The Effect of High-Pressure on Amino Acids.

Stephen A. Moggach

A Thesis submitted in fulfilment of the requirements for the degree of Doctor of Philosophy to the School of Chemistry, University of Edinburgh.

January 2006

Declaration

I declare that this thesis was written by myself and that the work detailed in this is my own, or I have contributed substantially to such work, except where specific reference is made to the work of another. This work has not been submitted for any other degree or professional qualification.

Stephen Moggach

Abstract

The crystal structure of L-serine has been determined at room-temperature at pressures between 0.3 and 4.8 GPa. The structure of this phase (hereafter L-serine-I), which consists of the molecules in their zwitterionic tautomer, is orthorhombic, space group $P2_12_12_1$; the cell dimensions at ambient pressure (CCDC refcode LSERIN01) are a = 8.599(5), b = 9.348(3), c = 5.618(2) Å; at 4.8 GPa the corresponding parameters are a = 8.2980(16), b = 8.600(3), c = 5.4663(10) Å. The least compressible cell-dimension (c), corresponds to chains of head-to-tail NH...carboxylate hydrogen bonds. The most compressible direction is along b, and the pressure-induced distortion in this direction takes the form of closing-up of voids in the middle of R-type hydrogen-bonded ring motifs. This occurs by a change in the geometry of hydrogen bonded chains connecting the hydroxyl groups of the -CH_2OH side chains. These hydrogen bonds are the longest conventional hydrogen bonds in the system at ambient pressure, having an O...O separation of 2.918(4) Å, and an O...O...O angle equal to 148.5(2)°; at 4.8 GPa these parameters are 2.781(11) Å and 158.5(7)°. Elsewhere in the structure one NH...O interaction reaches an N...O separation of 2.691(13) Å at 4.8 GPa. This is amongst the shortest of this type of interaction to have been observed in an amino acid crystal structure, and above 4.8 GPa the structure undergoes a single crystal to single crystal phase transition to a hitherto uncharacterized polymorph, which we designate L-serine-II. L-serine-II is orthorhombic, space group $P2_12_12_1$ with cell dimensions a = 6.9083(10), b = 9.644(3), c = 5.6166(8) Å at 5.4 GPa. The OH...OH hydrogen bonded chains of L-serine-I are replaced in L-serine-II by shorter OH...carboxyl interactions, which have an O...O separation of 2.62(2) Å. This occurs via a change from a *gauche* to *anti* conformation of the OH group, and a change in the $NC_\alpha CO$ torsion angle from -178.1(2)° at 4.8 GPa to -156.3(10)° at 5.4 GPa. Thus, the same topology appears in both crystal forms, which explains why it occurs from one single crystal form to another. The transition to L-serine-II is also characterized by closing-up of voids which occur in the centres of other R-type motifs elsewhere in the structure. There is a marked increase in CH...O hydrogen bonding in both phases relative to L-serine-I at ambient pressure.

The hydrostatic compression of L-serine-d_7 has been studied to 8.1 GPa by neutron powder diffraction. Over the course of this pressure range the compound undergoes two phase transitions, the first between 4.6 and 5.2 GPa, yielding L-serine-II, and the second between 7.3 and 8.1 GPa, yielding L-serine-III. All three polymorphs are orthorhombic, $P2_12_12_1$, and feature chains of serine molecules connected via head-to-tail

ND...O H-bonds formed between ammonium and carboxylate groups. The chains are linked into a ribbon by a second set of ND...O H-bonds. The hydroxyl moieties are distributed along the outer edges of the ribbon, and in phase-I they connect the ribbons into a layer by chains of OD...OD H-bonds. The layers are connected together by a third set of ND...O H-bonds, forming $R^3_4(14)$ rings with substantial voids at their centres. In the transition from phase-I to II these voids begin to close-up, but at the cost of breaking the OD...OD chains. The OD...OD H-bonds are replaced by shorter OD...O H-bonds to carboxylate groups. The results obtained here on compression of L-serine-d_7, were comparable to those obtained in our previous single-crystal X-ray diffraction experiment. At 7.3 GPa the O...O distance in the OD...O H-bonds measures only 2.516(17) Å, which is short, and we propose that the phase transition to phase-III that occurs between 7.3 and 8.1 GPa relieves the strain that has built up in this region of the structure. The hydroxyl D-atom now bifurcates between the OD...O contact that had been present in phase-II and a new OD...O contact formed to a carboxylate in another layer. Hirshfeld surface fingerprint plots show that D...D interactions become more numerous, while H-bonds actually begin to lengthen in the transition from phase II to III.

The crystal structure of hexagonal L-cystine has been determined at room temperature at pressures between 0.4 and 3.7 GPa; unit cell dimensions were measured up to 6.4 GPa. The structure of this phase consists of molecules in their zwitterionic form, and crystallises in the hexagonal space group $P6_122$. The structure consists of H-bonded layers which are strongly reminiscent of those seen in α-glycine, and consist of $R^4_4(16)$ H-bonded ring motifs. These layers are connected on one side by the disulfide bridges within the cystine molecules, and on the other by NH...O H-bonds to other glycine-like layers. The most compressible unit cell dimension, and the direction of greatest strain in the structure, is along the *c*-axis, and application of pressure pushes the layers closer together. The compression occurs approximately equally in the regions of the interlayer H-bonds and the disulfide bridges, in the latter changes in the C-S-S-C torsion angles allow the cystine molecules to act like springs. The effects of pressure can be interpreted in terms of closing-up of voids in the structure, and this leads to (*i*) a lessening of the N-C-C-O and C-S-S-C torsional angles, (*ii*) shortening of the N-H...O hydrogen bonds by 0.10 – 0.60 Å and (*iii*) a further shortening of an already short S...S contact from 3.444(4) Å to 3.264(4) Å.

The crystal structure of the orthorhombic phase of L-cysteine (hereafter L-cysteine-I) consists of chains of molecules linked via NH...O H-bonds. The chains are

linked into a layer by other NH...O H-bonds, forming $R^4_4(16)$ ring motifs. The layers are linked by further NH...O, disordered SH...S/SH...O interactions. The main effects of compression to 1.8 GPa are to contact voids in the middle of the $R^4_4(16)$ rings and to reduce S...S distances from 3.8457(10) Å to 3.450(4) Å. The latter is at the lower limit for S...S distances, and we suggest that strain about the S-atom is responsible for the formation of a new phase of L-cysteine, L-cysteine-III above 1.8 GPa. The phase transition is accompanied by a change in the NCCS torsion angle from *ca* 60° to *ca* -60° and small positional displacements, but with no major changes in the orientations of the molecules. The structure of L-cysteine-III contains similar *R*-type ring motifs to L-cysteine-I, but there are no S...S contacts within 3.6 Å. L-cysteine-III was found to be stable to at least 4.2 GPa. On decompression to 1.7 GPa, another single-crystal to single-crystal phase transition formed another previously uncharacterised phase, L-cysteine-IV. This phase is *not* observed on increasing pressure. The structure consists of two crystallographically independent cysteine molecules in the same conformations as those found in L-cysteine-I and L-cysteine-III. The structure separates into zones which are alternately phase-I-like and phase-III-like. L-cysteine-IV and can therefore be thought of as an unusual example of an intermediate phase. Further decompression to ambient pressure generates L-cysteine-I.

The crystal structure of α-glycylglycine (α-GLYGLY) has been determined at room temperature at pressures between 1.4 and 4.7 GPa; unit cell dimensions were measured up to 5.4 GPa. The structure can be considered to consist of layers of molecules which stack perpendicular to the (1 0 -1) direction. The arrangement of glycylglycine molecules within each layer resembles the anti-parallel β-sheet motif observed in proteins, except that in α-GLYGLY the motif is constructed through NH...O H-bonds rather than conventional covalent amide links. Compression of α-GLYGLY proceeds via a reduction in void sizes. Voids close in such a way as to decrease the distances of stabilising interactions like H-bonds and dipolar contacts. The largest reductions in interaction distances tend to occur for those contacts which are longest at ambient pressure. These longer interactions are formed between the β-sheet-like layers, and the largest component of the strain tensor lies in the same direction. The N...O distance in one NH...O H-bond measures 2.624(9) Å at 4.7 GPa. This is very short for this kind of interaction and the crystal begins to break up at above 5.4 GPa, presumably as the result of a phase transition. The changes that occur have been analysed using Hirshfeld surfaces. Changes in the

appearance of these surfaces enable rapid assessment of the structural changes that occur on compression.

Acknowledgements

I would like to start by thanking my Supervisor Dr Simon Parsons, not only for teaching me Crystallography, but for making the last three years a pleasure to work for him. Words can not describe.

Dr Colin Pulham and Dr Dave Allan for all their help during my PhD. Dave, my very own high-pressure guru, thanks for all your support and help, particularly for those long Daresbury trips. Dr Carole Morrison for all her computational help, sorry I bailed on that front, I promise to do more! Dr John Warren for all his help during the past few years on station 9.8. John, you really do make that station a fantastic place to work.

Thanks to everyone from the Chemical Crystallography group, including Patty (my little Spanish Friend), Fran (my cheeky Italian friend) and Laura (just little). To Pete and Fraser for all their great 'banter' over the last year, you made the office a nice place to be, sorry if I've been a bit grumpy while writing. To my friends Philip Van Kuyk, Emma Ashman and Nada, without you, I would not have made it this far! To Rachel Smith (Mrs Pete) for coping with my jokes, I promise to get some new material. To both Alice Dawson and Iain Oswald, not only for teaching me high-pressure techniques and crystallography, but for making me feel so welcome in the first few years of my PhD.

To my Edinburgh urban family, Michael Crane, Jennifer Todd and Rubah. Mike, the best flatmate, Jenny, the best cook and Rubah, the best cat. You have made living in Edinburgh the best.

To my Mum and Dad for supporting me through the entirety of my student life. To Sharron, Sean and Scot Moggach (the three maggots!) for all their support, and to Michelle Moggach and Philip Cooper for keeping Scot and Sharron in line. To both my Nanny and Grandad for all their help and support, and for giving me the best T.V. ever!

My final thanks go to Fiona Stefanowicz, pal, you are my best friend on the entire planet, you have kept me well fed, and taken care of me over the last four years. It just would not have been the same without you.

Contents

Chapter 1

Introduction

1.1 Introduction

The most important intermolecular interactions in the organic solid state are van der Waals forces, dipole-dipole and other polarised interactions and hydrogen bonding. Interaction energies can be estimated using a variety of techniques. One recent development in this area has been the introduction of the density sums or Pixel method. Calculations have been carried out on a variety of molecular dimers commonly found in the organic solid state, yielding a hierarchy of the packing forces (Gavezzotti, 2005). For example, typical interaction energies have been derived for acidic O-H...O=C interactions (30-40 kJ mol^{-1}), NH...O and NH...N hydrogen bonds in amides (15-25 kJ mol^{-1}), and OH...O hydrogen bonds in alcohols (20-25 kJ mol^{-1}). A hydrogen bond is not always the strongest intermolecular interaction in a structure. Stacking interactions between benzene rings for example are at the lower end of the H-bond hierarchy (10-15 kJ mol^{-1}), while C=O...C=O dipole-dipole energies have been shown to have interaction energies equivalent to more classical hydrogen bonds ($\leq$ 20 kJ $mo1^{-1}$) (Allen *et al.*, 1998). On the lower end of this hierarchy, CH...O/N interactions were found to have energies of <10 kJ mol^{-1}, however, this was only found when the donor hydrogen was highly acidic. Interactions between aliphatic CH groups and polar acceptors for example, involved energies of less than 5 kJ mol^{-1}.

Intermolecular interactions are thus much weaker than intramolecular covalent bonds and the ionic bonds that are characteristic of 'inorganic' solids. Mean bond enthalpies for C-C and C=O bonds are typically 348 and 743 kJ mol^{-1}, respectively, while the lattice enthalpies for NaCl and LiF are 787 and 1037 kJ mol^{-1}, respectively. Molecular solids are therefore relatively soft and compressible.

The compressibility of a solid can be quantified using the *bulk modulus* (B_0), which characterises the variation of the volume of a solid with increasing pressure at constant temperature, and can be defined as:

$$B_0 = -V_0(\partial P / \partial V)_{P=0}$$

Some representative values are NaCl (25 GPa), quartz (37 GPa), ceramics (50-300 GPa) and diamond (440 GPa) (Slebodnick *et al.* 2004). Molecular solids typically have B_0 < 30 GPa (Angel, 2004), and often much less (e.g. for 6.6 GPa $Ru_3(CO)_{12}$).

Application of pressure offers a useful tool with which to perturb structure and change the hierarchy of interactions in the solid state. This can be understood in terms of the work done (W) when a force per unit area (P) acts on a volume (V), given by:

$$W = -P\Delta V$$

On compressing molecular materials, W and P are both positive and therefore application of pressure constrains the ΔV term to be negative – that is pressure favours states with smaller volumes. The relation

$$\frac{\partial \Delta G}{\partial P} = \Delta V$$

shows that the perturbations which occur with pressure depend solely on volume, and as a result the changes that occur with pressure can be more straightforward to interpret than those that occur with temperature (Fourme *et al.*, 2001).

A recent goal in the field of small-molecule crystallography has been to gain an understanding of the changes which occur in molecular systems as a function of pressure at atomic resolution. The majority of studies have been carried out using single crystal diffraction below 10 GPa, the upper limit of conveniently available hydrostatic media. The work presented in this thesis focuses on the effects of high-pressure on the crystal structures of amino acids. This family of compounds offers several advantages for pressure studies as they are polyfunctional and form well-defined intermolecular interactions, most prominently hydrogen bonds.

1.2 Hydrogen Bonding

1.2.1 Definition of a Hydrogen Bond.

Pauling first defined the hydrogen bond in his book *Nature of the Chemical Bond* (1939): *Under certain conditions, an atom of hydrogen is attracted by rather strong forces to two atoms instead of one, so that it may be considered to be acting as a bond between them. This is called a hydrogen bond.*

More recently in a review by Steiner (2002), the definition of a hydrogen bond was developed further: *An D-H...A interaction is called a "hydrogen bond", if 1. it constitutes a local bond, and 2. D-H acts as a proton donor.*

D and A are referred to as hydrogen bond donor and acceptor atoms, respectively. In this description, D must be sufficiently electron withdrawing to enhance the acidic nature of

the hydrogen atom, while A usually has a region of high electron density, such as a lone pair of electrons.

Hydrogen bonding interactions are ideally classified as strong, moderate or weak on the basis of the energies of the interactions involved. However, in the absence of thermochemical data the classification is usually based on interatomic distances, or even the atom types forming the bond. Table 1.1 summaries a widely-accepted classification scheme, originally proposed by Jeffrey (1997). The main structural difference that distinguishes hydrogen bonds from van der Waals interactions is their directionality, in particular their preference for linearity. This is taken into consideration within Jeffrey's criteria for strong, moderate and weak hydrogen bonds, as the directional preference becomes weaker as the interaction becomes weaker (Table 1.1). Computational techniques have been used to partition hydrogen bonds into their different energy contributions. In a study by Morokuma, (1977) the main energy contribution to moderate hydrogen bonds was found to be the electrostatic term, and this has been confirmed by Gavezzotti's Pixel calculations (Gavezzotti, 2005).

	Strong	Moderate	Weak
Interaction type	mostly covalent	mostly electrostatic	electrostatic
Bond lengths			
H.....A (Å)	~1.2-1.5	~1.5-2.2	~2.2-3.2
D.....A (Å)	2.2-2.5	2.5-3.2	3.2-4.0
Bond angles(°)	175-180	130-180	90-150
Bond energy (kJ mol^{-1})	63-167	17-63	<17

Table 1.1: Strong, moderate and weak hydrogen bonds as defined by Jeffrey, (1997).

1.2.2 Hydrogen Bonds in Amino Acids at Ambient Pressure

L-α-Amino acids are the building blocks of proteins, and they have the general formula shown in Figure 1.1. The identity of an amino acid is determined by the side chain *R* group; for example glycine, serine and cysteine have *R* = H, CH_2OH and CH_2SH, respectively. The only achiral amino acid is glycine, most other naturally-occurring amino acid have the L configuration at the α carbon (Figure 1.1).

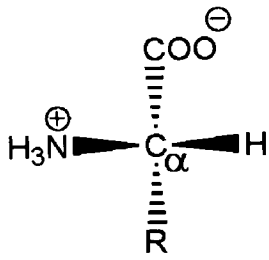

Figure 1.1: General structure of an L-α-amino acid.

In the solid state, amino acids exist in their zwitterionic form, where the ammonium and carboxyl groups respectively have positive and negative charges (Figure 1.1). Although ammonium-to-carboxylate NH...O hydrogen bonds dominate the crystal chemistry of amino acids, the variation of the *R*-side chains leads to a great diversity of possible hydrogen bond types, from N^+-H...O^- salt bridges to weak C-H...O interactions. Polar amino acids, such as serine and threonine for example both contain sp^3-hybridized hydroxyl groups which can act as both hydrogen bond donors and acceptors, while nonpolar amino acids such as methionine, which contain a sp^3-hybridized sulfur atom, are rarely involved in hydrogen bonding. It is common practice in the literature to designate hydrogen bonds based on N and O as 'moderate or conventional', while others such as CH...O and SH...SH are 'weak'.

1.2.3 Hydrogen Bond Geometries in Amino Acids

In a survey of the hydrogen bonding geometries of 32 amino acid structures as determined by neutron diffraction (Jeffrey & Maluszynska. 1982), the NH_3^+ group was found to always donate at least three hydrogen bonds, while the COO^- group was found to accept between four and six hydrogen bonds. This is unsymmetrical, and from this viewpoint, amino acid structures are proton deficient. This usually results in formation of a number of bifurcated (or three-centred) NH^+...^-OOC hydrogen bonds. Out of a total of 168 hydrogen bonds identified in the survey, 64 were found to be NH...O hydrogen bonds between the NH_3^+ and COO^- zwitterions; of these 46 were bifurcated. The geometry of the bifurcated NH...O bonds range from unsymmetrical, where the H atom is only slightly displaced towards the second acceptor, to more symmetrical where the two acceptor oxygen atoms become more equidistant.

The shortest hydrogen bonds observed within the subset of amino acid structures determined by neutron diffraction were OH...O=C interactions, formed between a

carboxylic acid hydroxyl to a carboxylate oxygen, and NH...O=C hydrogen bonds where the N atom was from a proline or histidine ring. Typical H...O distances in these H-bonds fall into the range 1.71 to 2.08 Å. Amongst the weak CH...O bonds the majority (64%) were from C_α-H donors. This is thought to be because the αH atom is activated by the electron withdrawing NH_3^+ group. CH...O interactions have H...O distances in the range 2.16-2.65 Å, and <CH...O angles in the range 140-174°.

1.2.4 Classification of Hydrogen bonding Patterns

One method for characterising complex three-dimensional hydrogen bonding patterns is through the use of Graph Set Analysis (Etter *et al.* 1990; Bernstein *et al.*, 1995). The main advantage of this technique is that it can be used to break down complex hydrogen bonded structures into small repeated motifs. The notation used by Etter *et al.* is $G_d^a(n)$, where *G* represents the pattern descriptor, *d* denotes the number of donor atoms, *a* designates the number of acceptor atoms and *n* represents the number of atoms used in the pattern or *degree*. There are four different pattern descriptors that can be used; *C*, *R*, *S* & *D*. *C* denotes an infinite hydrogen bonded chain, *R* denotes a ring pattern, *S* denotes an intramolecular bond and *D* represents a discrete hydrogen bond.

One of the major advantages of using graph set analysis is that it forms a systematic method for identifying and comparing H-bonding motifs in related crystal structures. For example, head to tail NH...OOC hydrogen bonds usually lead to the formation of *C*(5) chains. This is illustrated in Figure 1.2, where the crystal structures of both α-glycine and L-norleucine both show formation of *C*(5) chains (Boldyreva *et al.*, 2003b; Torii & Iitaka, 1973).

An example of an intermolecular ring motif is shown in Figure 1.3 for L-leucine and L-methionine (Gorbitz & Dalhus., 1996; Dalhus & Gorbitz, 1996).

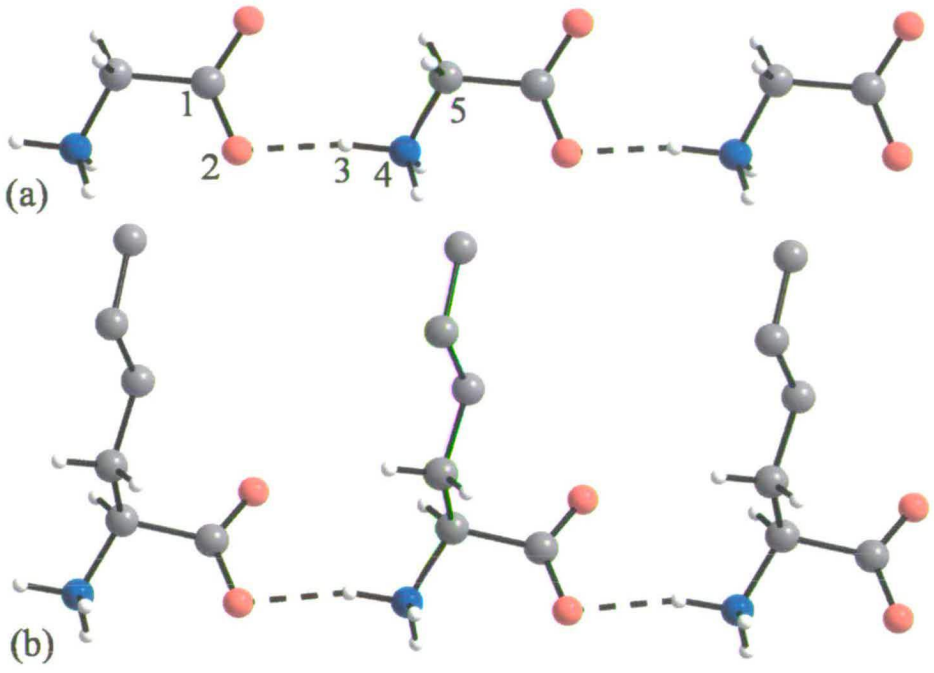

Figure 1.2: Formation of *C*(5) chains in the crystal structures of (a) α-glycine and (b) L-norleucine. In (a), the atoms which distinguish the chain have been labelled.

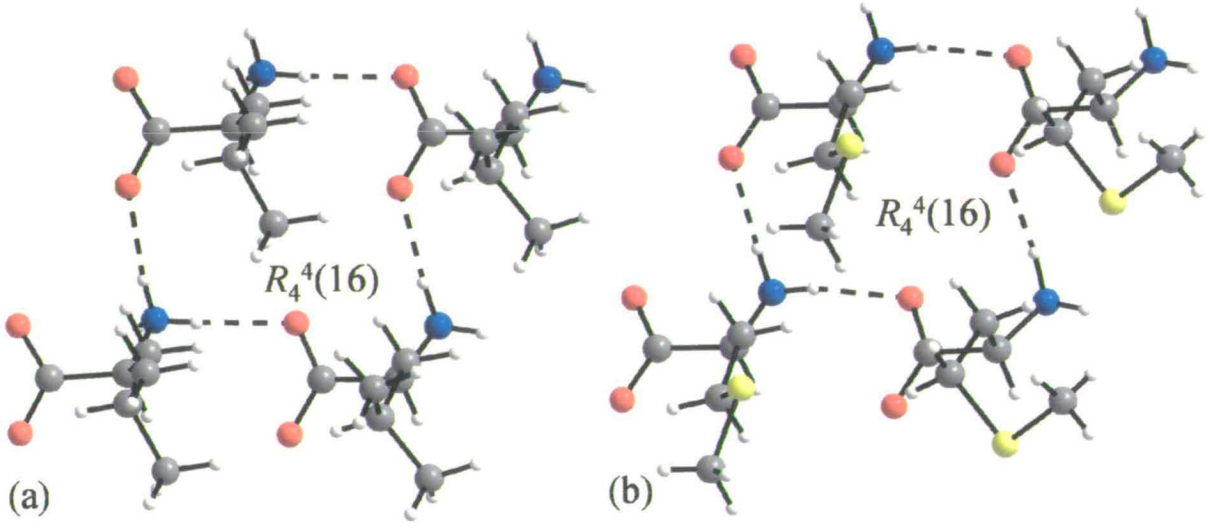

Figure 1.3: Formation of $R_4^4(16)$ ring motifs in both (a) L-leucine and (b) L-methionine.

1.3 Changes in Inter- and Intra-molecular bonds under Pressure

1.3.1 Vibrational Spectroscopy

Vibrational spectroscopy has been used extensively to investigate the changes that occur in solids under pressure. For example, in Fe-bearing wadsleyite (Cynn & Hofmeister, 1994) O-H stretching frequencies <3600cm^{-1} were shown to decrease in frequency, while those >3600cm^{-1} increased in frequency. It was suggested that the former involved those hydroxyl groups involved in hydrogen bonding, and the red shift was attributed to a broadening of the hydrogen bond potential as the D-H hydrogen bond acceptor approached the donor, increasing the strength of the H...A bond. For those hydroxyl groups not involved in H-bonding the reported increase in frequency was though to be a result of a decrease in the O-H bond length with increasing pressure.

Spectroscopic studies have also been used to measure the effect of pressure on metal-carbonyl interactions. The effect of pressure on $Mn(CO)_5Br$ was studied by Adams and Ekejiuba in 1982, where changes in the slopes of wavenumber versus pressure plots were used to identify a second order phase transition which took place at 2.3 GPa. In this case the frequency of the axial ν(CO) mode decreased slightly between ambient pressure to 2.3 GPa, while the other ν(CO) modes showed continuous, but positive shifts. Above 2.3 GPa, however, the pressure dependence of the axial ν(CO) mode became positive. Similar results were observed for isomorphous structures such as $Re(CO)_5Cl$.

Although vibrational spectroscopy can provide information on intramolecular geometry, normal modes consist of combinations of many different interatomic motions, and so it is difficult to correlate pressure induced shifts with changes in interatomic distances and intramolecular angles.

1.3.2 High Pressure Crystallography

Diffraction, most commonly single crystal X-ray diffraction, is the method of choice for studying intermolecular geometry. Though over 300 000 crystal structures are available in the Cambridge Crystallographic Database (CSD), only 189 of these (to August 2005) were determined at high pressure. Several carboxylic acids have been studied, including acetic acid, oxalic acid dihydrate, propionic acid and squaric acid. A number of substituted benzene derivatives have also been studied, including *p*-

dichlorobenzene, phenol and 1,4-di-iodobenzene. Recently, a number of compounds have been obtained *via* hydrothermal techniques, such as paracetamol methanol solvate, piracetam and phenanthrene. This approach can help overcome the kinetic barrier usually associated with the formation of new polymorphs at high-pressure (Fabbiani *et al.*, 2003, 2005). Several much simpler molecular compounds have been studied, including methane, methane dihydrogen and dimethane dihydrogen, reflecting the interests of planetary scientists.

Very few X-ray diffraction studies can be found on organometallic compounds, with one of the few exceptions, including structural studies on spin-crossover iron(II) complexes, such as $Fe(Phen)_2(NCS)_2$, (phen = 1,10-phenanthroline) and $Fe(Btz)_2(NCS)_2$, (Btz = 2,2'-bi-4,5-dihydrothiazine) (Granier *et al.*, 1993). More recently, an isolated high pressure study on $Ru_3(CO)_{12}$ was performed (Slebodnick *et al.*, 2004).

1.3.3 The effect of Pressure on Covalent bonds

Intramolecular bonds are expected to lengthen as intermolecular interactions strengthen with pressure. In paracetamol, for example, the shortening of an intermolecular OH...O(O=C) hydrogen bond is accompanied by a small elongation of the C=O bond (0.023 Å at 4 GPa) (Boldyreva *et al.*, 2003a). Studies of 2-methyl-1,3-cyclopentanedione, dimedone, and 1,3-cyclohexanedione also reveal similar variations with pressure (0.02 Å at 3GPa) (Katrusiak, 1992). However, these changes are very small, and in most cases are within experimental error. In an *ab initio* study on the effect of pressure on pentaerythritol tetranitrate, changes in calculated bond lengths on compression to 22.76 GPa showed that C-C bonds decreases by 0.05 Å, while CH and CO bonds decreased by only 0.01 Å (Brand, 2005). The largest change in bond angle in this study was 3.7°, while the largest change in torsion angle was 11°.

In high pressure crystallography, particularly when applied to low-symmetry crystal systems, shading by the pressure cell restricts the volume of reciprocal space that can be sampled. This leads to low data completeness and low data-to-parameter ratios during refinement. In severe cases data sets are pseudo two-dimensional. Bond distances and angles are generally restrained to ambient pressure and temperature values in order to alleviate these refinement problems. While such restraints can be justified below 10 GPa, this approximation is likely to become less accurate at higher pressures.

1.3.4 The effect of High Pressure on intermolecular bonds in amino acids

The first paper to describe the effect of pressure on the crystal structure of amino acid described a synchrotron powder study on a polymorphic mixture of glycine. Under ambient pressure conditions glycine exists in three different polymorphic forms designated α-, β- and γ-. The order of stability at atmospheric pressure and room temperature is γ > α > β. The effect of pressure on pure samples of all three polymorphs was studied by Dawson *et al.* (2005) using a combination of single crystal and powder methods.

α-Glycine has a 'double-layer' structure in which pairs of H-bonded layers interact via weaker CH…O bonds. These inter-later CH…O interactions shorten by up to 0.109 Å on compressing α-glycine to 6.2 GPa, causing the stacking distance between layers to be reduced. This, however, is not the direction of greatest strain in the structure, which actually resides within the layers. The main effect within these layers is to compress 'holes' at the centre of $R^4_4(16)$ H-bonded ring motifs (Figure 1.4).

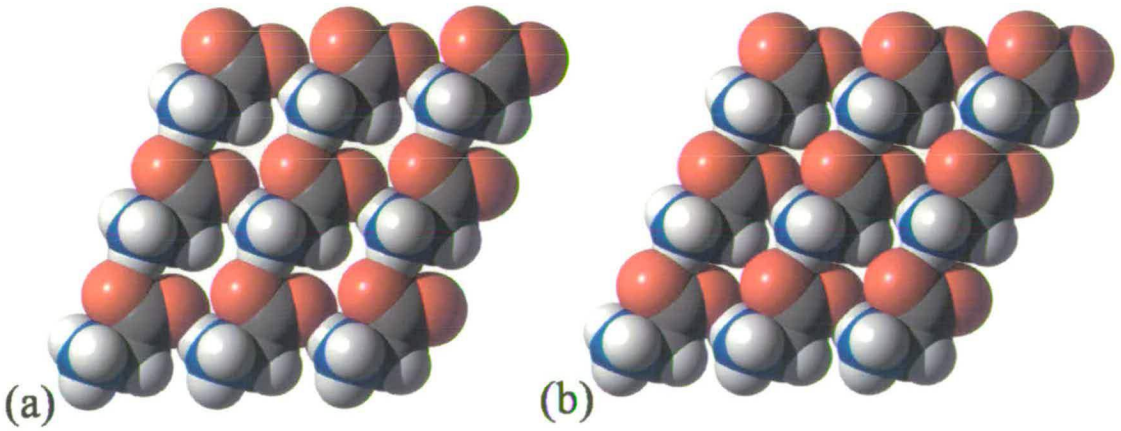

Figure 1.4: Space-filling plots of $R^4_4(16)$ ring motifs at (a) ambient pressure and (b) 6.2 GPa. Colour scheme is the same as Fig 1.2.

Although single-crystal data on α-glycine have been collected to 6.2 GPa, the structure has been reported, on the basis of Raman spectra, to be stable to 23 GPa (Murli et al., 2003).

β–glycine is the least stable phase under ambient pressure conditions, and on compression undergoes a reversible single-crystal to single-crystal phase transition at a very modest pressure (0.8 GPa) to a new high pressure phase, δ-glycine. The same transition has been observed by Raman spectroscopy. β–glycine crystallises in the

monoclinic space group $P2_1$, and the structure is composed of similar layers to that of the α polymorph, comprising $R^4_4(16)$ rings. δ-glycine crystallises in the centrosymmetric space group $P2_1/a$, and differs from that of β-glycine by the orientation of the glycine molecules. This is illustrated in Figure 1.5 where the NH...O hydrogen bond, N1H5...O1 in β-glycine points down, while in in δ-glycine, this hydrogen bond alternates between pointing down and up in consecutive $C(5)$ chains (Figure 1.5b).

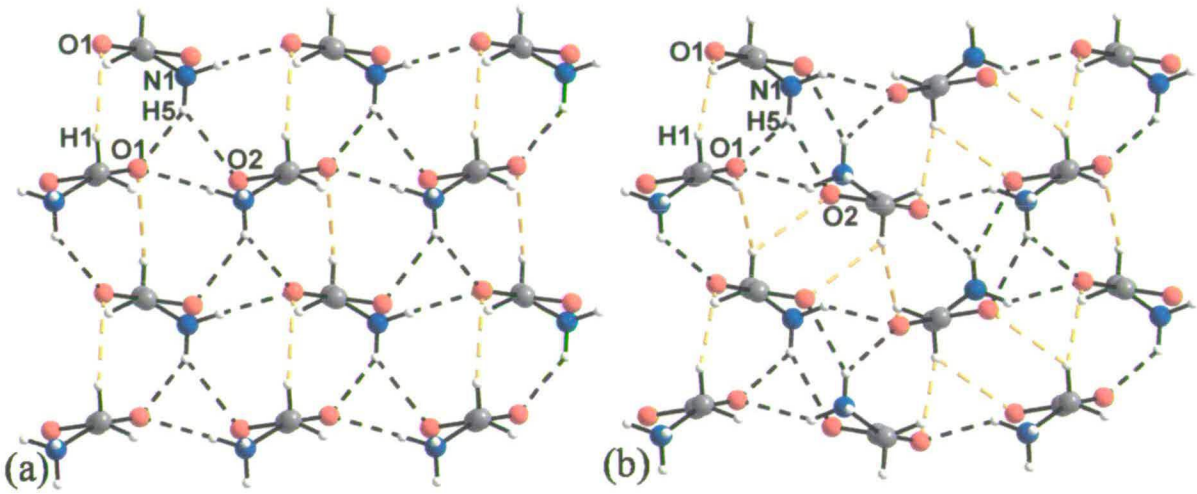

Figure 1.5: The crystal structure of (a) β-glycine at ambient pressure and (b) δ-glycine at 1.9 GPa. NH...O and CH...O interactions between layers, stacked along the *b*-direction are shown, drawn as black and orange dotted lines respectively.

Comparison of space-filling plots of the layers in β–glycine at ambient pressure, and δ-glycine at 1.9 GPa shows that one effect of the transition is to close up voids within $R^4_4(16)$ ring motifs, similar to the effect on compression of α-glycine (Figure 1.6).

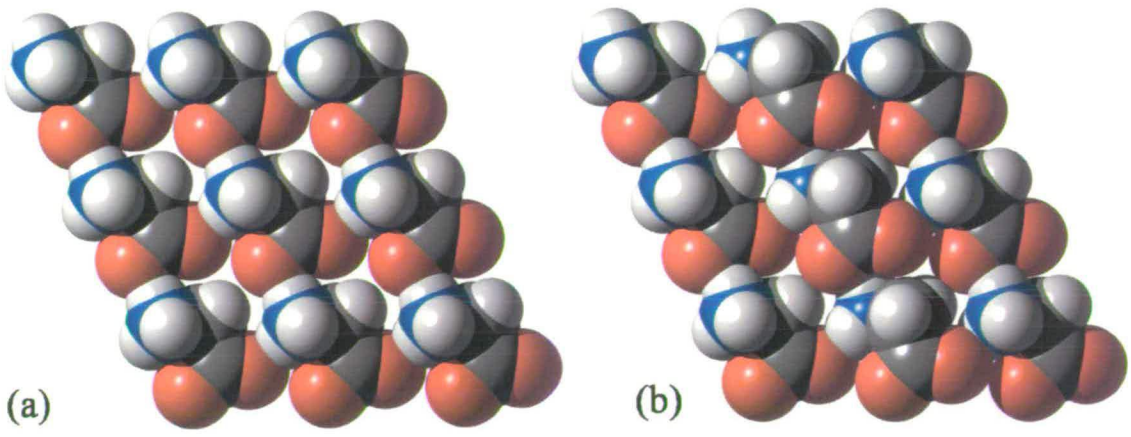

Figure 1.6: Space-filling plots of $R^4_4(16)$ ring motifs in (a) β-glycine at ambient pressure and (b) δ-glycine at 1.9 GPa. Colour scheme is the same as Fig 1.2.

γ-Glycine is trigonal and crystallises in $P3_1/P3_2$. Unlike the other phases of glycine mentioned thus far, γ-glycine does not contain layers, but instead forms a three dimensional hydrogen bonded network built from a helical arrangement of glycine molecules around the 3_1 screw axis (Figure 1.7).

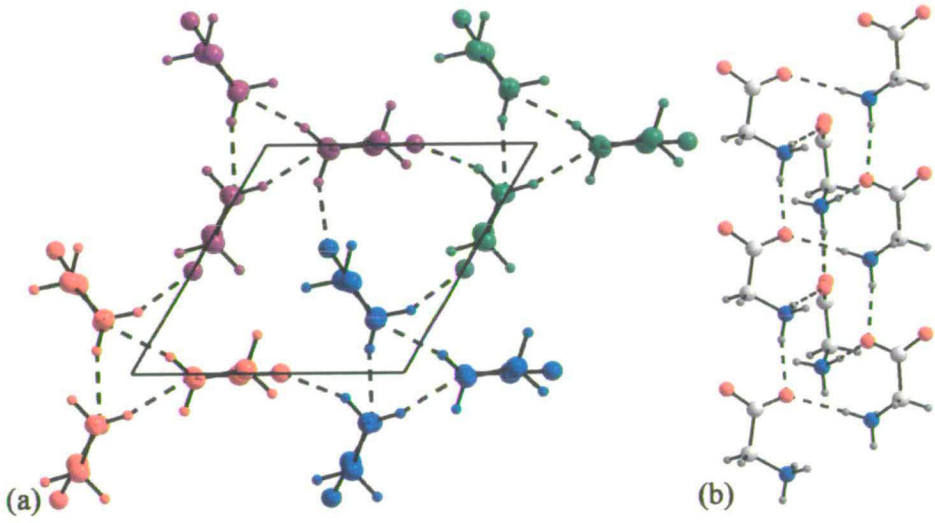

Figure 1.7: The crystal structure of γ-glycine at 1.3 GPa. (a) Helical arrangement of the molecules about the 3_1 screw axes is shown. Each helix is shown in different colours for clarity. (b) One of the helices taken on its own as viewed along **b**.

On increasing pressure on a single-crystal of γ-glycine above 1.3 GPa, it was found that the quality of the single-crystal deteriorated to such an extent that no useful intensity data could be obtained. By using high-pressure powder methods however, structural data were collected to 4.3 GPa, leading to the formation of a new high-pressure phase (ε-glycine). A structure of ε-glycine has been proposed on the basis of a similar powder diffraction study by Boldyreva *et al.* (2004), though some doubt was cast on the correctness of this structure by Dawson *et al.* (2005). However, both the interpretations of Boldyreva *et al.* and Dawson *et al.* were in agreement that ε-glycine crystallises in the monoclinic space group *Pn*, with its structure composed of irregularly spaced layers, as in α-glycine (Figure 1.8).

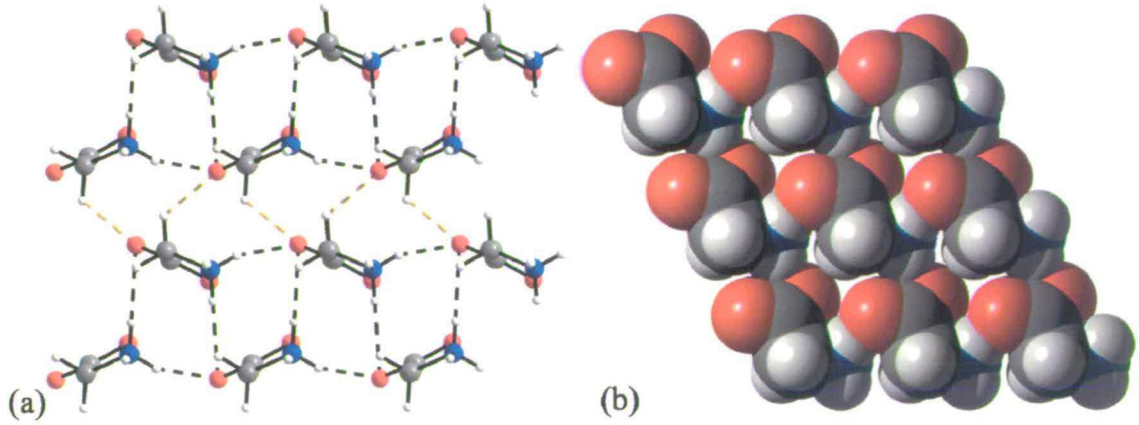

Figure 1.8: The crystal structure of ε-glycine at 4.3 GPa. (a) NH...O and CH...O interactions between layers, stacked along the *b*-direction and (b) Space-filling plot of $R^4_4(16)$ ring motifs. NH...O and CH...O interactions are drawn as black and orange dotted lines respectively. Colour scheme is the same as Fig 1.2.

Dawson *et al.* (2005) noted that that NH...O hydrogen-bond distances did not fall outside the range 2.6-3.1 Å in any of the glycine polymorphs. This range does not fall outside that observed for structures determined under ambient conditions, suggesting that super-short hydrogen bonds are not formed at pressures below approximately 10 GPa. It seemed that the effect of pressure on individual hydrogen bonds could be rationalized by other changes, such as closing-up of voids or CH...O bond formation which occur under compression.

1.3.5 The effect of High Pressure on macromolecules.

Application of pressure to biological systems has been known to have major effects for some time, with observations of proteins made as early as 1914 by Bridgeman, where he described the coagulation of the white of an egg when subjected to hydrostatic pressure at room temperature, its appearance becoming much like that of a hard-boiled egg.

More recently, spectroscopic methods have been utilised yielding information about the secondary structure of proteins at high pressure. Examples include an infrared study of chymotrypsinogen in H_2O to 3.0 GPa by Wong & Heremans (1988). In this study, an irreversible denaturation was induced at 0.76 GPa, where the contributions of random coil and turn conformational substructures to the protein structure were found to increase dramatically at the expense of the contributions of the α-helix and β-sheet

substructures. The on-set pressure of denaturation increased when the external pressure was applied more slowly.

The ability to obtain atomic resolution high-pressure data is of great importance in understanding the effects of pressure on the primary structure of biological systems under pressure. Several structural studies have appeared on the behaviour of proteins under non ambient pressure conditions, including those on tetragonal hen egg-white lysozyme (t-HEWL) and sperm whale myoglobin (Kundrot & Richards, 1986; Urayama *et al.*, 2002). The first crystal structure of a macromolecular assembly under high-pressure, however, was not obtained until recently (Girard *et. al.* 2005). In this study, the effect of pressure on cubic Cowpea mosaic virus crystals at 0.03 GPa were described, where on application of pressure, a disorder-order transition was induced resulting in greatly enhanced diffraction. A much larger number of ordered water molecules were observed than at ambient pressure; the thermal parameters were also lower. Hydrogen bond lengths were found to shorten, with those acting between residues reducing on average by 0.034 Å. For those hydrogen bonds between a residue and a water molecule, a mean reduction of 0.048 Å was observed. One of the most noticeable effects was a reduction in the size and occurrence of cavities within the structure at high-pressure, with the mean cavity volume for the icosahedral unit reducing from 113.4 $Å^3$ to 65.9 $Å^3$ between ambient pressure and 0.03 GPa.

The findings in macromolecular systems parallel those in glycine, where relative compressibility along different crystallographic directions could be rationalised in terms of the distributions and shapes of intermolecular voids. Hydrogen bonds and other intermolecular interactions formed along the directions in which voids compress shorten substantially, while other such interactions may be left relatively unchanged. CH...O hydrogen bonds also increase in strength and number. It was notable that compression continued until the minimum distance as observed for a specific interaction (*e.g.* the N...O distance in an N-H...O hydrogen bond) under ambient pressure has been reached, and it was at this point in γ-glycine that a phase transition occurred. However, the extent to which these observations have any generality still needs to be established, and this forms the subject of this thesis.

1.4 References

Adams, D. M. & Ekejiuba, I. O. C. (1982). *J. Chem. Phys.*, **77**, 4793-4795.

Allen, F. H., Baalham, C. A., Lommerse, J. P. M. & Raithby, P. R. (1998). *Acta Cryst. B***54**, 320-329.

Bernstein, J., Davis, R. E., Shimoni, L. & Chang, N-L. (1995). *Angew. Chem. Int. Ed. Engl.* **34**, 1555-1573.

Boldyreva, E. V. (2003a). *J. Mol. Struct.* **647**, 159-179.

Boldyreva, E. V., Ahsbahs, H. & Weber, H.-P. (2003b). *Z. Krist*, **218**, 231-236.

Boldyreva, E. V., Ivashevskaya, S. N., Sowa, H., Ahsbahs, H. & Weber, H.-P. (2004). *Doklady. Phys. Chem.*, **396**, 111-114.

Brand, H. V. (2005). *J. Phys. Chem. B.* **109**, 13668-13675.

Cynn, H. & Hofmeister, A. M. (1994). *J. Geophy. Res.*, **99**, 17717-17727.

Dawson, A., Allan, D. R., Belmonte, S. A., Clark, S. J., David,W. I. F., McGregor, P. A., Parsons, S., Pulham, C. R. & Sawyer, L. (2005). *Cryst. Growth Des.* **5**, 1415-1427.

Dalhus, B. & Goerbitz, C. H. (1996). *Acta. Chemica. Scand.*, **50**, 544-548.

Etter, M. C., MacDonald, J. C. & Bernstein, J. (1990). *Acta Cryst. B***46**, 256-262.

Fabbiani, F. P. A., Allan, D. R., Dawson, A., David, W. I. F., McGregor, P. A., Oswald, I. D. H., Parsons, S. & Pulham, C. R. (2003). *Chem. Comm.* **24**, 3004-3005.

Fabbiani, F. P. A.., Allan, D. R., Marshall, W. G., Parsons, S., Pulham, C. R.. & Smith, R. I. (2005). *J. Cryst. Growth.*, **275**, 185-192.

Fourme, R., Kahn, R., Mezouar, M., Girard, E., Hoerentrup, C., Prange, T. & Ascone, I. (2001). *J. Synchrotron Rad.* **8**, 1149-1156.

Gavezzotti, A. (2005). *J. Chem. Theory Comput.* **1**, 834-840.

Girard, E., Kahn, R., Mezouar, M., Dhaussy, A-C., Lin, T., Johnson, J.E. & Fourme, R. (2005). *Biophysical Journal.*, **88**, 3562-3571.

Goerbitz, C. H. & Dalhus, B. (1996b). *Acta. Cryst, C***52**, 1754-1756.

Granier, T., Gallois, B., Gaultier, J., Real, J. A. & Zarembowitch, J. (1993). *Inorg. Chem.*, **32**, 5305-5312.

Jeffrey, G. A. (1997). *An Introduction to Hydrogen Bonding*, Oxford University Press, Oxford, UK.

Jeffrey, G. A. & Maluszynska, H. (1982). *Int. J. Biol. Macro.* **3**, 173-185.

Katrusiak, A. (1992). *J. Mol. Struct.*, **269**, 329-354.

Kundrot, C. E. & Richards, F. M. (1986). *J. Appl. Cryst.*, **19**, 208-213.

Morokuma, K. (1977). *Acc. Chem. Res.* **10**, 294-300.

Slebodnick, C., Zhao, J., Angel, R., Hanson, B. E., Song, Y., Liu, Z. & Hemley, R. J. (2004). *Inorg. Chem.* **43**, 5245-5252.

Steiner, T. (2002). *Angew. Chem. Int. Ed.* **41**, 48-76.

Torii, K. & Iitaka, Y. (1973). *Acta. Cryst.*, *B***29**, 2799-807.

Urayama P., Phillips G. N Jr. & Gruner S. M. (2001). *Structure.*, **10**, 51-60.

Wong, P. T. T. & Heremans, K. (1988). *Biochim. Biophys. Acta.*, **956**, 1-9.

Chapter 2

The Effect of Pressure on the Crystal Structure of L-Serine: The Crystal Structure of L-Serine-II at 5.4 GPa.[i]

[i] Moggach, S. A., Allan, D. R., Morrison, C. A., Parsons, S. & Sawyer, L. (2005). *Acta Cryst.*, ***B*61**, 58-68.

2.1 *Synopsis*

The crystal structure of L-serine has been determined at room temperature at pressures from 0.3 to 4.8 GPa. Above 4.8 GPa the structure transforms to a new polymorph, the structure of which has been determined at 5.4 GPa.

2.2 *Introduction*

Molecular crystals display a wide range of intermolecular interactions, from strong ionic and hydrogen bonding to weak van der Waals contacts. The application of high pressure to organic materials is a very powerful way to probe the nature of these interactions. The magnitudes of the effects which are observed are generally greater than those observed on cooling. Pressure-induced polymorphism occurs in a number of systems. We have characterized, for example, new high pressure phases in alcohols (Allan & Clark, 1999, Allan *et al.*, 2001, Allan *et al.*, 2002), carboxylic acids (Allan *et al.*, 1998, Allan *et al.*, 2000), acetone (Allan *et al.*, 1999), and, very recently, glycine (Dawson *et al.*, 2004*b*). A different high-pressure phase of glycine has also been recently reported by Boldyreva *et al.* (2004). The number of high-pressure studies on molecular systems that have actually been carried out is still rather small, and systematic trends have yet to emerge. However, this is a rapidly emerging area of structural science, and it has been the subject of a number of recent reviews, for example Boldyreva (2003, 2004*a*, 2004*b*, 2004*c*), Katrusiak (2004) and Hemley & Dera (2000).

Organic compounds crystallize predominantly in low-symmetry crystal systems, and the effect of application of pressure is generally quite anisotropic. The compressibility along different crystallographic directions can occasionally be rationalized in terms of the strengths of hydrogen bonds made along different directions. For example, both Boldyreva *et al.* (2003) and we (Dawson *et al.*, 2004*b*) have shown that the least compressible lattice-direction of α-glycine corresponds to the direction of strongly hydrogen-bonded chains. However, in $[Co(NH_3)_5NO_2]Cl_2$ some hydrogen bond lengths actually increase with pressure (Boldyreva *et al.*, 1998), and it is clear that the behaviour of hydrogen bonds under high pressure depends not only on the bonds themselves, but also on their relationship to other features of a structure, such as other intermolecular interactions and crystal packing.

The extent to which compressibility can be explained, and how far a structure can be compressed before it undergoes a phase transition, are key issues of current interest in this area of crystallography. In this paper we attempt to address them in a study of the effect of pressure on L-serine. Amino acids have been studied extensively at ambient pressure both by neutron and X-ray diffraction; they are highly crystalline, and their structures are dominated by hydrogen bonding (Jeffrey & Maluszynska, 1982). Weak CH...O hydrogen bonds occur frequently, and play an important role in supporting more familiar medium-strength hydrogen bonds, e.g. NH...O (Desiraju & Steiner, 1999; Derewenda *et al.*, 1995). Amino acids therefore make excellent candidates for this kind of study, but we hope that the results will additionally be useful for the development of inter-residue potentials which can be used to model the nature of pressure effects in proteins and other complex systems.

2.3 Experimental

2.3.1 Crystal growth

L-serine (99%) was purchased from Aldrich (catalogue number S2,60-0). One small, block-shaped crystal was obtained directly from the sample bottle and loaded into a diamond anvil cell.

2.3.2 High Pressure Crystallography

High-pressure experiments were carried out using a Merrill-Bassett diamond anvil cell (half-opening angle 40°), equipped with 600μm culets and a tungsten gasket (Merrill & Bassett, 1974). A 1:1 mixture of *n*-pentane and isopentane was used as a hydrostatic medium. A small ruby chip was also loaded into the cell as the pressure calibrant, with the ruby fluorescence method utilized to measure the pressure. Measurements were carried out by excitation with a 632.417 nm line from a He-Ne laser, the fluorescence being detected with a Jobin-Yvon LabRam 300 Raman spectrometer.

Diffraction data were collected on a Bruker SMART APEX diffractometer with graphite-monochromated Mo-Kα radiation (λ = 0.71073 Å). A hemisphere of data was collected at room temperature using the crystal before it was mounted in the Merrill-Bassett cell. The crystal was orthorhombic, and its unit cell dimensions were a = 8.579(4), b = 9.349(4), c = 5.613(3) Å based on 783 data $8 < 2\theta < 45°$. The L-serine coordinates of Kistenmacher *et al.* (1974) were refined against these data to yield a

conventional *R*-factor of 0.0293 for 408 data with $I > 2\sigma(I)$. The aim of this experiment was simply to establish the starting phase of the sample used in this pressure study, and crystallographic data are not given here.

Data collection and processing procedures for the high-pressure experiments were as described by Dawson *et al.* (2004*a*). Integrations were carried out using the program SAINT (Bruker-AXS, 2003), and absorption corrections with the programs SADABS (Sheldrick, 2004) and SHADE (Parsons, 2004). Data collections were taken in approximately 1.0 GPa steps from 0.3 GPa up to a final pressure of 5.4 GPa. Determinations of the cell constants at 5.4 GPa showed that a single-crystal to single-crystal phase transition had occurred to a new polymorph (L-serine-II). The pressure was then reduced back down to ambient pressure and the sample removed from the pressure cell. Once removed, a hemisphere of X-ray diffraction data was collected at room temperature. The phase on return to ambient pressure was identified as the L-serine-I on the basis of the unit cell constants [orthorhombic, a = 8.531(9), b = 9.249(10), c = 5.581(6) Å] and structure refinement of L-serine-I coordinates yielded a conventional *R*-factor of 0.0412. This experiment aimed simply to establish the phase of serine after removal from the cell, and further data are not given here.

Refinements of the compressed form of L-serine-I were carried out starting from the published co-ordinates determined at ambient pressure. The structure of the new phase (L-serine-II) was solved by the global minimisation method using the program DASH (David *et al.*, 2001), and was refined as described above. Refinements were carried out against $|F|^2$ using all data (CRYSTALS, Betteridge *et al.*, 2004). Because of the low completeness of the data-sets, all 1,2 and 1,3 distances were restrained to the values observed in the ambient pressure structure, and all carbon, nitrogen and oxygen atoms were refined with isotropic displacement parameters.

Hydrogen atoms attached to carbon and nitrogen were placed geometrically and not refined. At ambient pressure Kistenmacher *et al.* (1974) showed that the hydroxyl hydrogen atom (H7) eclipses C3-H2 with r(OH) = 0.88 Å and <COH = 107°; we have confirmed these results. This feature is ascribable to formation of intermolecular OH...OH hydrogen bonds (see section *2.4 Results and Discussion*). In placing the hydroxyl H-atom (H7) in the structures between 0.3 and 4.8 GPa, we initially assumed that the ambient pressure conformation of the CH_2OH side chain was retained, and this atom was placed in an ideal position for OH...OH hydrogen bonding. However, the positional parameters of H7 were refined subject to the restraints r(O-H) = 0.88(1) Å and

< COH = 107(1)°, so enabling the HOCC torsion angle to optimize. In all except the 4.8 GPa data set the O3-H7 eclipsed C2-H2 as it does at ambient pressure. At 4.8 GPa O3-H7 appeared to adopt a staggered orientation with respect to the neighbouring CH_2 group; refinements in which it was restrained in an eclipsed position failed to converge. Of course, the standard uncertainties on the positional parameters of H7 are so large that difference between the two models are not statistically significant, but in the 4.8 GPa model presented here H7 is left in its refined position. A definitive statement regarding the position of H7 at 4.8 GPa is not possible from these data, but neutron diffraction experiments would clarify this issue. At 5.4 GPa H7 was observed in a difference map, but treated during refinement in the same way as at lower pressure. All distances and angles involving H quoted in this paper were calculated after normalizing the H-atom position to mimic those that might be obtained by neutron diffraction [r(C-H) = 1.083, r(N-H) = 1.009, r(O-H) = 0.983 Å].

Listings of crystal and refinement data are given in Table 2.1.

Crystal structures were visualized using the programs CAMERON (Watkin *et al.*, 1993) and MERCURY (Bruno *et al.*, 2002). Analyses were carried out using PLATON (Spek, 2004), as incorporated in the WIN-GX suite (Farrugia, 1999). Searches of the Cambridge Database (Allen, 2002; Allen & Motherwell, 2002) utilized the program CONQUEST and version 5.25 of the database with updates up to April 2004.

The numbering scheme used is the same as CSD refcode LSERIN01 (Kistenmacher *et al.* 1974) and is given in Scheme 2.1.

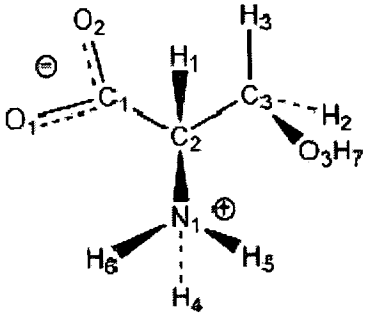

Scheme 2.1: Chemical structure diagram showing atomic numbering scheme.

In macromolecular structures our C2, C3 and O3 would be designated CA, CB and OG, respectively. The settings of the structures reported here are the same as used in LSERIN01; that used for the L-serine-II was chosen to facilitate comparison with L-serine-I.

Pressure / GPa	0.3	1.4	2.9
Formula	C3 H7 N1 O3	C3 H7 N1 O3	C3 H7 N1 O3
Weight	105.09	105.09	105.09
Radiation	Mo-Kα	Mo-Kα	Mo-Kα
Crystal system	Orthorhombic	Orthorhombic	Orthorhombic
Space Group	$P2_12_12_1$	$P2_12_12_1$	$P2_12_12_1$
a/Å	8.5213(13)	8.4365(10)	8.3702(10)
b/Å	9.172(2)	8.9506(19)	8.7699(19)
c/Å	5.5847(8)	5.5512(6)	5.5103(6)
Volume/Å^3	436.47(15)	419.18(11)	404.49(11)
No. reflections for cell	246	270	258
$2\theta_{max}$(°)	46	46	47
Z	4	4	4
*D*c (Mg/m^3)	1.599	1.665	1.726
μ (mm^{-1})	0.143	0.149	0.154
Reflections collected	1169	1006	1112
No. Unique [R_{int}]	151 [0.138]	146 [0.127]	134 [0.119]
No. $F>4\sigma(F)$	140	135	133
T_{min}/ T_{max}	0.695 , 1.000	0.552 , 1.000	0.711 , 1.000
Parameters	33	33	33
R_1 [$F>4\sigma(F)$]	0.0827	0.0733	0.0649
wR_2 (F^2, all data)	0.2137	0.1641	0.1536
S	1.0678	1.1438	1.0679
$\Delta\rho_{max}$ / eÅ^{-3}	0.30	0.37	0.26
$\Delta\rho_{min}$ / eÅ^{-3}	-0.23	-0.27	-0.24

(a)

Pressure / GPa	4.1	4.8	5.4
Formula	C3 H7 N1 O3	C3 H7 N1 O3	C3 H7 N1 O3
Weight	105.09	105.09	105.09
Radiation	Mo-Kα	Mo-Kα	Mo-Kα
Crystal system	Orthorhombic	Orthorhombic	Orthorhombic
Space Group	$P2_12_12_1$	$P2_12_12_1$	$P2_12_12_1$
a/Å	8.3266(13)	8.2980(16)	6.9083(10)
b/Å	8.665(3)	8.600(3)	9.644(3)
c/Å	5.4851(8)	5.4663(10)	5.6166(8)
Volume/Å^3	395.75(15)	390.09(17)	374.19(14)
No. reflections for cell	258	247	313
$2\theta_{max}$(°)	47	44	46
Z	4	4	4
*D*c (Mg/m^3)	1.764	1.789	1.865
μ (mm^{-1})	0.158	0.160	0.167
Reflections collected	1112	1068	1990
No. Unique [R_{int}]	130 [0.080]	129 [0.083]	140 [0.081]
No. $F>4u(F)$	129	128	122
T_{min}/ T_{max}	0.721 , 1.000	0.739 , 1.000	0.666 , 1.000
Parameters	32	33	32
R_1 [$F>4u(F)$]	0.0664	0.0603	0.0562
wR_2 (F^2, all data)	0.1648	0.1219	0.1185
S	1.0635	1.1552	1.1479
$\Delta\rho_{max}$ / eÅ^{-3})	0.25	0.19	0.21
$\Delta\rho_{min}$ / eÅ^{-3}	-0.20	-0.21	-0.18

(b)

Table 2.1: Crystallographic data for L-serine at increasing pressures (a) 0.3 to 2.9 GPa and (b) 4.1 to 5.4 GPa.

2.4 *Results and Discussion*

2.4.1 *The structure of L-serine-I at ambient pressure*

Prior to this work there was only one known crystalline form of anhydrous L-serine, and this crystallizes with one molecule in the asymmetric unit in space group $P2_12_12_1$. We refer to this form as L-serine-I. The structure was determined using X-ray diffraction by Beneditte *et al.* (1972) and then later by Kistenmacher *et al.* (1974). The serine molecule is in its zwitterionic form (see Scheme 2.1), with the CH_2OH side-chain in the *gauche* conformation with respect to the ammonium and carboxyl groups (χ_1 = 61.5°). This conformation is observed under all conditions investigated during this work.

The structure of L-serine-I is dominated by hydrogen bonding (Figures 2.1*a*-2.3*a* show projections of the structure along **a, b** and **c**, respectively). Many amino acid crystal structures have one cell dimension of near 5.5 Å, and this is associated with a head-to-tail chain motif formed by NH...OOC interactions. This is observed in L-serine-I, where the molecules form a chain *via* lattice repeats along the crystallographic *c*-direction through three-centre N1H5...O1/2 interactions (Figure 2.1*a*). Jeffrey and Maluszynska (1982) have shown that such interactions can take on varying degrees of asymmetry, and the one observed here is relatively symmetrical, with distances of 1.91 Å (H5...O2) and 2.29 Å (H5...O1). If the weaker hydrogen bond is ignored, the graph-set descriptor of this chain is $C(5)$ (Bernstein *et al.*, 1995).

A second $C(5)$ chain, generated by the 2_1 about **c**, is linked to the first via N1H6...O1 hydrogen bonds [N1...O1 = 2.840(4) Å)] to form a ribbon. The N1H6...O1 interactions also generate primary level $C(5)$ chains along the ribbon. Along the length of the ribbon the combination of the two $C(5)$ chains forms secondary-level $R^3_3(11)$ ring motifs. The CH_2OH side chains are distributed along the outside edges of the ribbons, and these interact via $C(2)$ ...O3H7...O3H7 hydrogen bonds to link the ribbons into layers. The hydrogen bonds between the hydroxyl groups are quite weak, with O3...O3 measuring 2.918(4) Å under ambient conditions. The combination of the $C(2)$ and $C(5)$ N1H5...O2 chains generates secondary-level $R^3_3(13)$ ring motifs (Figure 2.1*a*).

The layers are stacked along **a**, having a sinusoidal appearance when viewed in projection onto (001) (Figure 2.3*a*). The layers are linked by N1H4...O2 interactions which form yet another primary level $C(5)$ chain which runs along **a** (Figure 2.2*a*). The intersection of the N1H5...O2 and N1H4...O2 $C(5)$ chains along **a** and **c** builds a third set of secondary level ring motifs, these having the descriptor $R^3_4(14)$.

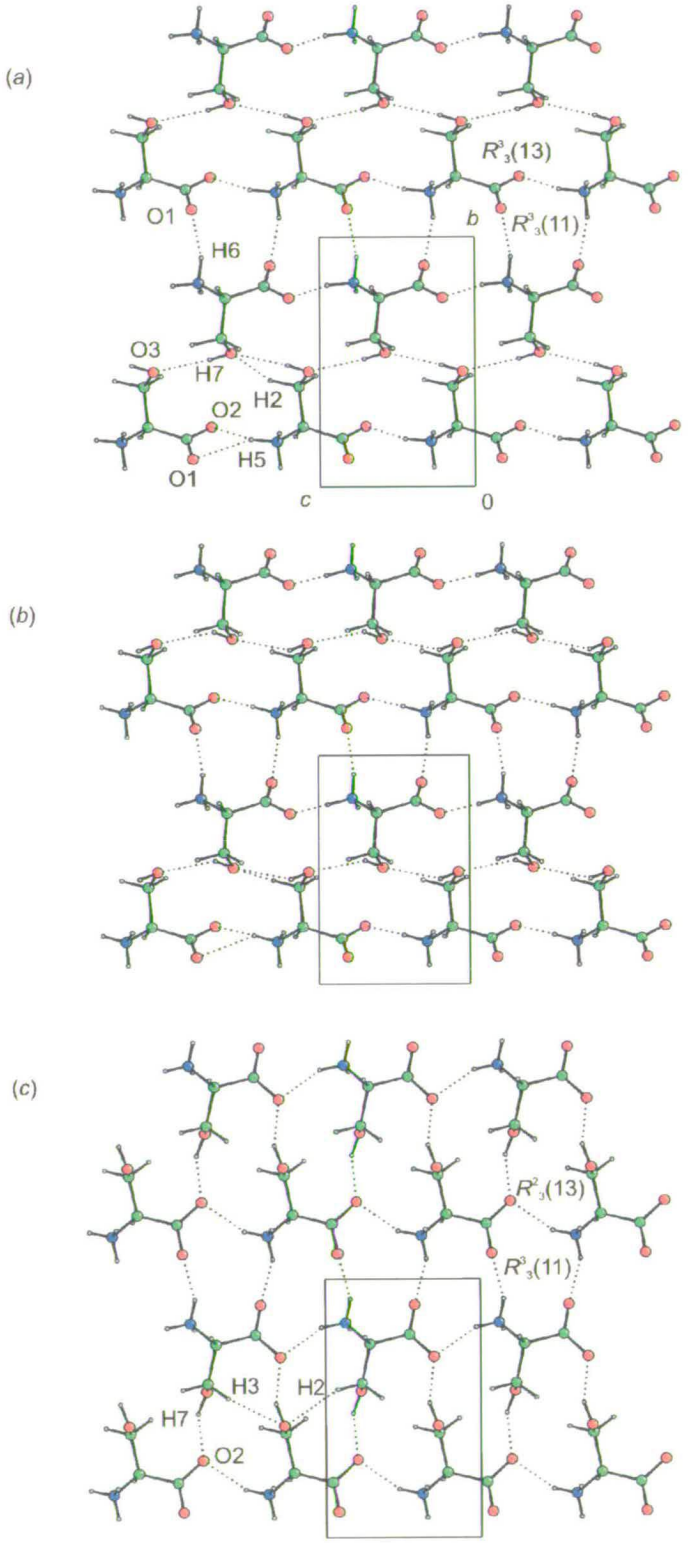

Figure 2.1: Effect of pressure on the crystal structure of L-serine as viewed along **a**: (*a*) L-serine-I at ambient pressure; (*b*) L-serine-I at 4.8 GPa; (*c*) L-serine-II at 5.4 GPa. This layer is referred to as the *A-layer* in the text. The colour scheme is red: oxygen, blue: nitrogen, green: carbon and white: hydrogen. The orientations of all diagrams are the same; the scale is the same as that used in Figures 2.2 and 2.3. The bifurcation of the N1H5…O1/2 and CH…O bonding are shown only in the bottom left fragment of the diagram.

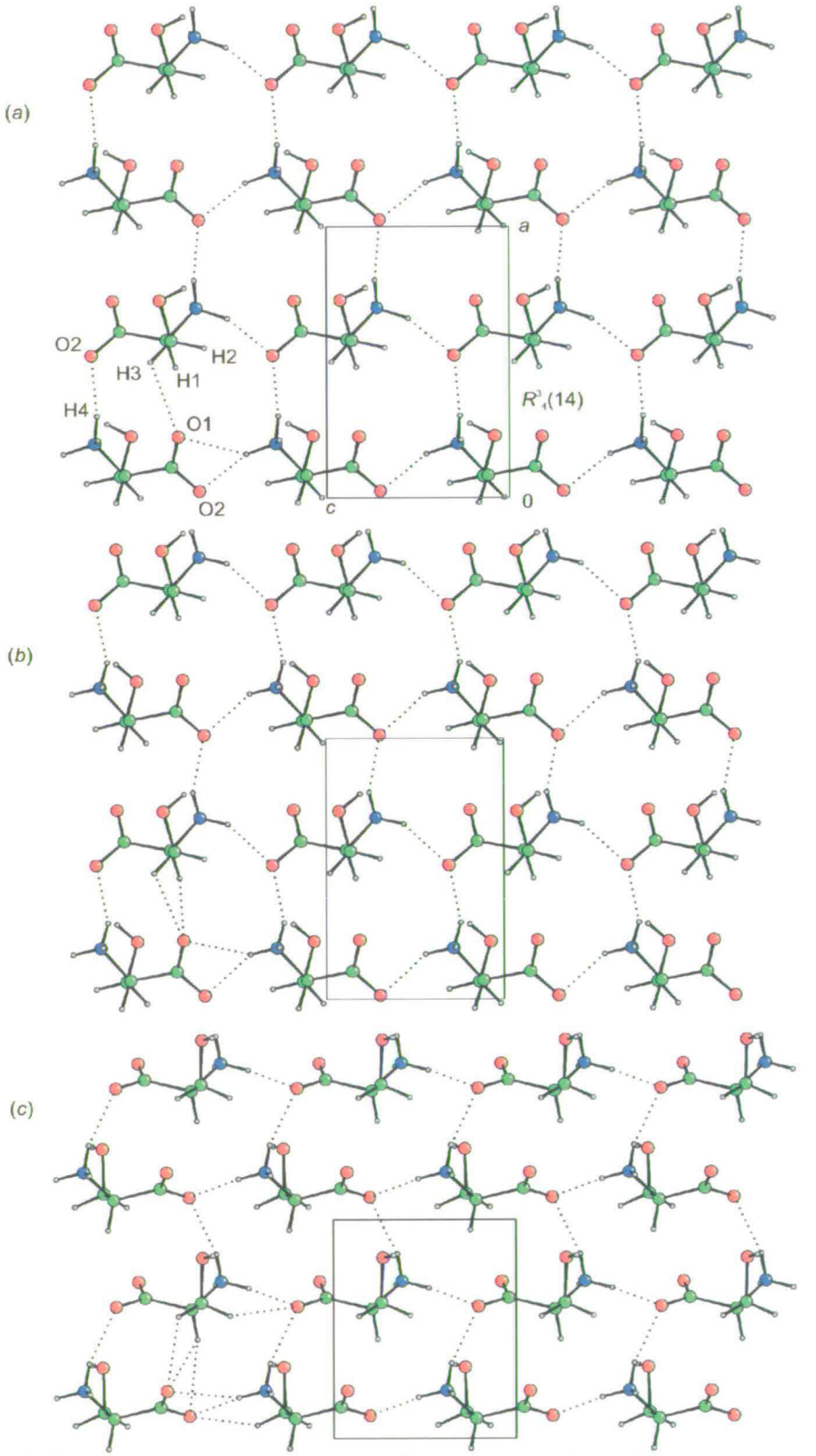

Figure 2.2: Effect of pressure on the crystal structure of L-serine as viewed along **b**: (*a*) L-serine-I at ambient pressure; (*b*) L-serine-I at 4.8 GPa; (*c*) L-serine-II at 5.4 GPa. This layer is referred to as the *B-layer* in the text. The orientations of all diagrams are the same; the scale is the same as that used in Figures 2.1 and 2.3. The bifurcation of the N1H5…O1/2 and CH…O bonding are shown only in the bottom left fragment of the diagram. The colour scheme is as in Figure 2.1.

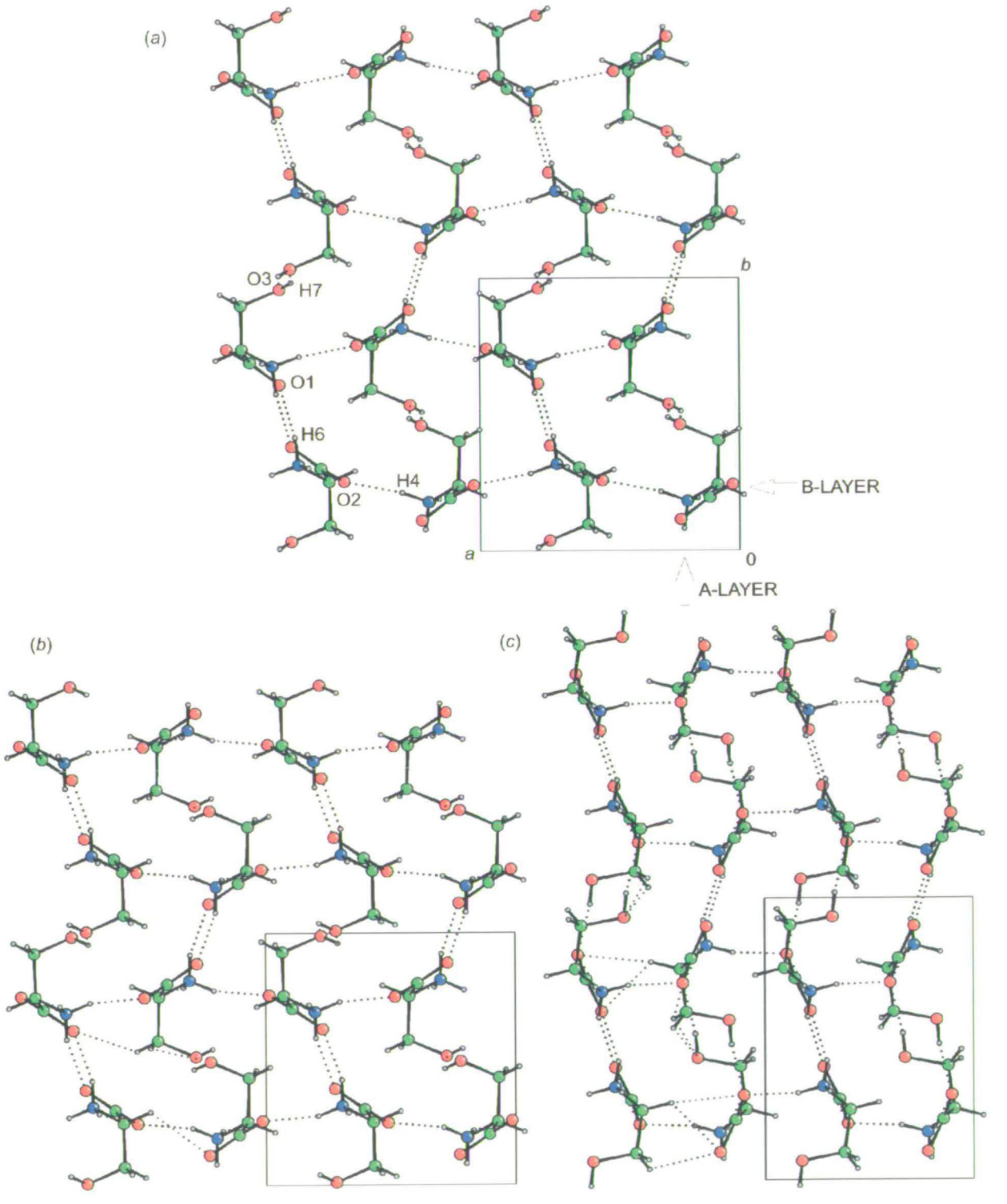

Figure 2.3: Effect of pressure on the crystal structure of L-serine as viewed along **c**: (*a*) L-serine-I at ambient pressure; (*b*) L-serine-I at 4.8 GPa; (*c*) L-serine-II at 5.4 GPa. The A-layers run vertically, the B-layers horizontally. The orientations of all diagrams are the same; the scale is the same as that used in Figures 2.1 and 2.2. The CH…O bonding is shown only in the bottom left fragment of the diagram. The colour scheme is as in Figure 2.1.

The N1H5...O2 and N1H4...O2 interactions actually build another layer which is parallel to the *ac* plane (Figure 2.2*a*). Overall then, the structure consists of two sets of layers: one stacks along *a* and contains $R^3_3(11)$ and $R^3_3(13)$ ring motifs, the other is more planar, stacks along *b*, and contains $R^3_4(14)$ rings. We shall refer to these as the A and B layers, respectively. The N1H4...O2 interactions which occur *within* the B-layers can also be viewed as interactions *between* the A-layers; similarly the N1H6...O1 and O3H7...O3H7 interactions within the A-layers serve to link the B-layers (Figure 2.3*a*). The N1H5...O2 hydrogen bonds are common to both layers.

Plots of the cell dimensions and volume of L-serine as a function of pressure are given in Figure 2.4. L-serine-I is stable to 4.8 GPa (48 kbar). Above this pressure it undergoes a single-crystal to single-crystal phase transition to a new phase, which we designate L-serine-II. We prefer this I-, II-... phase nomenclature to the α-, β-... nomenclature for amino acids, even though the polymorphs of glycine are denoted α, β, γ... because the symbols α and β are used for other purposes in amino acid chemistry.

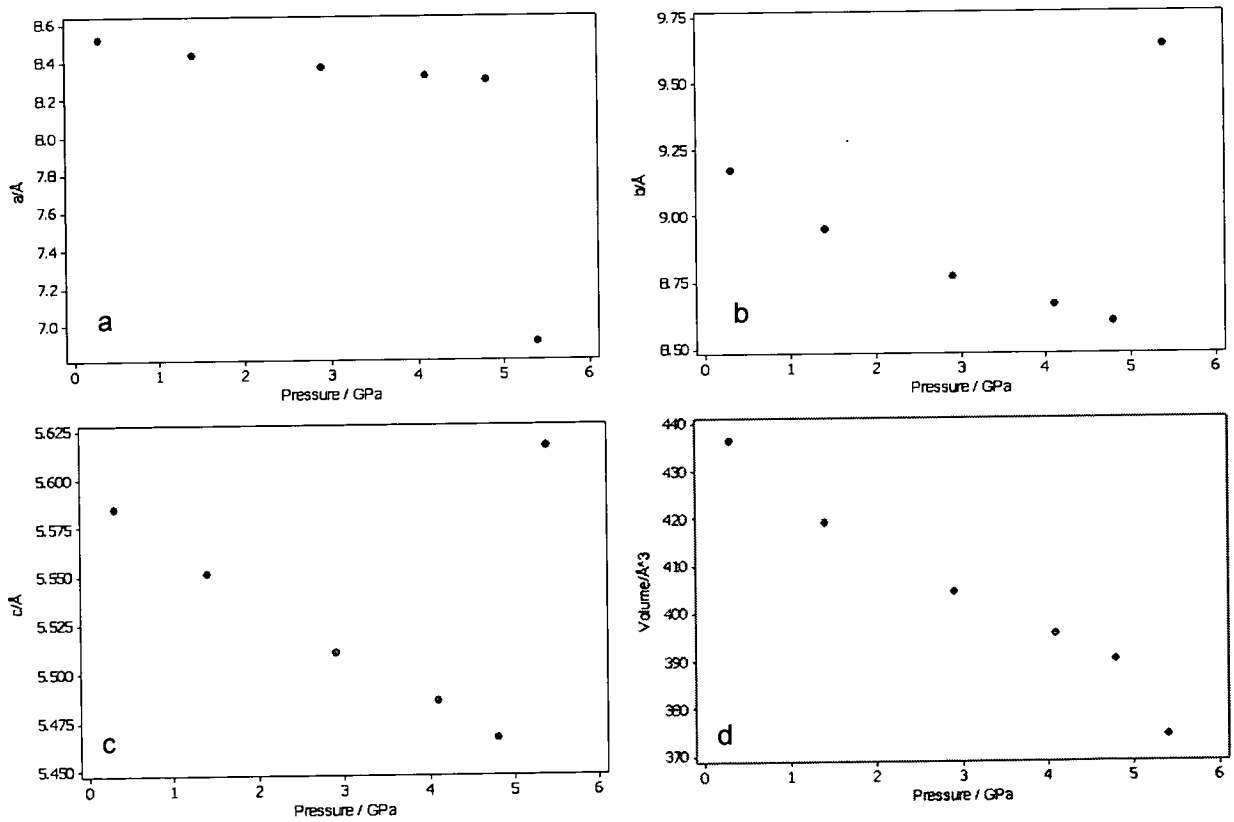

Figure 2.4: Variation of the lattice parameters (*a*- c, Å) and volume (*d*, Å^3) of L-serine as a function of pressure (GPa).

2.4.2 The response of L-serine-I to pressure up to 4.8 GPa

The response of the unit cell dimensions of L-serine-I to high pressure is anisotropic (Figure 2.4), though, since the crystal system is orthorhombic, the principal axes of the strain tensor must be coincident with the crystallographic axes. The largest reduction occurs in the *b*-axis (6.2%), while the *a*- and *c*-axes change by 2.6 and 2.1%, respectively. The volume changes most rapidly between 0.2 and 2.9 GPa, and then the trend flattens-off up to 4.8 GPa; above 4.8 GPa all three axis lengths change suddenly during the transition to L-serine-II. Figure 2.5 shows the superposition of the structures of L-serine-I at ambient pressure at 4.8 GPa where the molecules are represented by their inertial tensors. The orientations of the molecules change slightly, but the large compression along **b** is readily apparent.

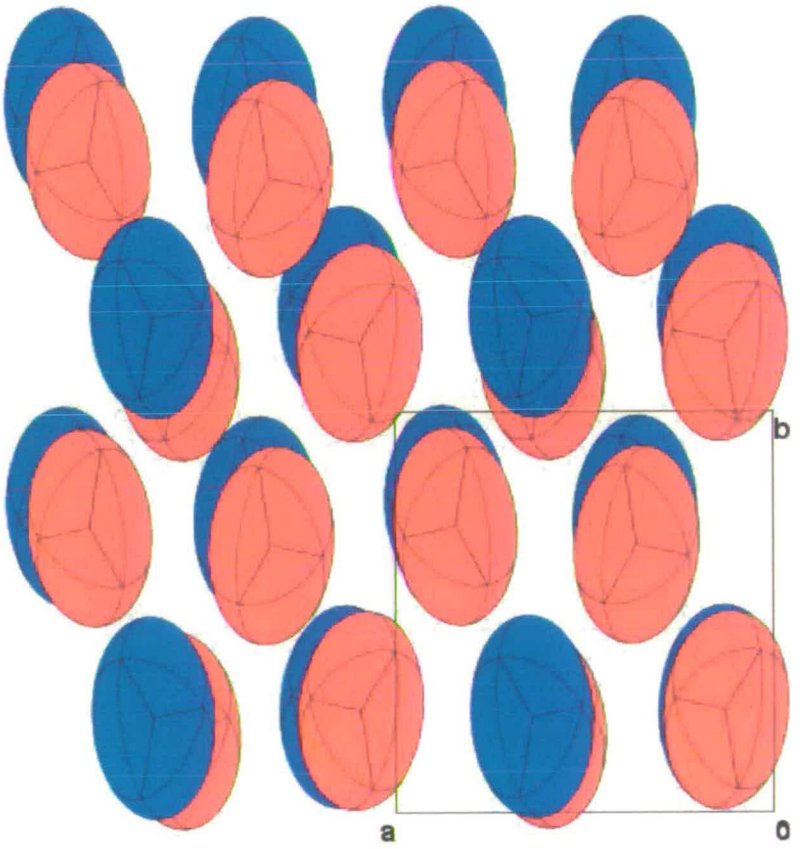

Figure 2.5: Comparison of packing in the structures of L-serine-I at ambient pressure (blue) and 4.8 GPa (red). Molecules are represented by their inertial tensor ellipsoids. The unit cell shown corresponds to the ambient pressure phase. Note that the molecules do not greatly change orientation.

The variation of hydrogen bonding parameters in L-serine-I between 0.3 and 4.8 GPa is presented in Table 2.2. The N1H4...O2 shortens from N...O = 2.887(4) Å at ambient pressure to 2.691(13) Å at 4.8 GPa (Figure 2.2*b*). A search of the Cambridge Database reveals that there are only three amino acid structures (out of 213) in which NH...O interactions are shorter than this, the shortest, 2.661 Å, being observed in L-arginine D-glutamate trihydrate (DUSMAF, Suresh *et al.*, 1986). The shortening of this distance occurs quite smoothly between 0.3 and 4.8 GPa. N1H6...O1 is formed approximately along the b^*-axis (Figure 2.1*b*), and reflection data along this direction of reciprocal space were severely shaded by the pressure cell. This distance is therefore not very precisely determined in the present study, but it, too, shortens from 2.840(4) to 2.72(3) Å.

The least compressible interaction is the head-to-tail, bifurcated, N1H5...O1/2 chain-forming interaction along **c**. The length of the shorter of the two O...O interactions which constitute the three-centre hydrogen bond along this direction decreases from O...O = 2.871(3) Å to 2.775(13) Å between ambient pressure and 4.8 GPa. The longer bond in this bifurcated motif decreases 3.118(3) to 2.981(12) Å, which corresponds to an enhancement of the bifurcated character of this hydrogen bond. The crystal structure of α-glycine also contains head-to-tail chains of molecules, and, in that structure as well, an increase in bifurcation is also observed with pressure (Dawson *et al.*, 2004*b*). The crystallographic direction parallel to this chain in α-glycine is the least compressible in the system (Boldyreva *et al.*, 2003), as it is here.

Pressure/GPa	0	0.3	1.4	2.9	4.1	4.8
N1H5..O2[iv]						
H5..O2	1.91	1.94	1.89	1.86	1.86	1.86
N1..O2	2.871(3)	2.862(15)	2.814(14)	2.786(12)	2.775(12)	2.775(13)
<N1H5O2	158(2)	153	152	153	150	150
N1H5..O1[iv]						
H5..O1	2.29	2.30	2.28	2.24	2.22	2.19
N1..O1	3.118(3)	3.106(15)	3.070(14)	3.028(11)	3.010(12)	2.981(12)
<N1H5O1	139(2)	138	136	136	136	136
N1H4..O2[i]						
H4..O2	1.90	1.89	1.86	1.82	1.80	1.78
N1..O2	2.887(4)	2.825(16)	2.796(15)	2.751(12)	2.709(13)	2.691(13)
<N1H4O2	167(2)	153	153	153	150	149
N1H6..O1[v]						
H6..O1	1.87	1.86	1.81	1.80	1.79	1.76
N1..O1	2.840(4)	2.81(3)	2.76(3)	2.75(2)	2.75(3)	2.72(3)
<N1H6O1	162(2)	158	157	157	159	158
O3H7..O3[iii]						
H7..O3	2.02	1.98	1.98	2.00	1.92	2.08
O3..O3	2.918(4)	2.882(16)	2.842(14)	2.807(12)	2.790(12)	2.781(11)
<O3H7O3	153(3)	153(14)	147(7)	139(6)	147(6)	129(7)
<O3..O3..O3	148.5(2)	151.2(14)	155.4(12)	158.1(8)	158.9(7)	158.5(7)
C2H1..O1[ii]						
H1..O1	2.75	2.67	2.56	2.48	2.45	2.44
C2..O1	3.368(4)	3.307(16)	3.222(15)	3.153(13)	3.113(13)	3.106(13)
<C2H1O1	118.3(13)	118	120	121	120	120
C3H2..O3[iii]						
H2..O1	2.56	2.57	2.54	2.51	2.50	2.48
C3..O1	3.214(4)	3.182(17)	3.147(16)	3.099(14)	3.076(13)	3.062(13)
<C3H2O3	117.6(12)	116	116	115	114	114
C3H3..O1[ii]						
H2..O1	2.55	2.48	2.46	2.44	2.43	2.42
C3..O1	3.053(4)	3.005(14)	2.942(13)	2.905(11)	2.876(11)	2.871(11)
<C3H3O1	109.4(18)	110	107	107	105	105

Symmetry Operators

i	1/2+x,1/2-y,-z
ii	-1/2+x,1/2-y,-z
iii	1/2-x,1-y,1/2+z
iv	x,y,1+z
v	1/2-x,-y,1/2+z

Table 2.2: Hydrogen bonding parameters in L-serine-I. Distances to hydrogen have been normalized to neutron values (see *Experimental*). Distances are in Å, and angles in °.

The hydrogen bonds in the OH...OH...OH chain formed by the side-groups of the serine molecules are longer those formed between the ammonium and carboxylate groups, and the O...O distances measure 2.918(4) Å at ambient pressure. These interactions also decrease in length to 2.781(11) Å. Brock and Duncan (1994) quote a range of 2.55 – 3.05 Å for the O...O distances in this type of interaction at ambient pressure, with an average of 2.79(1) Å. The angles subtended at O3 in these chains increases from 148.5(2)° at ambient pressure to 158.5(7)° at 4.8 GPa.

We have recently described the crystal structure of α-glycine at 6.2 GPa (Dawson *et al.*, 2004*b*). The structure consists of a stack of hydrogen-bonded bi-layers which interact via CH...O hydrogen bonds. Within the layers sets of $C(5)$ chains intersect to form $R^4_4(16)$ ring motifs. The effect of pressure was described in terms of the closing-up of holes in the middle of the $R^4_4(16)$ rings, and the formation or shortening of CH...O hydrogen bonds both across the $R^4_4(16)$ rings and between the bilayers. It is interesting to investigate whether similar features can be observed in the compression of L-serine-I.

Inspection of space-filling plots (Figure 2.6*a-f*) shows that there are holes in the centres of each of the $R^3_3(11)$, $R^3_3(13)$ and $R^3_4(14)$ ring motifs formed in L-serine-I. The shortening of the NH...O hydrogen bonds (even N1H4...O2, which became very short) is not enough to close-up the holes in the middle of the $R^3_3(11)$ and $R^3_4(14)$ rings, which occur in the A and B layers, respectively. Closure of the hole in the centre of the $R^3_3(13)$ ring does occur though, and as this occurs along the *b*-axis direction, this may explain the greater compressibility in this direction compared with *a* and *c*. The closure occurs not only by a shortening of the O3...O3 distance from 2.918(4) to 2.781(11) Å, but also an increase in the O3...O3...O3 angles made along the chains of hydroxyl groups from 148.5(2)° to 158.5(7)° (the angle made by the vector between the central O3 and the mid-point of the two flanking O3s and [0 1 0] is 15.4°; Figure 2.1*b*). As these appear to be comparatively weak hydrogen bonds this is presumably a rather 'soft' parameter, which deforms easily under pressure.

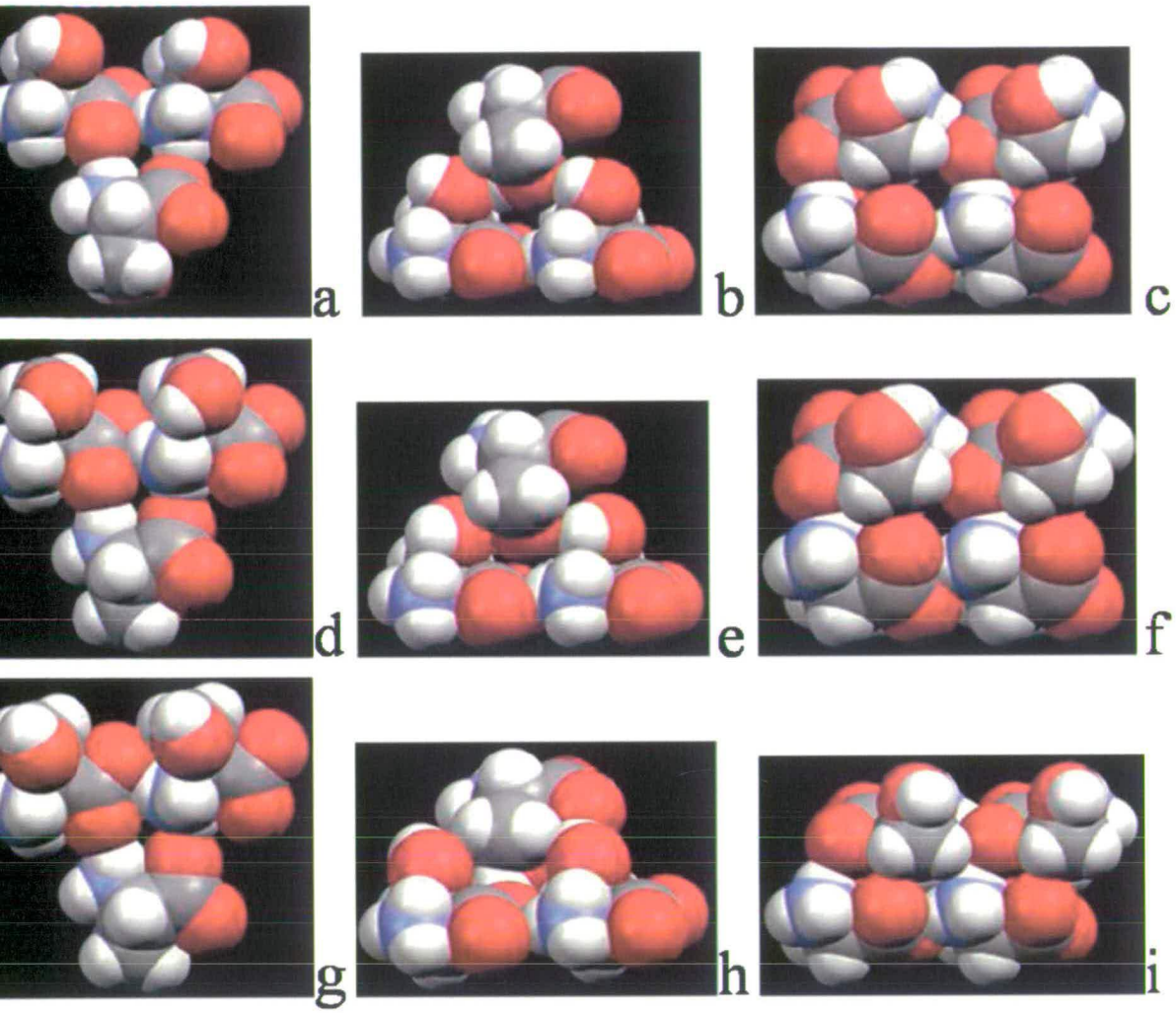

gure 2.6: Space-filling plots showing *R*-type graph sets which occur in L-serine phases I d II as a function of pressure. The top middle and bottom rows correspond the L-serine-I at nbient pressure, L-serine-I at 4.8 GPa and L-serine-II at 5.4 GPa, respectively. On the left the diagram (*a*), (*d*) and (*g*) are all $R^3_3(11)$ motifs which occur in the A-layers (*cf.* Figure 1); the hole in this small ring does not become very much smaller with increasing pressure. the middle column of the diagram (*b*) and (*e*) show $R^3_3(13)$ motifs, which also occur in the -layers (*cf.* Figure 2.1). Note that the hole in the middle of the ring is significantly smaller 4.8 GPa than at ambient pressure. At 5.4 GPa (*h*) this has been converted into a $R^2_3(13)$ otif after the phase transition from form-I to form-II. On the right of the figure (*c*), (*f*) and show the $R^3_4(14)$ rings. Although the hole in the middle of this ring does not close-up in rm-I between ambient (*c*) and 4.8 GPa (*f*), in L-serine-II at 5.4 GPa (*i*) the hole has been osed up.

CH...O interactions occur frequently in the structures of amino acids and in proteins (Desiraju & Steiner, 1999). A survey of amino acid crystal structures determined by neutron diffraction showed that the most common H...O distances are around 2.4 Å, with a minimum of 2.15 Å (Jeffrey & Maluszynska, 1982). Generally, it is the hydrogen atom attached to the α-carbon atom which is involved in this type of interaction, as this is activated by the neighbouring ammonium and carboxylate groups (Derewenda *et al.*, 1995; Desiraju & Steiner, 1999); the hydrogen atoms of side chains are involved less frequently. L-serine under ambient conditions does not conform to this general trend, and under ambient conditions the strongest CH...O interactions are formed by the CH_2 group to the oxygen atoms of neighbouring hydroxyl and carboxylate groups at normalized distances of 2.55 and 2.56 Å for C3H3...O1 and C3H2...O3, respectively. The shortest CH...O contact made by the αH-atom is 2.75 Å at ambient pressure. CH...O hydrogen bonding from the $C_\alpha H$ group becomes more significant at high pressure, and the normalized C2H1...O1 distance becomes 2.44 Å at 4.8 GPa. Most of the shortening in this interaction occurs between 0.3 and 2.9 GPa. The C3H3...O1 interaction shortens to 2.42 Å, and together these interactions form a pair of contacts to the same O1 atom across the $R^3_4(14)$ rings in the B-layers. These CH...O interactions can also be considered to support the N1H4...O1 interactions formed between the A-layers.

So, while compression of α-glycine was characterized by the closing up of voids in *R* motifs with concomitant shortening of weak CH...O hydrogen bonds, that in L-serine-I is associated with deformation and shortening of rather weak OH...OH hydrogen bonds. Though different interactions are involved in the two amino acids, both might be considered easily deformable. The formation of CH...O hydrogen bonds between the layers in the α-glycine structure is paralleled in L-serine-I by CH...O bond formation between the A-layers (Figure 2.3*b*).

One interesting conclusion of the, admittedly limited, research that has been carried out on hydrogen bonded molecular systems is that super-short hydrogen bonds are not formed by application of pressures below about 10 GPa. The lower distance limits for such interactions which apply at ambient pressure also seem to apply at high pressure. In serine at 4.8 GPa at least one N...O distance (N1H4...O2) approaches the lower limit for this kind of interaction observed in the Cambridge Database. Above this pressure a phase change occurs to a hitherto uncharacterized phase, L-serine-II.

2.4.3 *L-Serine-II at 5.4 GPa.*

The transition from L-serine-I to L-serine-II occurs with a marked reduction in the volume of the unit cell (Figure 2.4). The volume per non-hydrogen atom is only 13.4 Å^3. Remarkably, the transition proceeds from one single crystal of L-serine-I to a single crystal of L-serine-II, and this is fully reversible.

The observation that this transition occurs from one single crystal to another strongly implies that the overall topologies of phases I and II are similar to each other. This proves to be the case, and the structure also consists of two sets of layers which are stacked along the *a*- and *b*-directions (Figures 2.1*c* and 2.2*c*; hydrogen bonding information is presented in Table 2.3). In terms of hydrogen bonds formed, the structure of the B-layers is the same as in L-serine-I. Chains are formed by lattice repeats along **c** in which the molecules interact via three-centre N1H5...O1/2 bonds. In a reversal of the trend established during the compression of L-serine-I, these bonds are less symmetrical than the equivalent ones in L-serine-I at 4.8 GPa.

	H..A	D..A	<D-H..A
N1H5..O2^{iv}	1.86	2.810(14)	155
N1H5..O1^{iv}	2.30	3.145(11)	141
N1H4..O2^{ii}	1.89	2.850(10)	159
N1H6..O1^{i}	1.76	2.64(2)	143
O3H7..O2^{v}	1.71	2.62(2)	152
C2H1..O1^{iii}	2.50	3.059(13)	111
C2H1..O2^{iii}	2.37	3.411(10)	162
C3H2..O2^{iv}	2.40	3.149(13)	125
C3H2..O3^{v}	2.45	3.276(15)	132
C3H3..O3^{vi}	2.37	3.207(15)	133
C3H3..O1^{iii}	2.42	2.982(10)	111

Symmetry operators:

i	1/2+x,1/2-y,-z
ii	-1/2+x,1/2-y,-z
iii	1/2-x,1-y,1/2+z
iv	x,y,1+z
v	1/2-x,-y,1/2+z
vi	1/2-x,1-y,-1/2+z

Table 2.3: Table of H-bonding parameters for L-serine-II at 5.4 GPa. H-atom coordinates have been normalized to neutron values. Distances are in Å, angles in °.

Neighbouring chains are linked into a B-layer by N1H4...O2 hydrogen bonds, to build $R^3_4(14)$ motifs (Figure 2.2*c*). These are completely analogous to those in the B-layers of L-serine-I, but the rings in L-serine-II are longer and thinner (compare Figures 2.2*a-c*). This change occurs by (*i*) opposite displacements of the molecules in successive N1H5...O2 chains along the *c*-direction, (*i.e.* the chains slide across each other), and (*ii*) compression of the distance between the chains along the *a*-direction. This enables compression of the $R^3_4(14)$ rings without further shortening the N1H4...O1 hydrogen bond. Inspection of space-filling plots shows that this closes up the voids which occur in the centre of the $R^3_4(14)$ rings in L-serine-I even at 4.8 GPa (compare Figures 2.6*c*, *f* and *i*). The dimensions of the ring are equal to *a*/2 and *c*, and so this effect is reflected in the lengths of the *a* and *c* unit cell axes, the former sharply decreasing and the latter increasing slightly relative to L-serine-I.

As in L-serine-I, the structure of the A-layers consists of ribbons in which $C(5)$ chains formed by N1H5...O2 hydrogen bonds are linked by N1H6...O1 hydrogen bonds (Figure 2.1*c*). The N1...O1 distances $R^3_3(11)$ rings so-formed appear to be somewhat shorter than in L-serine-I at 4.8 GPa, though the standard uncertainties are high. There is a substantial change in the way the ribbons are connected into a layer. In L-serine-I this was achieved through OH...OH interactions, but in L-serine-II these are replaced by much stronger O3H7...O2 hydroxyl to carboxylate hydrogen bonds. This generates $R^2_3(13)$ motifs which replace the $R^3_3(13)$ motifs. The hydroxyl hydrogen atom, H7, was located in a difference Fourier map, and is clearly attached primarily to O3. Its position was also optimized in a plane-wave DFT calculation, with results consistent with those implied by the difference map (details of these calculations will be described in another publication). The length of the new hydrogen bond is very short, with an O3...O2 distance of 2.62(2) Å, though the (normalized) H7...O2 distance 1.71 Å. In order to accommodate this interaction the N1-C2-C1-O2 torsion angle changes from -178.1(2)° at 4.8 GPa to -156.3(10)° at 5.4 GPa. The orientation of the O3H7 group changes from being *gauche* to *anti* with respect to C2-C3. This movement of the hydrogen atom implies that the $C(5)$ chains which run along **c** must move apart slightly, with the result that the *b*-axis is actually *ca* 0.5 Å longer in L-serine-II than in L-serine-I.

The formation of L-serine-II is also characterized by a marked increase in CH...O hydrogen bonding, with each H-atom making two interactions. These occur within the A-layers between the CH_2 groups and the hydroxyl and carboxylate groups of neighbouring molecules involved in the new $R^2_3(13)$ ring motifs. In the B-layers they are formed across the

$R^3_4(14)$ rings in the direction of the *a*-axis; they can therefore be considered to stabilize the compression of these rings.

2.5 *Conclusions*

We have described the effect of high pressure on the crystal structure of L-serine. The structure can be considered to consist of two sets of layers, which stack along the *a* and *b* axes of the unit cell, and which have been referred to above as the A and B layers. The A-layers contain NH...O and OH...OH interactions which combine to give $R^3_3(11)$ and $R^3_3(13)$ ring motifs; NH...O interactions in the B-layers form $R^3_4(14)$. The $R^3_4(14)$ motifs *within* the B-layers can also be viewed as connections *between* the A-layers. This structure remains stable up to 4.8 GPa. It undergoes anisotropic compression in which the principal structural effect is to compress voids in the middle of the $R^3_3(13)$ rings of the A-layers by deforming the rather 'soft' hydrogen-bonded hydroxyl chains. The stacking distance between the A-layers also decreased, with a shortening of NH...O hydrogen bonds supported by the formation of CH...O hydrogen bonds. This latter effect continued until, at 4.8 GPa, the length of the NH...O hydrogen bonds approached the minimum value observed for this kind of interaction. Above 4.8 GPa a single crystal to single crystal phase change to L-serine-II occurs.

The phase change from L-serine-I to L-serine-II is accomplished by the change in two torsion angles and small positional displacements, and there are no major changes in the orientations of the molecules. The observation that the transformation occurs from one single crystalline form to another is therefore readily understood. In the new phase the hydrogen bonded links in the A-layers between OH...OH groups are replaced by stronger, shorter OH...carboxyl interactions. The layers also move closer together by closing-up voids which occur in the centres of the $R^3_4(14)$ rings. All three hydrogen atoms which are attached to carbon take part in two CH...O interactions. The *b* and *c* axes are longer in L-serine-II than in L-serine-I, but the *a* axis is substantially shorter, and the overall effect is a reduction in the volume of the unit cell. This reduction is ascribable to the closing-up of the voids in the $R^3_4(14)$ rings.

In L-serine high pressure closes up voids which occur in *R*-motifs and decreases the interactions between layers by CH...O hydrogen bond formation. Similar comments apply to the behaviour of glycine under pressure. We are currently investigating the effect of pressure on other α-amino acids, and it will be interesting to discover to what extent these same effects apply in those systems.

2.6 References

Allan, D. R. & Clark, S. J. (1999). *Phys. Rev. B*, **60**, 6328-6334.

Allan, D. R., Clark, S. J., Brugmans, M. J. P., Ackland, G. J. & Vos, W. L. (1998). *Phys. Rev. B*, **58**, R11809-R11812.

Allan, D.R., Clark, S.J., Dawson, A., McGregor, P.A. & Parsons, S. (2002). *Acta Cryst. B***58**, 1018-1024.

Allan, D.R., Clark, S.J., Ibberson, R.M., Parsons, S., Pulham, C.R. & Sawyer, L. (1999). *Chem. Comm.*, 751-752.

Allan, D.R., Clark, S.J., Parsons, S. & Ruf, M. (2000). *J. Phys.: Condensed Matter*, **12**, L613-L620.

Allan, D.R., Parsons, S. & Teat, S.J. (2001). *J. Synchrotron Rad.*, **8**, 10-17.

Allen, F.H. (2002). *Acta Cryst. B***58**, 380-388.

Allen, F. H. & Motherwell, W. D. S. (2002). *Acta Cryst. B***58**, 407-422.

Benedetti, E., Pedone, C. & Sirigu, A. (1972). *Cryst. Struct. Commun.*, **1**, 35-37.

Bernstein, J., Davis, R.E., Shimoni, L. & Chang, N-L. (1995). *Angew. Chem. Int. Ed. Engl.*, **34**, 1555-1573.

Betteridge, P.W., Carruthers, J.R., Cooper, R.I., Prout, K. & Watkin, D.J. (2003). *J. Appl. Cryst.*, **36**, 1487.

Boldyreva, E.V. (2003). *J. Mol. Struct.*, **647**, 159-179.

Boldyreva, E.V. (2004*a*). *J. Mol. Struct.*, **700**, 151-155.

Boldyreva, E.V. (2004*b*). *Crystal Engineering*, **6**, 235-254.

Boldyreva, E.V. (2004*c*). NATO Science Series, II: Mathematics, Physics and Chemistry, **140**, 495-512. Ed. A. Katrusiak & P.F. McMillan, Kluwer, Dordrecht, 2004.

Boldyreva, E.V., Ahsbahs, H. & Weber, H.-P. (2003). *Z. Krist.*, **218**, 231-236.

Boldyreva, E.V., Ivashevskaya, S.N., Sowa, H., Ahsbahs, H. & Weber, H.-P. (2004). *Doklady Phys. Chem.*, **396**, 358-361.

Boldyreva E. V., Naumov D.Yu. & Ahsbahs H. (1998). *Acta Cryst.*, *B***54**, 798-808.

Boldyreva, E.V., Shakhtshneider, T.P., Vasilchenko, M.A., Ahsbahs, H. & Uchtmann, H. (2000). *Acta Cryst. B***56**, 299-309.

Brock, C. P. & Duncan, L. L. (1994). *Chem. Mater.* **6**, 1307-1312

Bruker-AXS (2003). SAINT version 7. Bruker-AXS, Madison, Wisconsin, USA.

Bruno, I.J., Cole, J.C., Edgington, P.R., Kessler, M., Macrae, C.F., McCabe, P. Pearson, J. & Taylor, R. (2002). *Acta Cryst. B***58**, 389-397.

David, W. I. F., Shankland, K., Cole, J., Maginn, S., Motherwell, W. D. S. & Taylor, R. (2001). *DASH User's Manual.* Cambridge Crystallographic Data Centre, Cambridge, UK.

Dawson, A., Allan, D.R., Clark, S.J., Parsons, S. & Ruf, M. (2004*a*). *J. Appl. Cryst.*, **37**, 410-416

Dawson, A., Allan, D.R., Belmonte, S.A., Clark, S.J., David, W.I.F., McGregor, P.A., Parsons, S., Pulham, C.R. & Sawyer, L. (2004*b*). *Submitted for publication, Cryst. Growth Des.*.

Derewenda, Z.S., Lee, L. & Derewenda, U. (1995). *J. Mol. Biol.*, **252**, 248-262.

Desiraju, G.R. & Steiner, T. (1999). *The Weak Hydrogen Bond.* IUCr Monographs on Crystallography No. 9. Oxford University Press, Oxford, UK.

Farrugia, L. J. (1999). *J. Appl. Cryst.* **32**, 837-838.

Hemley, R.J. & Dera, P. (2000). *Rev. Mineral. Geochem.*, **41**, 335-419.

Jeffrey, G.A. & Maluszynska, H. (1982). *Int. J. Biol. Macromol.*, **4**, 173-185.

Katrusiak, A. (2004). NATO Science Series, II: Mathematics, Physics and Chemistry, **140**, 513-520. Ed. A. Katrusiak & P.F. McMillan, Kluwer, Dordrecht, 2004.

Kistenmacher, T.J., Rand, G.A. & Marsh, R.E. (1974). *Acta Cryst. B***30**, 2573-2578.

Merrill, L. & Bassett, W.A. (1974). *Rev. Sci. Instrum.*, **45**, 290-294.

Parsons, S. (2004). *SHADE.* Program for empirical absorption corrections to high pressure data. The University of Edinburgh, Scotland.

Sheldrick, G. M. (2004). *SADABS.* Bruker-AXS, Madison, Wisconsin, USA.

Spek, A. L. (2004). *PLATON- A Multipurpose Crystallographic Tool*, Utrecht University, Utrecht, The Netherlands.

Suresh, C.G., Ramaswamy, J. & Vijayan, M. (1986). *Acta Cryst. B***42**, 473-478

Watkin, D. J., Pearce, L. & Prout, C. K. (1993). *CAMERON - A Molecular Graphics Package.* Chemical Crystallography Laboratory, University of Oxford, England.

Chapter 3

A high-pressure neutron diffraction study of L-serine-I and L-serine-II, and the structure of L-serine-III at 8.1 GPa.[ii]

[ii] Moggach, S. A., Marshall, W. G. & Parsons, S. (2005). *Submitted for publication*

3.1 Synopsis

The hydrostatic compression of L-serine-d_7 has been studied to 8.1 GPa by neutron powder diffraction. Over the course of this pressure range the compound undergoes two phase transitions, the first between 4.6 and 5.2 GPa, and the second between 7.3 and 8.1 GPa.

3.2 Introduction

Pressure is an important thermodynamic variable in the study of molecular systems as it provides a useful tool for changing the hierarchy of interactions in the solid state. For example, H-bonding interactions are usually regarded as being 'structure-directing', but as pressure increases the need to pack molecules efficiently is expected to begin to assume more importance. The application of pressure, unlike temperature also allows structural studies to be performed that depend on changes in volume alone, and not the simultaneous effects of volume and thermal energy (Fourme *et al.*, 2001).

The importance of pressure is well known in marine biology and deep sea diving physiology. Application of pressure to biological systems has been known to have major effects, from deactivation of enzymes (Somero *et al.*, 1992) to killing bacteria (Johnson *et al.*, 1974). In fact, the structural effects of pressure were observed in proteins by Bridgeman as early as 1914, when the white of an egg subjected to hydrostatic pressure at room temperature became coagulated, becoming in appearance much like hard-boiled egg. Recent work by Fourme *et al.*, (2001) has opened up the possibility of collecting high-resolution, high-pressure data on large macromolecules using short wavelength X-rays (*ca* 0.3 Å). More recently, the first crystal structure of a macromolecular assembly under high-pressure was published on the structure of cubic cowpea mosaic virus crystals (Girard *et al.*, 2005).

A recent goal in the field of small-molecule crystallography has been to gain an understanding of the changes which occur in molecular systems as a function of pressure at atomic resolution [Boldyreva (2004), Katrusiak (2004), Hemley & Dera (2000)]. Amino acids have several advantages in this area, as they are polyfunctional and form well-defined intermolecular interactions such as hydrogen bonds and dipolar contacts; the results also have some relevance to the macromolecular work described above. In recent years a number of crystallographic studies have been carried out on amino acids and related compounds,

including glycine (Dawson *et al*, 2005; Boldyreva *et al.*, 2003) cystine (Moggach *et al.*, 2005c) and cysteine (Moggach *et al.*, 2005a).

We recently described the effect of pressure on the anhydrous orthorhombic phase of L-serine (Scheme 3.1), L-serine-I, which undergoes a single-crystal to single-crystal phase transition at 5.4 GPa to a new high pressure phase, L-serine-II (Moggach *et al.*, 2005b). This transition occurs with no change in symmetry. The reduction in volume is achieved by compression of interstitial voids. In addition, the strain present in some H-bonded interactions, which become very short just below the transition pressure, is also relieved during the phase transformation.

Our previous study on serine was carried-out using X-ray diffraction, and certain inferences regarding H-atom positions were made on the basis of N and O positions. We now describe a study of the compression of L-serine by neutron powder diffraction, which enables statements on H-atom positions to be made with a greater degree of certainty. Recently, a second phase transition was observed in L-serine *via* a high-pressure Raman study, the transition taking place at 7.8 GPa (Kolesnik *et al.*, 2005). Here we confirm this reported transition to a third high-pressure phase of serine, L-serine-III, at 8.1 GPa, and describe its structure for the first time.

3.3 *Experimental*

L-Serine-d_7 (98.2 atom% D, Scheme 3.1) was purchased from CDN isotopes (catalogue number D-6466). One small crystallite was removed directly from the sample bottle and shown to be L-serine-I by single crystal diffraction (Kirstenmacher *et al.*, 1974).

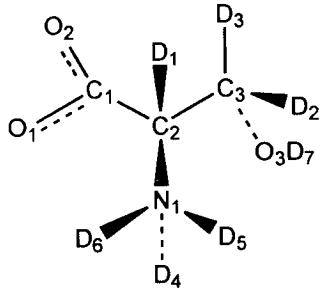

Scheme 3.1: Chemical structure diagram showing atomic numbering scheme.

3.3.1 Neutron Powder Diffraction at High Pressure

Note: The work carried out in this section was done in collaboration with Dr William G. Marshall; beamline scientist on the PEARL beamline high-pressure facility (HiPr) at ISIS.

Ambient temperature, high-pressure neutron powder diffraction data were collected by the time-of-flight technique at the PEARL beamline high-pressure facility (HiPr) at ISIS. Approximately 50mm^3 of L-Serine-d_7 was gently ground into a fine powder and loaded into a Paris–Edinburgh (P–E) high-pressure cell. The P-E cell ram pressure was monitored and controlled by means of a computer controlled hydraulic system. The sample was loaded into a null-scattering Ti-Zr alloy capsule gasket (Marshall & Francis, 2002). A pellet of lead was included as a pressure marker.

Time-of-flight neutron powder diffraction data suitable for structure refinement were obtained by electronically focusing the 1080 individual detector element spectra of the main PEARL/HiPr 2-theta=90° detector bank. The summed pattern was then normalised with respect to the incident beam monitor and the scattering from a standard vanadium calibration sample. Lastly, the diffraction pattern intensities were corrected for the wavelength and scattering-angle dependence of the neutron attenuation by the P-E cell anvil (WC) and gasket (TiZr) materials.

In order to ensure that the pressure applied to a crystal held in a pressure cell is uniform, it is necessary to immerse the sample in a medium which displays hydrostatic behaviour throughout the pressure range of interest. A 4:1 mixture of methanol and ethanol is commonly used in high pressure work, though L-serine has some solubility in this mixture. A 1:1 mixture of deuterated pentane and isopropanol was therefore used for an initial survey. Data were collected in approximately 0.7 GPa steps from 0.1 GPa to a final pressure of 4.3 GPa. Peak broadening occurred above 4.3 GPa, suggesting that conditions became non-hydrostatic at high pressures.

Based on our previous work on crystal growth from solutions at high pressure, the solubility of L-serine was expected to decrease at elevated pressures (Fabbiani *et al.*, 2005). In order to extend the pressure range for this study a second sample of L-serine was loaded with a 4:1 mixture of MeOD:EtOD as the hydrostatic medium. Diffraction data were collected in approximately 1 GPa steps from 4.6 GPa to a final pressure of 8.1 GPa. On increasing pressure to 5.2 GPa, the phase transition from L-serine-I to L-serine-II was observed, a transition which we have observed previously in a single-crystal high-pressure X-ray diffraction experiment on a non-deuterated sample of L-serine-I (Moggach *et al.*, 2005b). On increasing pressure further to 8.1 GPa, another phase transition was observed to a hitherto uncharacterized phase of L-serine which we have designated L-serine-III.

3.3.2 Structure solution and Refinement.

Powder indexing, structure solution and Rietveld refinements were carried-out using TOPAS-A (Coelho, 2005). Rietveld refinement of phases I and II was carried out starting from the 4.8 GPa and 5.4 GPa coordinates of Moggach *et al.*, (2005b) for L-serine-I and L-serine-II respectively.

The structure of the new phase (L-serine-III) was indexed on an orthorhombic unit cell, a = 6.5574 Å, b = 9.5397 Å, c = 5.6101 Å, in the space group $P2_12_12_1$ using the method of Coelho (2003). The structure was then solved by simulated annealing. During refinement the serine molecules were treated as variable metric rigid groups using the Z-matrix formalism available in TOPAS.

Lead (included in the sample as a pressure marker), tungsten carbide and nickel were also included in the refinement models. The weak tungsten carbide and nickel peaks both

arise from the P-E cell anvil cores which consist of cemented WC with a Ni binder. The refined cell dimensions of lead were used to calculate the applied pressure using a Birch-Murnaghan equation of state (Birch, 1947) using $V_0 = 30.3128$ Å^3, $B_0 = 41.92$ GPa, $B' = 5.72$. These parameters were derived by Fortes (2004) as averages of the values in Kuznetsov *et al.* (2002), Miller & Schuele (1969) and Waldorf & Alers (1962).

All intramolecular bond distances and angles were constrained to their ambient pressure values for all but the hydroxyl group, whose O-D distance and C-O-D angle were refined. All torsion angles were also refined. All N-D and C-D distances were constrained to 1.009 Å and 1.083 Å, respectively. All non-hydrogen atoms were refined with a common isotropic thermal parameter; the displacement parameters of the D-atoms were equal to 1.5 times this value. The final Rietveld fit for L-serine-III is shown in Figure 3.1. Unit cell dimensions and refinement parameters for L-serine-I at 4.6 GPa, L-serine-II at 5.2 and 7.3 GPa, and L-serine-III at 8.1 GPa are included in Table 3.1.

Crystal structures were visualized using the programs MERCURY (Bruno *et al.*, 2002) and DIAMOND (Crystal Impact, 2004). Analyses were carried out using PLATON (Spek, 2004), as incorporated in the WIN-GX suite (Farrugia, 1999). Hirshfeld surface analysis was performed using the program CrystalExplorer (Wolff *et al.*, 2005).

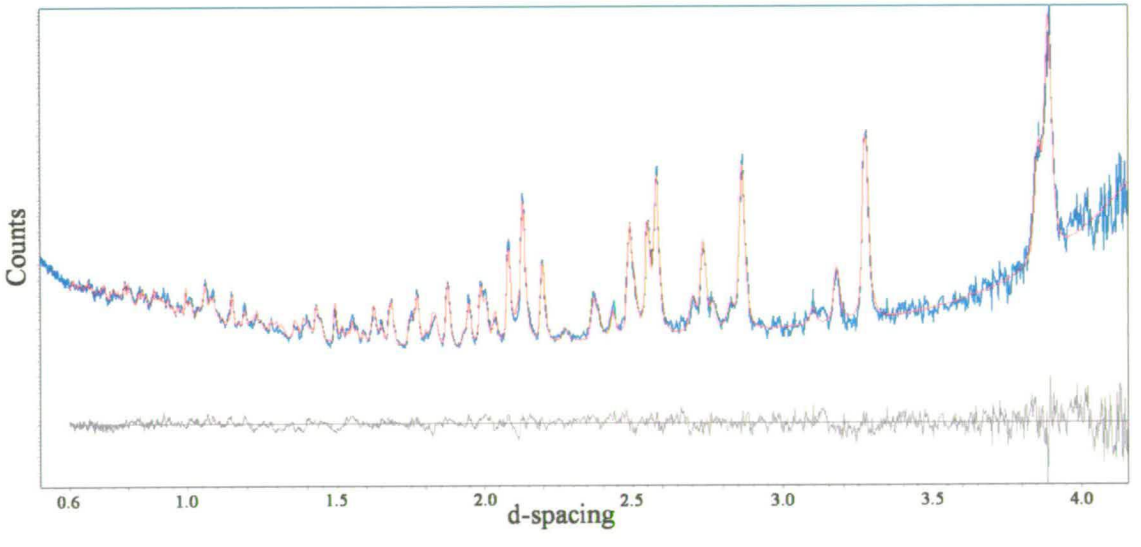

Figure 3.1: Rietveld refinement plot of L-serine-III. Blue and red lines correspond to observed and calculated powder patterns, respectively; the difference plot is shown in grey.

Pressure (GPa)	**4.6**	**5.2**	**7.3**	**8.1**
Crystal data				
Chemical formula	C3D7NO3	C3D7NO3	C3D7NO3	C3D7NO3
M_r	112.11	112.11	112.11	112.11
Cell setting, space group	Orthorhombic, $P2_12_12_1$	Orthorhombic, $P2_12_12_1$	Orthorhombic, $P2_12_12_1$	Orthorhombic, $P2_12_12_1$
a, b, c (Å)	8.3096 (3), 8.5950 (3), 5.4647 (3)	6.8700 (3), 9.6396 (5), 5.6058 (3)	6.6874 (3), 9.5815 (6), 5.5619 (3)	6.5477 (4), 9.5405 (6), 5.6092 (4)
α, β, γ (°)	90, 90, 90	90, 90, 90	90, 90, 90	90, 90, 90
V (Å^3)	390.29 (3)	371.24 (3)	356.38 (4)	350.40 (4)
Z	4	4	4	4
D_x (Mg m^{-3})	1.908	2.006	2.089	2.125
Radiation Type	Neutron	Neutron	Neutron	Neutron
Temperature (K)	298	298	298	298
Specimen form, colour	Powder, colourless	Powder, colourless	Powder, colourless	Powder, colourless
Data collection				
Diffractometer	ISIS, PEARL	ISIS, PEARL	ISIS, PEARL	ISIS, PEARL
Collection method	Time of flight	Time of flight	Time of flight	Time of flight
Range of d (Å)	0.6-4.3	0.6-4.3	0.6-4.3	0.6-4.3
Refinement				
Method	Rietveld	Rietveld	Rietveld	Rietveld
R_p	2.985	2.907	3.299	3.463
R_{wp}	4.140	4.146	4.735	4.921
S	0.385	0.377	0.386	0.381
No. reflections	1101	1064	1018	1004
Background	6-term Chebychev polynomial	6-term Chebychev polynomial	6-term Chebychev polynomial	6-term Chebychev polynomial
Profile function	Back-to-back exponential convoluted with Voigt function	Back-to-back exponential convoluted with Voigt function	Back-to-back exponential convoluted with Voigt function	Back-to-back exponential convoluted with Voigt function
No. Parameters	39	39	39	39
Weighting scheme	$1/\sigma^2$	$1/\sigma^2$	$1/\sigma^2$	$1/\sigma^2$
$(\Delta/\sigma)_{max}$	<0.001	<0.001	<0.001	<0.001

Table 3.1: Crystal and refinement parameters

3.4 *Results and Discussion*

3.4.1 The response of L-serine-I-d7 to 4.5 GPa

We have previously investigated the response of L-serine-I to pressure using single-crystal X-ray diffraction (Moggach *et al.*, 2005b). Boldyreva *et al.* (2005) also studied L-serine-I to 4.4 GPa, obtaining similar results. While deuterated materials can sometimes display different phase behaviour to their per-hydrogenated analogues, the response of deuterated L-serine-d_7-I is essentially the same as that of L-serine-h_7-I up to 4.6 GPa. On increasing pressure to 5.2 GPa, the sample underwent a phase transition to L-serine-II. The phase transition from L-serine-I to L-serine-II is marked by a sudden decrease in volume (Figure 3.2).

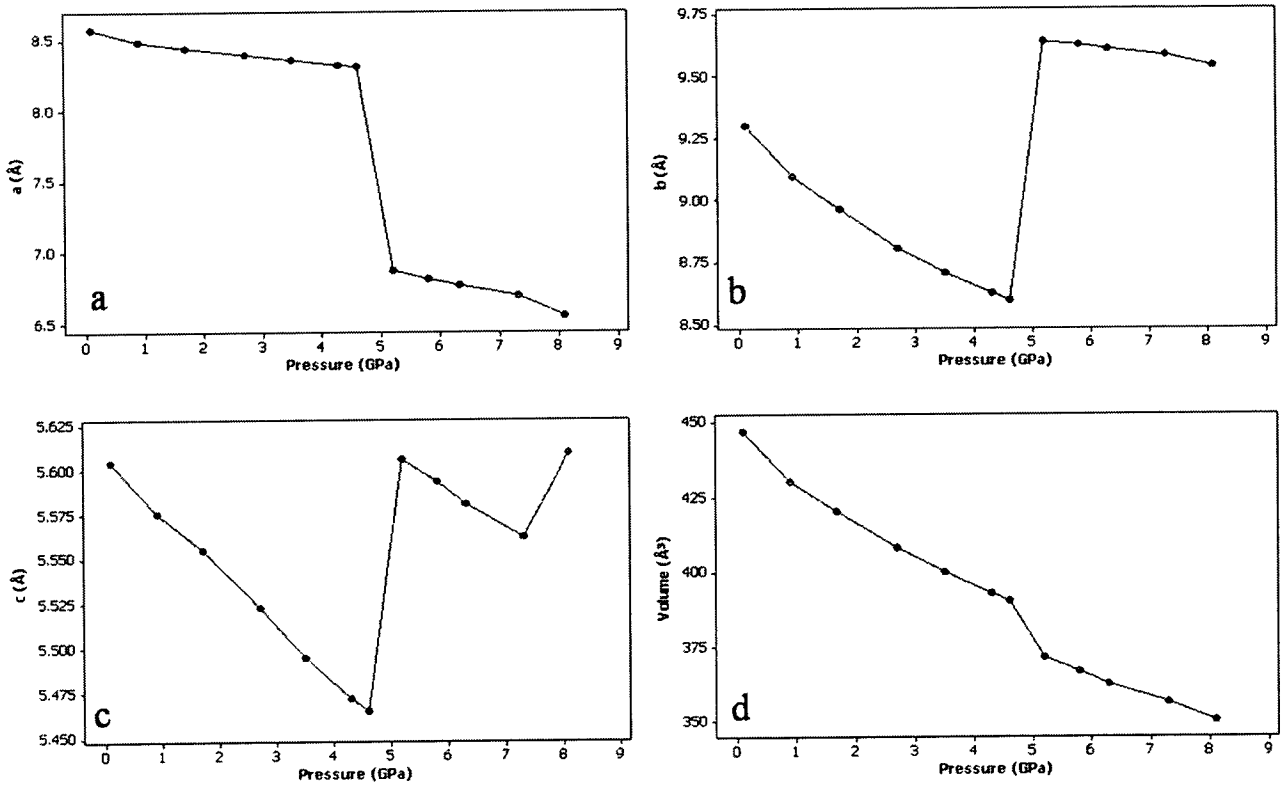

Figure 3.2: Variation of the lattice parameters (*a*- c, Å) and volume (*d*, Å^3) of L-serine as a function of pressure (GPa).

3.4.2 Description of Phases I and II

We have discussed the structures of L-serine-I and II in detail in Moggach *et al.* (2005c), and our motive for including a summary here is to highlight H-bonded motifs relevant to the development of L-serine-III, described below.

C(5) chains are formed in both L-serine-I and II along **c** by N1D5...O2 H-bonds (Figure 3.3a,b). A second *C*(5) chain, generated from the first *via* a 2_1 operation, is linked to the first through N1D6...O1 H-bonds, and together the N1D5...O2 and N1D6...O1 interactions form ribbons containing successive $R^3_3(11)$ ring motifs. The CD_2OD side chains are distributed along the outside edges of these ribbons. In L-serine-I these link the ribbons into a layer via OD...OD...OD interactions (Figure 3.3a). In L-serine-II the ribbons are connected into a layer by O3D7...O2 H-bonds formed between the alcohol and carboxyl moieties (Figure 3.3b). The graph-sets so-formed are $R^3_3(13)$ and $R^2_3(13)$, and the layers are stacked along the *a*-axis in both phases.

The layers are linked together in both phases I and II by N1D4...O2 interactions, which build another primary-level *C*(5) chain. The combination of the N1D5...O2 and N1D4...O2 *C*(5) chains along **a** and **c** builds a third set of secondary level ring motifs, these having the descriptor $R^3_4(14)$ (Figure 3.4a,b). In fact these chains can be viewed as building up another layer which is parallel to the *ac* plane. Overall then, the structure consists of two sets of layers: one stacks along **a** and contains $R^3_3(11)$ and $R^3_3(13)$ ring motifs, the other stacks along **b**, and contains $R^3_4(14)$ rings. In Moggach *et al.* (2005b) we referred to these as the *A* and *B*-layers, respectively.

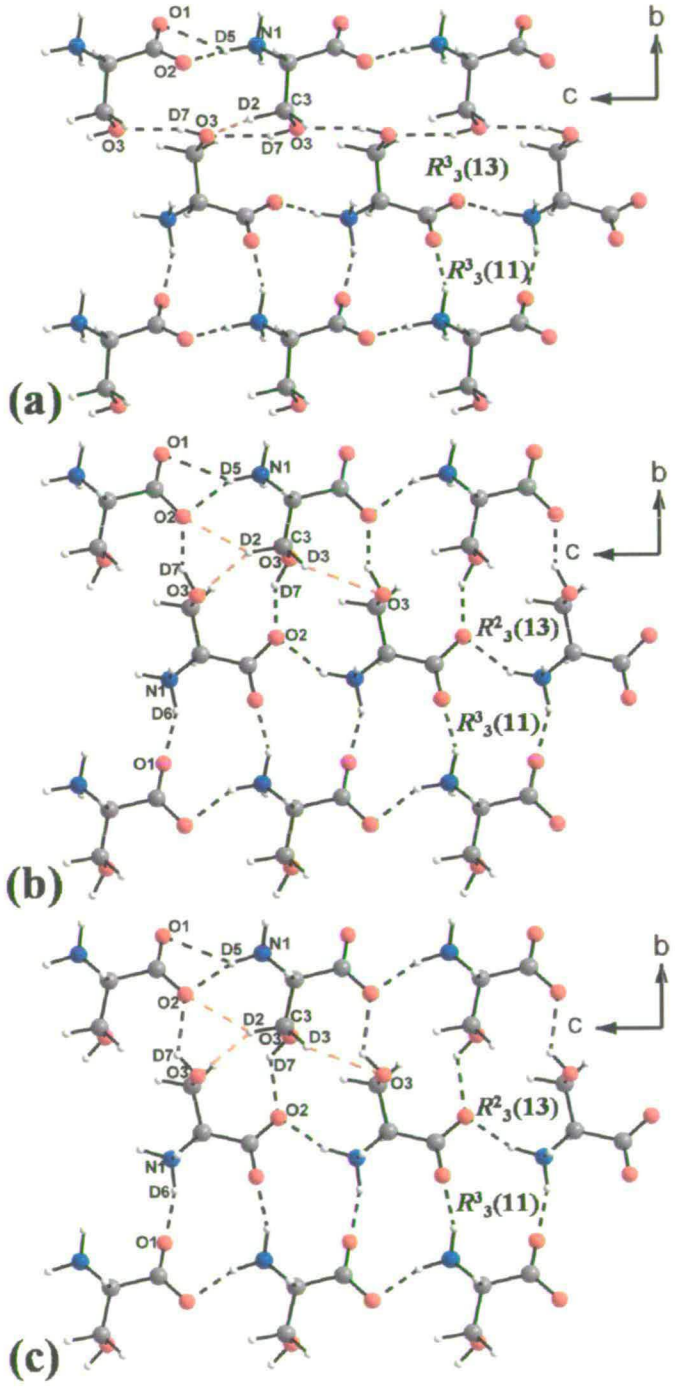

Figure 3.3: (a) L-serine-I at 4.6 GPa, (b) L-serine-II at 5.2 GPa and (c) L-serine-III at 8.1 GPa as viewed along **a**. $R^3_3(13)$, $R^2_3(13)$ and $R^3_3(11)$ ring motifs are shown. ND...O and OD...O H-bonds are drawn as black dotted lines while CD...O interactions are drawn as orange dotted lines. For clarity, the bifurcated interaction N1D5...O1/O2, and CD...O interactions are shown only in the top left corner. These layers are referred to as the *A*-layers in the text. Colour scheme C grey, H white, N blue and O red.

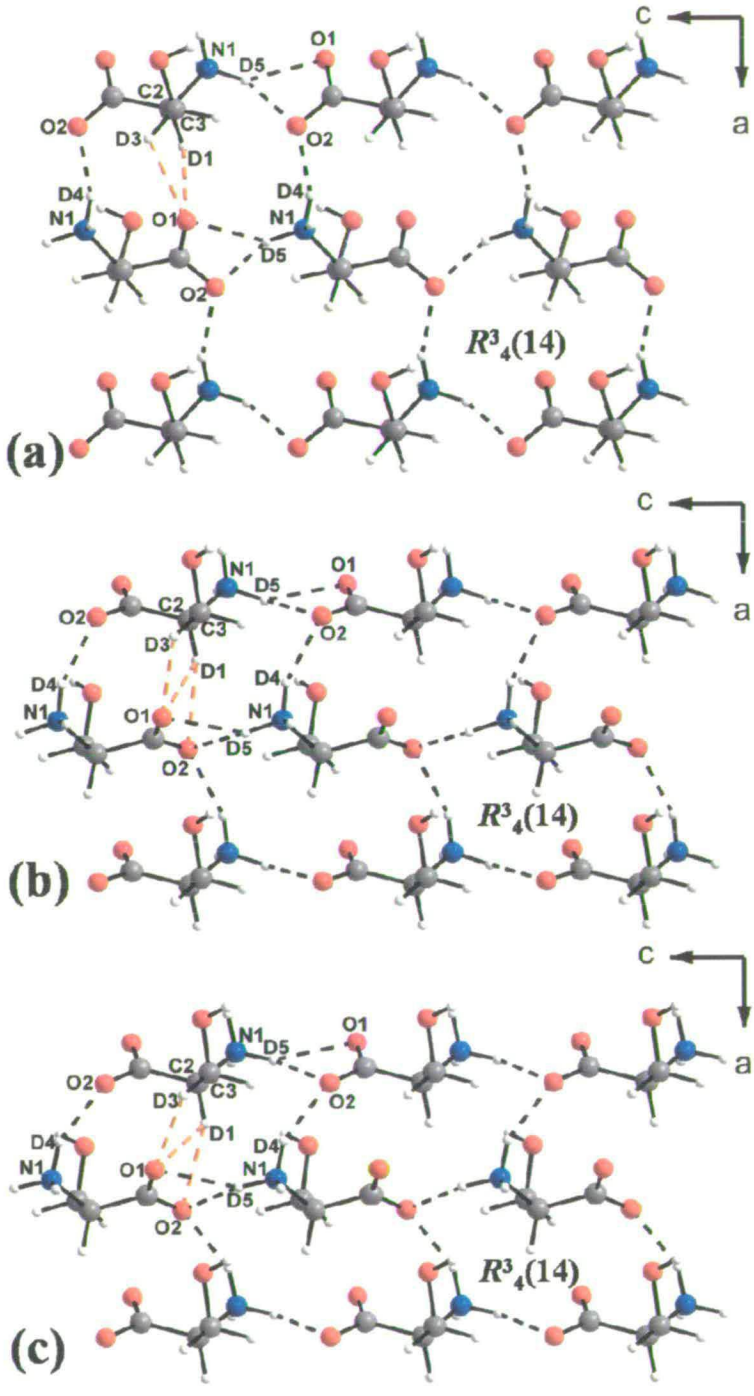

Figure 3.4: (a) L-serine-I at 4.6 GPa, (b) L-serine-II at 5.2 GPa and (c) L-serine-III at 8.1 GPa as viewed along **b**. $R^3_4(14)$ ring motifs are shown. ND...O and OD...O H-bonds are drawn as black dotted lines while CD...O interactions are drawn as orange dotted lines. . For clarity, the bifurcated interaction N1D5...O1/O2, and CD...O interactions are shown only in the top left corner. These layers are referred to as the *B*-layers in the text. Colour scheme is the same as Figure 3.3.

3.4.3 Comparison of L-serine-I at 4.5 GPa and L-Serine-II at 5.2 GPa.

One difference between L-serine-I and II is the position of the hydroxyl H-atom. In our original X-ray study the position of this H-atom was rather imprecisely-determined, but our conclusions are confirmed by the present neutron study. The O...O and D...O distances in the O3D7...O2 hydroxyl-carboxyl H-bonds in phase-II are substantially shorter than the O3D7...O3 hydroxyl-hydroxyl H-bonds in phase-I (Table 3.2).

The conformations of the $R^3_4(14)$ rings in L-serine-I and II represent a second difference between the crystal structures of the two phases. Voids observed in L-serine-I-*d*7 at 4.6 GPa at the centres of the $R^3_4(14)$ ring motifs are closed-up on undergoing the transition (Figure 3.5a,b). This is accomplished by (*i*) a displacement along the **+c** and **–c** directions by successive $C(5)$ chains formed by N1D5...O2 H-bonds, and (*ii*) a shortening of the distance between the chains along the *a*-direction (Figures 3.6a and b). The opposite directions of displacement of the $C(5)$ chains breaks the O3D7...O3 hydroxyl-hydroxyl H-bonds which are replaced by O3D7...O2 hydroxyl-carboxylate H-bonds in phase-II.

CD...O contacts are also more numerous in L-serine-II than in L-serine-I. All C-H bonds act as donors in two H-bonding interactions which span the $R^2_3(13)$ and $R^3_4(14)$ rings (Table 3.2, Figures 3.3b and 3.4b).

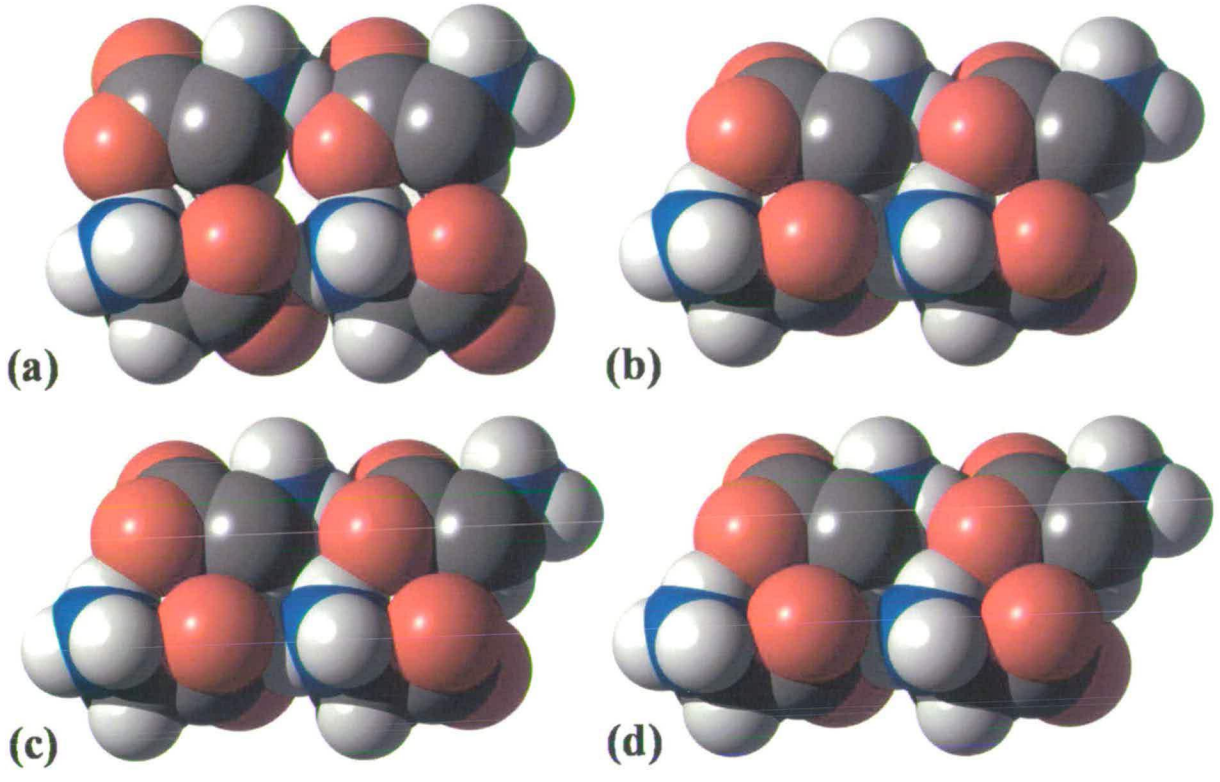

Figure 3.5: Space-filling plots for $R^3_4(14)$ ring motifs in (a) L-serine-I at 4.6 GPa, (b) L-serine-II at 5.2 GPa, (c) L-serine-II at 7.3 GPa and (d) L-serine-III at 8.1 GPa as viewed along **b**. The CD_2OD side groups have been removed for clarity. Colour scheme is the same as in Figure 3.3.

Pressure/GPa	4.6[I]	5.2[II]	7.3[II]	8.1[III]
N1D4..O2[i]				
N1..O2	2.743(11)	2.821(17)	2.764(18)	2.836(15)
D4...O2	1.839(11)	1.877(19)	1.85(2)	1.890(16)
<N1D4O2	147.3(5)	154.3(12)	149.3(12)	154.8(7)
N1D5..O1[ii]				
N1..O1	3.012(5)	3.071(4)	3.008(4)	3.085(3)
D5...O1	2.215(8)	2.243(8)	2.168(8)	2.304(7)
<N1D5O1	134.8(5)	138.4(5)	139.6(5)	133.3(4)
N1D5..O2[ii]				
N1..O2	2.714(10)	2.823(10)	2.829(11)	2.776(9)
D5...O2	1.762(13)	1.875(13)	1.902(15)	1.796(11)
<N1D5O2	155.7(5)	155.2(9)	151.3(10)	162.9(4)
N1D6..O1[iii]				
N1..O1	2.631(14)	2.642(15)	2.640(17)	2.694(18)
D6...O1	1.683(14)	1.733(14)	1.735(16)	1.710(18)
<N1D6O1	154.6(5)	147.8(6)	147.1(7)	164.2(8)
O3D7..O3[iv]				
O3..O3	2.780(5)			
D7..O3	1.954(18)	-	-	-
<O3D7O3	156(2)			
O3D7..O2[iv]				
O3..O2		2.576(16)	2.516(17)	2.638(15)
D7..O2	-	1.67(3)	1.56(3)	2.05(3)
<O3D7O2		168(3)	174(3)	122(2)
O3D7..O1[v]				
O3..O1				2.775(13)
D7..O1	-	-	-	1.95(3)
<O3D7O1				152(2)

Table 3.2: Hydrogen bonding parameters in L-serine. Distances are in Å, and angles in °. Roman numerals refer to the phase of L-serine.

Pressure/GPa	4.6[I]	5.2[II]	7.3[II]	8.1[III]
C2D1..O1[vi]				
D1..O1	2.499(14)	2.438(16)	2.350(17)	2.341(16)
<C2D1O1	119.2(4)	111.1(4)	109.7(4)	105.9(4)
C2D1..O2[vi]				
D1..O2	-	2.385(15)	2.338(16)	2.322(14)
<C2D1O2		159.6(4)	157.9(4)	154.7(4)
C3D2..O2[ii]				
D2..O2	-	2.389(12)	2.297(12)	2.378(11)
<C3D2O2		128.2(7)	129.7(8)	129.2(7)
C3D2..O3[iv]				
D2..O3	2.41(3)	2.44(3)	2.39(3)	2.32(2)
<C3D2O3	114.5(5)	131.3(8)	132.5(9)	152.7(7)
C3D3..O3[vii]				
D3..O3	-	2.37(3)	2.32(2)	2.26(2)
<C3D3O3		132.9(10)	134.1(11)	157.2(12)
C3D3..O1[vi]				
D3..O1	2.420(15)	2.36(2)	2.32(2)	2.229(17)
<C3D3O1	105.7(6)	109.5(7)	109.5(7)	113.4(6)

Symmetry Operators

i	-1/2+x,3/2-y,1-z	v	1-x,-1/2+y,3/2-z
ii	x,y,1+z	vi	1/2+x,3/2-y,1-z
iii	3/2-x,2-y,1/2+z	vii	3/2-x,1-y,-1/2+z
iv	3/2-x,1-y,1/2+z		

Table 3.2 (cont'd): Hydrogen bonding parameters in L-serine. Distances are in Å, and angles in °. Roman numerals refer to the phase of L-serine.

3.4.4 L-Serine-II between 5.2 and 7.3 GPa

As the pressure on L-serine-II is increased from 5.2 to 7.3 GPa the largest compression occurs along the **a** direction, with the *a*-axis decreasing in length by 2.7%; the *b* and *c*-axes reduce by only 0.6% and 0.8%, respectively. The relative displacement of the N1D5...O2 *C*(5) chains and the diminution of the distance between the chains both continue up to 7.3 GPa, leading to further compression of voids within $R^3_4(14)$ ring motifs (Figures 3.6a, 3.6b and 3.5c).

The most compressible ND...O H-bond, N1D5...O1, decreases by 0.075(11) Å between 5.2 and 7.3 GPa. This H-bond is the longest of its type at 5.2 GPa, and it shortening increases the bifurcation in the interaction N1D5...O1/O2. N1D6...O1, which is short anyway at 5.2 GPa, remains relatively unchanged. The largest change occurs for O3D7...O2, which was formed in the transition from phase-I to phase-II: by 7.3 GPa the O...O distance in this contact measures only 2.516(17) Å, which is very short. Though it is short, O3D7...O2 is unsymmetrical, with O3-D7 and D7...O2 measuring 0.97(2) Å and 1.56(3) Å, respectively.

The shortest OH...O H-bond found under ambient pressure conditions [2.474(2) Å] occurs in CSD refcode AMHACY (Leban., 1974). This, however, corresponds to a symmetrical H-bond where the H-atom is shared equally between adjacent carboxyl groups from neighbouring molecules. Strong hydrogen bonds of this type are common when formed between acids and complementary bases Steiner (2002). If this search is limited to H-bonding interactions between a free hydroxyl group donor (bonded to an alkyl CH_2) and carboxyl group acceptor, the shortest interaction observed under ambient conditions measures 2.584(2) Å for GOLWIN (Tusvik *et al.*, 1999). The O3D7...O2 H-bond, therefore, appears to be pushed to below this lower limit observed under ambient pressure conditions, and on increasing pressure further, the structure undergoes another phase transition to a second high-pressure phase, L-serine-III.

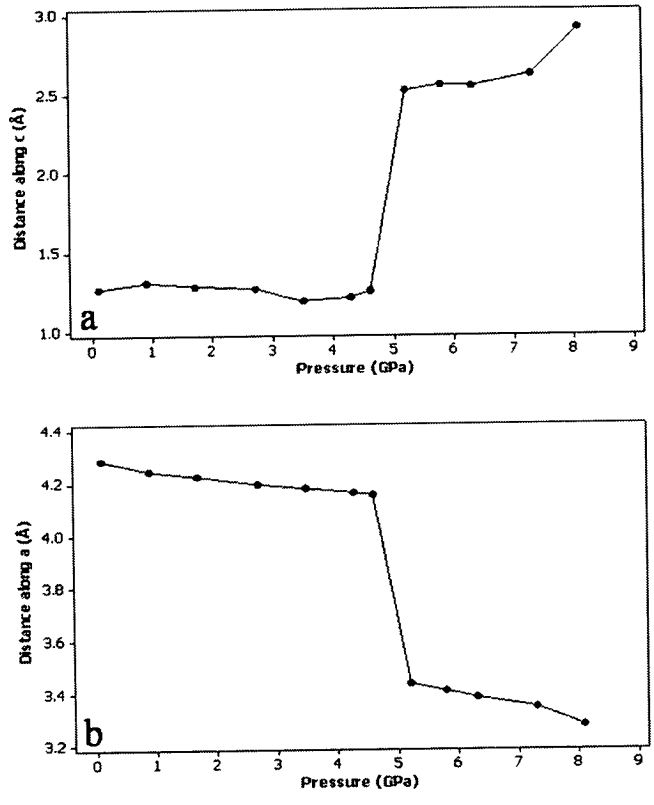

Figure 3.6: Graphs showing distances between centroids of molecules in neighbouring $C(5)$ chains along (a) **c** and (b) **a**.

3.4.5 The structure of L-serine-III at 8.1 GPa.

The phase transition from L-serine-II to L-serine-III, unlike that from phase I to II occurs with only a modest decrease in volume (Figure 3.2d); the volume per non-Hydrogen atom at 8.1 GPa is only 12.5 Å^3. Overall the structure is closely-related to the structures of phases I and II (Figures 3.3c and 3.4c), and the structure can again be considered in terms of layers which stack along the **a** and **b** directions.

The $R^3_4(14)$ ring motifs in the B-layers appear longer and thinner than they do in L-serine-I and II (Figure 3.4b,c), and over the course of the II-to-III phase transition the relative displacement of neighbouring N1D5...O2 $C(5)$ chains in the +**c** and –**c** directions continues (Figure 3.6a). The associated compression along the a direction also continues (Figure 3.6b), and at 8.1 GPa there are no visible voids within the $R^3_4(14)$ rings (Figure 3.5d). Small voids present at the centre of $R^2_3(13)$ ring motifs of the A-layers remain essentially unchanged

through the transition, while no observable voids can be observed at the centres of $R^3_3(11)$ ring motifs in phase-II or III.

The phase transition from L-serine-I to L-serine-II was, in part, characterised by a change in the H-bonds formed by the hydroxyl group, O3D7. A further change in H-bonding in this region of the structure also occurs in the transition from phase-II to phase-III. In phase-II the H-bonding from O3D7 was confined to one *A*-layer, but in phase-III the H-bonding from D7 becomes bifurcated between the same O3D7...O2 interaction that was present in phase-II, and a new O3D7...O1 H-bond which connects different *A*-layers together. This change in the H-bonding environment of the O3D7 group may explain the findings of Kolesnik *et al.*, (2005) who observed that the largest changes in the Raman spectra of L-serine on undergoing the transition from phase-II to III occurred in bands at 1250cm^{-1} (HOC bend) and 1430cm^{-1} (CO_2 sym. str). When viewed in projection the *A* and *B*-layers seem very similar in phases II and III: the difference lies in the way they are connected together, and this is clearer in the *c*-axis projection illustrated in Figure 3.7.

The O3...O2 distance within the O3D7...O2 hydrogen bonds in phase-II is very short [2.516(17) Å] at 7.3 GPa, and the structure presumably experiences significant strain in this region. It seems reasonable to suggest that the II-to-III transition is driven by the need to alleviate close contacts about O3 in L-serine-II as pressure is increased beyond 7.3 GPa.

In general, at elevated pressures the influence of H-bonds as structure-directing interactions is expected to diminish relative to the need to pack molecules more efficiently, and several of the ND...O and OD...O H-bonds in phase III at 8.1 GPa are longer than in phase-II at 7.3 GPa. In L-serine-II the H-bonding capacity of the C-D bonds is saturated and so the transition from phase-II to III does not result in an increase in number of CD...O interactions, with the six interactions present in L-serine-II, still observed in L-serine-III.

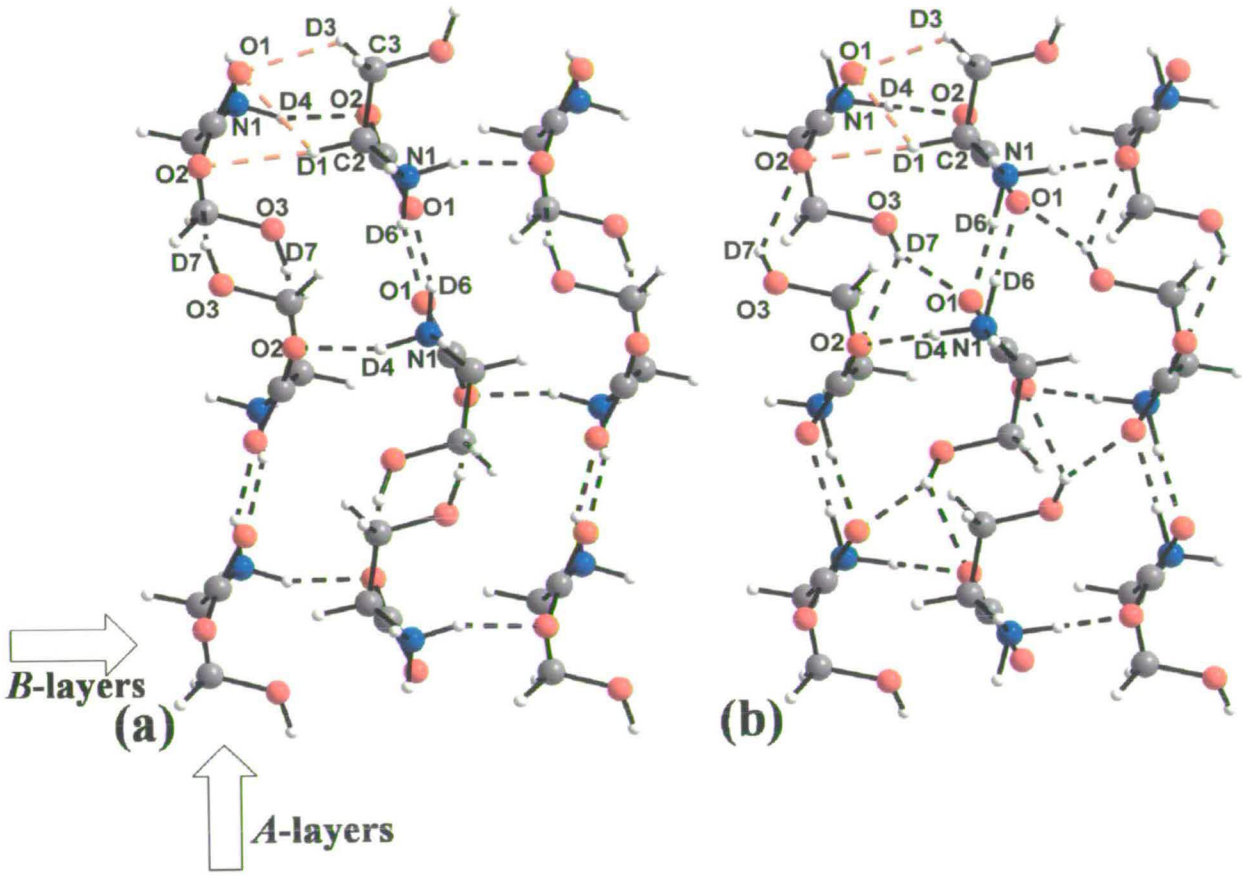

Figure 3.7: (a) L-serine-II at 5.2 GPa and (b) L-serine-III at 8.1 GPa as viewed along **c**. *A*- and *B*-layers as referred to in the text are labelled. ND...O and OD...O H-bonds are drawn as black dotted lines while CD...O interactions are drawn as orange dotted lines. For clarity, CD...O interactions are shown only in the top left corner. Note the formation of the O1D7...O1 interaction in L-serine-III at 8.1 GPa. Colour scheme is the same as Figure 3.3.

3.4.6 *Changes in CD...O and D...D interactions: Hirshfeld Fingerprint Plot Analysis.*

McKinnon *et al.* (2004) have recently described how Hirshfeld surface analysis can assist in the interpretation of differences between related crystal structures. Hirshfeld surfaces are created by partitioning space within a crystal structure into regions where the electron density from a sum of spherical atoms (the promolecule) dominates over the sum of the electron density of the crystal (the procrystal). The surfaces surround each molecule in a crystal structure, enabling various properties relating to packing to be calculated. Two such properties are d_e (the distance from the surface to the nearest atom in another molecule) and d_i (the distance from the surface to the nearest atom in the molecule itself). Plots of d_e against d_i are referred to as *fingerprint plots*, and they encode information on overall three-dimensional packing characteristics in a two-dimensional diagram. Fingerprint plots for the structures obtained in this study are shown in Figure 3.8.

On increasing pressure in L-serine-I between 0.1 to 4.6 GPa, the drive to compress H-bonding interactions is represented clearly on the fingerprint plots with d_e values driven to shorter distances (Figure 3.8a & b). In particular the two long spikes present in all fingerprint plots represent ND...O and OD...O H-bonding interactions, which can clearly be observed moving toward smaller values of d_e in L-serine-I (Figures 3.8a & b). The number of points at larger values of d_e and d_i also decrease on increasing pressure, giving a more compact plot at 4.6 GPa; the fingerprint plot is still more compact at 5.2 GPa (Figure 3.8c). This illustrates the compression of voids within $R^3_3(11)$ and $R^3_4(14)$ ring motifs within *A* and *B*-layers respectively. A 'hump' appears between the spikes at 4.5 GPa, becoming more prominent at 5.2 GPa. This corresponds to close D...D contacts. The shortest of these contacts at 4.6 GPa, D3...D6, forms between *A*-layers between D atoms from CD_2 and ammonium groups of adjacent molecules respectively. D...D contacts become more numerous at 5.2 GPa, for example a D3...D6 distance formed along the *a*-direction decreases from 2.19 Å to 2.08 Å.

On increasing pressure further to 7.3 GPa, the fingerprint plots look much the same, although a slight movement of the NH...O/OD...O spikes toward lower values of d_e can be observed (Figure 3.8c & d). The 'hump' between the spikes at 7.3 GPa also appears to sharpen, and move to *larger* values of d_e. This is accounted for by the movement of the hydroxyl OD group, which at 5.2 GPa forms the shortest D...D contact [D7...D3, 1.91 Å]. On

increasing pressure to 7.3 GPa, this close contact is actually relieved by the hydroxyl group, which twists, making the O3D7...O2 hydrogen bond more linear, while increasing the D7...D3 distance [1.98 Å]. This movement of the hydroxyl group can be quantified by comparing the D7-O3-C3-C2 torsion angle at 5.2 GPa [-178.5°], and 7.3 GPa [+172.3°]. Nevertheless, on increasing pressure to 7.3 GPa, the number of close D...D contacts does increase, represented in Figure 3.8d as an increase in the green colour within the 'hump' region of the plot.

At 8.1 GPa the spikes corresponding to ND...O H-bonds appear at larger values of d_e; this is caused by the *increased* lengths of ND...O and OD...O contacts in phase-III referred to above (Figure 3.8d & e). We have suggested above that the II-to-III transition is driven by the need to relieve short intermolecular contacts, and the similarity of the volumes of phases-II and III suggests that the transition does not result in markedly more efficient packing. However, there is a pronounced increase in the number of close D...D contacts between the spikes in the fingerprint plot shown in Figures 3.8d and e. Close contacts between hydrogen atoms are characteristic of the fingerprint plots obtained for alkanes (McKinnon *et al.*, 2004), and in serine their gradually increasing prominence illustrates much more graphically than tables of data the tendency for efficient packing to compete with H-bonding as structure-directing phenomena.

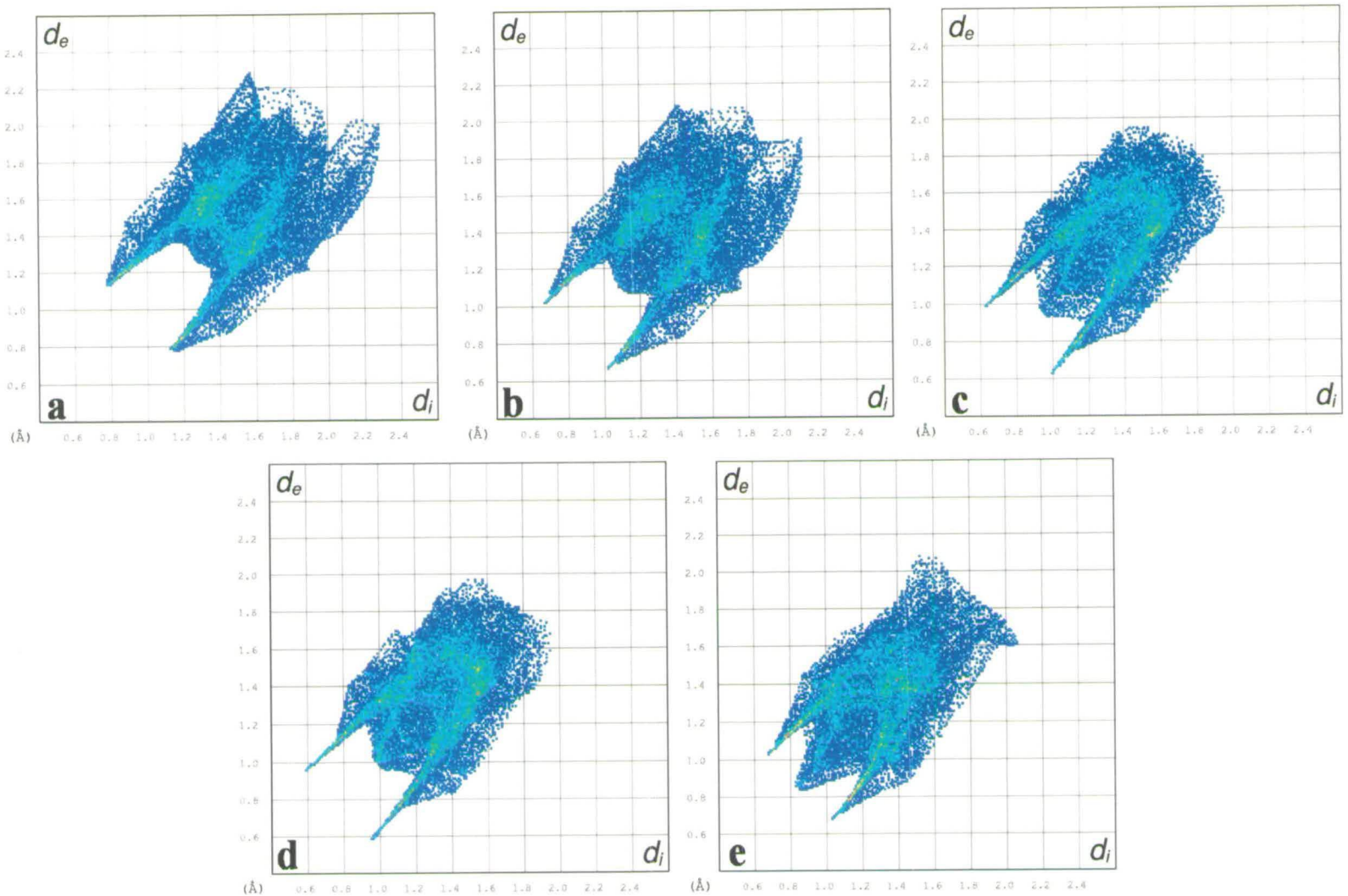

Figure 3.8: Two-dimensional fingerprint plots for (a) L-serine-I at 0.1 GPa, (b) L-serine-I at 4.6 GPa, (c) L-serine-II at 5.2 GPa, (d) L-serine-II at 7.3 GPa and (e) L-serine-III at 8.1 GPa.

3.5 *Conclusions*

We have previously described a single crystal X-ray study in which we observed a single-crystal to single-crystal phase transition from L-serine-I to an orthorhombic high-pressure phase, L-serine-II between 4.8 and 5.4 GPa. The same transition has also been observed by neutron powder diffraction in perdeuterated L-serine between 4.6 and 5.2 GPa. The I-to-II transition is accompanied by a large reduction in volume, achieved by opposite displacements of successive *C*(5) chains formed by ND...O H-bonds, and a shortening of the distance between the chains. Overall, this closes up voids present in H-bonded ring motifs, enabling the reduction in volume to occur. The opposite direction of the displacements of the *C*(5) chains breaks OD...O hydroxyl-hydroxyl H-bonds present in phase-I. These are replaced by OD...O hydroxyl-carboxylate interactions in phase-II. The change in position of the hydroxyl hydrogen atom was clearly demonstrated in this study.

Compression of L-serine-II from 5.2 to 7.3 GPa caused the O...O distance in the newly formed OD...O hydroxyl-carboxylate interaction to decrease to a very low 2.516(17) Å. This is very short, and it is possible that relief of the strain associated with this contact is responsible for a phase transition to a third form of serine as the pressure is increased from 7.3 to 8.1 GPa. In phase-III the short OD...O hydroxyl-carboxylate interaction is replaced by a bifurcated interaction in which the OD interacts with two carboxylate moieties with O...O distances of 2.638(15) and 2.775(13) Å. The trend towards opposite displacements of successive *C*(5) chains formed by N1D5...O2 H-bonds, and a shortening of the distance between the chains continued through the II-to-III transition leading to very efficient packing of chains in phase-III.

Hirshfeld fingerprint plots showed the changes in the balance of intermolecular interactions as a function of pressure. The increasing importance of D...D interactions at high pressure was particularly apparent. H-bonds seem to be longer in L-serine-III than L-serine-II, and the increase in D...D interactions revealed in the fingerprint plots point to the compromise between H-bonding and efficient packing that must be reached at elevated pressures.

3.6 References

Birch, F. (1947). *Phys. Rev.* **71**, 809-824.

Boldyreva, E. V. (2004). *NATO Science Series, II: Mathematics, Physics & Chemistry*, edited by A. Katrusiak & P. F. McMillan, Vol. 140, pp. 495-512. Dordrecht: Kluwer Academic Publishers.

Boldyreva, E. V., Ahsbahs, H., & Weber, H.-P. (2003). *Z. Kristallogr.* **218**, 231-236.

Boldyreva, E.V., Kolesnik, E.N., Drebushchak, T.N., Ahsbahs, H., Beukes, J.A. & Weber, H-P. (2005). *Z. Krist.* **220**, 58-65.

Bruker-Nonius (2004a. APEX. Area-Detector Software Package, Madison, Wisconsin, USA.

Bruker-Nonius (2004b. COSMO. Area-Detector Collection Strategy Optimisation Software Package, Madison, Wisconsin, USA.

Bruno, I. J., Cole, J. C., Edgington, P. R., Kessler, M., Macrae, C. F., McCabe, P., Pearson, J. & Taylor, R. (2002). *Acta Cryst.* **B58**, 389-397.

Coelho, A. (2003). *J. Appl. Cryst.* **36**, 86-95.

Coelho, A. (2005). *Topas-A: General Profile and Structure Analysis Software for Powder Diffraction Data.* http://pws.prserv.net/Alan.Coelho/.

Crystal Impact (2004). *DIAMOND*. Version 3.0. Crystal Impact GbR, Postfach 1251, 53002 Bonn, Germany. http://www.crystalimpact.com/diamond.

Dawson, A., Allan, D. R., Belmonte, S. A., Clark, S. J., David,W. I. F., McGregor, P. A., Parsons, S., Pulham, C. R. & Sawyer, L. (2005). *Cryst. Growth Des.* **5**, 1415-1427.

Dawson, A., Allan, D. R., Clark, S. J., Parsons, S. & Ruf, M. (2004). *J. Appl. Cryst.* **37**, 410-416.

Fabbiani, F. P. A.., Allan, D. R., Marshall, W. G., Parsons, S., Pulham, C. R.. & Smith, R. I. (2005). *J. Cryst. Growth* **275**, 185-192.

Farrugia, L. J. (1999). *J. Appl. Cryst.* **32**, 837-838.

Fortes, A. D. (2004). Ph.D. Thesis: *Computational and Experimental Studies of Solids in the Ammonia-Water System*, Department of Earth Sciences, University College, University of London.

Fourme, R., Kahn, R., Mezouar, M., Girard, E., Hoerentrup, C., Prange, T. & Ascone, I. (2001). *J. Synchrotron Rad.* **8**, 1149-1156.

Girard, E., Kahn, R., Mezouar, M., Dhaussy, A-C., Lin, T., Johnson, J.E. & Fourme, R. (2005). *Biophysical Journal.* **88**, 3562-3571.

Hemley, R.J.& Dera, P. (2000). *Rev. Mineral. Geochem.*, **41**, 335-419.

Johnson, F.H., Eyring, H. & Stover, B.J. (1974). *The Theory of Rate Processes in Biology and Medicine.* Wiley, New York.

Katrusiak, A. (2004). *NATO Science Series, II: Mathematics, Physics and Chemistry*, edited by A. Katrusiak & P. F. McMillan, Vol. 140, pp. 513-520. Dordrecht: Kluwer Academic Publishers.

Kistenmacher, T.J., Rand, G.A. & Marsh, R.E. (1974). *Acta Cryst.* **B30**, 2573-2578.

Kolesnik, E. N., Goryainov, S. V. & Boldyreva, E. V. (2005). *Doklady Phys Chem.* **404**, 61-64.

Kuznetsov. A. Z., Dmitriev, V., Dubrovinsky, L., Prakapenka, V. & Weber, H.-P. (2002). *Solid State Comm.* **122**, 125-127.

Leban, I. (1974). *Cryst. Struct. Commun.* **3**, 237-9.

Marshall, W. G. & Francis, D. J. (2002). *J. Appl. Cryst.* **35**, 122-125.

McKinnon, J. J., Spackman, M. A. & Mitchell, A. S. (2004). *Acta Cryst, B***60**, 627-668.

Miller. R. A. & Schuele, D. E. (1969). *J. Phys. Chem. Solids* **30**, 589-600.

Moggach, S. A., Allan, D. R., Clark, S. J., Gutmann, M. J., Parsons, S., Pulham, C. R., & Sawyer, L. (2005a). *Acta Cryst.* B. In press.

Moggach, S. A., Allan, D. R., Morrison, C. A., Parsons, S. & Sawyer, L. (2005b). *Acta Cryst.* B**61**, 58–68.

Moggach, S. A., Allan, D. R., Parsons, S., Sawyer, L. & Warren, J. E. (2005c). *J. Synchrotron Rad.* **12**, 598–607.

Somero, G.N. (1992). *Annu. Rev. Physiol.* **54**, 557-577.

Spek, A. L. (2003). *J. Appl. Cryst.* **36**, 7-13.

Tusvik, P. H., Mostad, A., Dalhus, B. & Rosenqvist, E. (1999). *Acta Cryst.* C**55**, 1113-1115.

Waldorf, D. L. & Alers, G. A. (1962). *J. Appl. Phys.* **33**, 3266-3269.

Wolff, S. K., Grimwood, D.J., McKinnon, J.J., Jayatilaka, D. & Spackman, M.A. (2005), CrystalExplorer 1.5. University of Western Australia.
http://www.theochem.uwa.edu.au/crystal_explorer/

Chapter 4

The Effect of Pressure on the Crystal Structure of Hexagonal L-Cystine.[iii]

[iii] Moggach, S. A., Allan, D. R., Parsons, S., Sawyer, L. & Warren, J. E. (2005). *J. Synchrotron Rad.* **12**, 598–607.

4.1 *Introduction*

The application of pressure is becoming an ever-more popular technique with which to analyse the nature of intermolecular interactions [for example Oswald *et al.* (2005*a* and *b*), Wunschel *et al.*, 2003., Boldyreva (2004*a* and *b*), Allan *et al.*, 2002]. Application of pressure (up to *ca* 10 GPa, approximately 10^5 atm) to non-cubic organic crystals commonly results in the anisotropic closure of voids in the structure along with an increase in the number and strength of weak interactions, such as CH...O hydrogen bonds. In some cases, the discovery of new phases of materials is observed with increasing pressure (Moggach *et al.*, 2005). In α-amino acids, the compression of numerous weak CH...O interactions may be extremely important, as they have a supporting role to medium strength hydrogen bonds under ambient pressure conditions, e.g. NH...O (Desiraju & Steiner, 1999; Derewenda *et al.*, 1995). The compression of such interactions has been discussed in other studies, such as the compression of L-serine-I (Moggach *et al.*, 2005).

Most molecular systems that have been studied previously are relatively simple with small unit cells with volumes ranging from a few hundred up to a few thousand Å^3. In this study, the effect of pressure on hexagonal L-cystine (I) was studied on Station 9.8 at the CCLRC Daresbury Laboratory (Cernik *et al.*, 1997) as part of our on-going research of the effect of pressure on amino acids and related compounds. Although L-cystine is a moderately small organic molecule containing 14 non-hydrogen atoms, it crystallises in a high symmetry space group ($P6_122$), with an unusually long axis (c = 55.9 Å). Attempts to study the compound at high pressure in the home-lab were frustrated by difficulties in resolving data along c^*. The low-divergence of synchrotron radiation, however, enabled this difficulty to be overcome, and we report here a compression study of L-cystine carried out using the high-pressure facilities on Station 9.8 at SRS Daresbury Laboratory. Structural data to 3.7 GPa, and unit cell dimensions up to 6.4 GPa are reported.

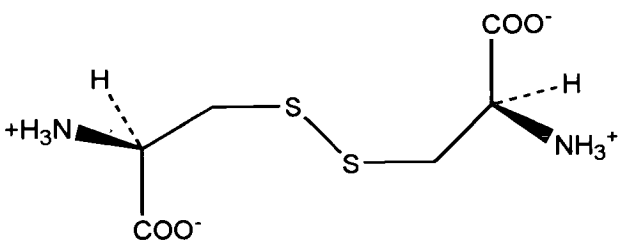

I

L-cystine is a dimer of L-cysteine produced by oxidation of the side chain thiols to form the so-called disulfide bridge. The disulfide bridge is a structurally important feature in proteins, being the only common covalent linkage to occur within and between polypeptide chains. Naturally occurring disulphide bridges are found in many proteins that are secreted by cells where their presence adds stability to the generally fragile protein structure. Common examples include the defensive immunoglobulin proteins, the hydrolytic enzymes like trypsin and lysozyme, and structural proteins like keratin. Initial analyses of the conformations adopted by cystine in globular proteins (Thornton, 1981; Richardson, 1981; Morris *et al.*, 1992) reveals that left- (-C-S-S-C- = $\chi3$ = -90°) and right-handed disulphides are equally distributed in globular proteins. The distributions of the $\chi1$ and $\chi2$ angles are also more or less as expected. $\chi1$ favours the -60° or g^+ conformation since there is less crowding between the S and the adjacent peptide carbonyl; $\chi2$ also tends to adopt the g^+ conformation. A more recent analysis, including that of the disulphide bridge environment by Bhattacharaya *et al.* (2004) confirms and extends these results using data from 1266 polypeptide chains in the PDB (Berman *et al.*, 2000) with *R*-factors $\leq$ 20% and data resolution $\leq$ 2 Å. It includes an analysis of the S to main-chain (carbonyl) oxygen distances that determines the average distance to be 3.6(2) Å, about a quarter of which are interactions with their own carbonyl oxygen.

4.2 Experimental

4.2.1 Crystal growth

All starting materials were purchased from Sigma-Aldrich and used as received. L-cystine (1.48 g, 6.16 mmol) was dissolved in warm ammonium hydroxide solution (ACS reagent, NH_3 28.0-30.0%, 8 cm^3) and crystallised on cooling to ambient temperature (Dahaoui *et al.*, 1999). A high-quality, hexagonally-shaped crystal of dimensions 0.1 x 0.2 x 0.2 mm^3 was then loaded into a Merrill-Bassett diamond anvil cell (DAC, Merrill & Bassett, 1974).

4.2.2 High-Pressure Crystallography, General Procedures

High-pressure experiments were carried out with a Merrill-Bassett diamond anvil cell equipped with 600μm culet-cut diamonds and a tungsten gasket. The sample and a chip of ruby (as a pressure calibrant) were loaded into the DAC with a 1:1 mixture of

pentane and isopentane as a hydrostatic medium. The ruby fluorescence method was utilised to measure the pressure (Piermarini *et al.*, 1975).

4.2.3 Data Collection, Reduction and Refinement

A sphere of data was collected on a crystal of L-cystine at ambient temperature and pressure in order to provide data for comparison with the high pressure studies, which were also performed at ambient temperature (see below). Diffraction data were collected on a single crystal of L-cystine on a Bruker SMART APEX diffractometer with graphite-monochromated Mo Kα radiation (λ = 0.71073 Å). These data were integrated using the program SAINT (Bruker-AXS, 2003), while the absorption correction was carried out with the program SADABS (Sheldrick, 2004). Refinement was carried out against $|F|^2$ using all data (CRYSTALS; Betteridge *et al.*, 2003) starting from the low-temperature (110 K) coordinates of Dahaoui *et al.*, (1999). The final conventional *R*-factor was 0.0476 for 898 data. Listings of crystal and refinement data are given in Table 4.1.

High pressure diffraction data were collected with synchrotron radiation on a Bruker APEX II diffractometer at the CCLRC Daresbury Laboratory on Station 9.8 (λ = 0.6774Å), see below. Data were collected in ω-scans in 8 settings of 2θ and φ with a frame and step size of one second and 0.2°, respectively. This data collection strategy was based on that described by Dawson *et al.* (2004). The data were integrated using the program SAINT using 'dynamic masks' to avoid integration of regions of the detector shaded by the body of the pressure cell (Dawson *et al.*, 2004). Additional masks were also added to mask-out the three most intense powder rings (100, 002 and 101) from the beryllium backing disks. This additional mask was required because the low divergence of synchrotron radiation gave the beryllium powder pattern a much more textured, spotty, appearance than if collected using a sealed-tube laboratory X-ray source. Application of this additional mask removed the possibility of unreliable measurements of sample reflections which coincided with the beryllium rings and was shown to improve the merging statistics slightly. Absorption corrections for the DAC and sample were carried out with the programs SHADE (Parsons, 2004) and SADABS, respectively. Data collections were taken in approximately 1.0 GPa steps from 0.4 GPa up to a final pressure of 6.4 GPa.

Pressure / GPa	0	0.4	1.4	2.3	3.7
Crystal data					
Chemical formula	$C_6H_{12}N_2O_4S_2$	$C_6H_{12}N_2O_4S_2$	$C_6H_{12}N_2O_4S_2$	$C_6H_{12}N_2O_4S_2$	$C_6H_{12}N_2O_4S_2$
M_r	240.30	240.30	240.30	240.30	240.30
Cell setting, space group	Hexagonal, $P6_122$	Hexagonal, $P6_122$	Hexagonal, $P6_122$	Hexagonal, $P6_122$	Hexagonal, $P6_122$
a, c (Å)	5.4203 (5), 55.980 (12)	5.4030 (1), 55.984 (4)	5.3524 (2), 55.087 (14)	5.3141 (1), 54.291 (3)	5.26630 (10), 53.549 (5)
V (Å^3)	1424.3 (4)	1415.40 (10)	1366.7 (4)	1327.75 (8)	1286.17 (13)
Z	6	6	6	6	6
D_x (Mg m^{-3})	1.681	1.691	1.752	1.803	1.861
Radiation type	Mo $K\alpha$	Synchrotron	Synchrotron	Synchrotron	Synchrotron
No. of reflections for cell parameters	1792	3156	1652	3365	3341
θ range (°)	9–46	9–54	9–53	9–53	9–51
μ (mm^{-1})	0.55	0.56	0.57	0.59	0.61
Temperature (K)	293	293	293	293	293
Crystal form, colour	Hexagonal block, colourless	Hexagonal block, colourless	Hexagonal block, colourless	Hexagonal block, colourless	Hexagonal block, colourless
Crystal size (mm)	0.32 × 0.17 × 0.15	0.20 × 0.20 × 0.10	0.20 × 0.20 × 0.10	0.20 × 0.20 × 0.10	0.20 × 0.20 × 0.10

Table 4.1: Crystallographic data for hexagonal L-cystine at ambient temperature and pressure, and at increasing pressures.

Pressure / GPa	0	0.4	1.4	2.3	3.7
Data collection					
Diffractometer	Bruker APEX	Bruker APEX II	Bruker APEX II	Bruker APEX II	Bruker APEX II
Data collection method	ω	ω	ω	ω	ω
Absorption correction	Multi-scan	Multi-scan	Multi-scan	Multi-scan	Multi-scan
T_{min}	0.81	0.71	0.62	0.64	0.56
T_{max}	0.92	0.95	0.94	0.94	0.94
No. of measured, independent and observed parameters	16236, 965, 898	4719, 539, 490	4645, 492, 464	4229, 492, 438	4229, 467, 439
Criterion for observed reflections	$I > 2.00u(I)$	$I > 2.00u(I)$	$I > 2.00u(I)$	$I > 2.00u(I)$	$I > 2.00u(I)$
Completeness (%)	99.0	45.4	45.5	45.5	45.9
R_{int}	0.085	0.047	0.047	0.053	0.063
θ_{max} (°)	26.4	28.5	28.1	28.1	27.9
Range of h, k, l	$-6 \rightarrow h \rightarrow 6$	$-7 \rightarrow h \rightarrow 7$	$-6 \rightarrow h \rightarrow 6$	$-7 \rightarrow h \rightarrow 6$	$-6 \rightarrow h \rightarrow 6$
	$-6 \rightarrow k \rightarrow 6$	$-7 \rightarrow k \rightarrow 6$	$-7 \rightarrow k \rightarrow 7$	$-7 \rightarrow k \rightarrow 6$	$-6 \rightarrow k \rightarrow 6$
	$-64 \rightarrow l \rightarrow 68$	$-29 \rightarrow l \rightarrow 29$	$-28 \rightarrow l \rightarrow 28$	$-28 \rightarrow l \rightarrow 28$	$-28 \rightarrow l \rightarrow 28$
Refinement					
Refinement on	F^2	F^2	F^2	F^2	F^2
$R[F^2 > 2\sigma(F^2)]$, $wR(F^2)$, S	0.048, 0.105, 1.07	0.035, 0.089, 1.06	0.036, 0.089, 1.05	0.048, 0.112, 1.05	0.093, 0.214, 1.09
No. of relections	956 reflections	513 reflections	485 reflections	458 reflections	451 reflections
No. of parameters	64	64	64	64	34
H-atom treatment	Not refined	Not refined	Not refined	Not refined	Not refined
Weighting scheme	Calculated $w = 1/[\sigma^2(F^2) + 0.03 + 3.29P]$ where $P = (\max(F_o^2,0) + 2F_c^2)/3$	Calculated $w = 1/[\sigma^2(F^2) + 0.05 + 0.8P]$ where $P = (\max(F_o^2,0) + 2F_c^2)/3$	Calculated $w = 1/[\sigma^2(F^2) + 0.05 + 1.06P]$ where $P = (\max(F_o^2,0) + 2F_c^2)/3$	Calculated $w = 1/[\sigma^2(F^2) + 0.03 + 3.33P]$ where $P = (\max(F_o^2,0) + 2F_c^2)/3$	Calculated $w = 1/[\sigma^2(F^2) + 0.00 + 18.85P]$ where $P = (\max(F_o^2,0) + 2F_c^2)/3$
$(\Delta/\sigma)_{max}$	0.001	<0.0001	<0.0001	<0.0001	<0.0001
$\Delta\rho_{max}$, $\Delta\rho_{min}$ (e Å^{-3})	0.35, –0.35	0.14, –0.19	0.22, –0.17	0.27, –0.21	0.54, –0.60

Table 4.1 (cont'd): Crystallographic data for hexagonal L-cystine at ambient temperature and pressure, and at increasing pressures.

Refinements of L-cystine were carried out starting from the published low temperature co-ordinates (Dahaoui, *et. al.*, 1999). Refinements were carried out against $|F|^2$ using all data (CRYSTALS). Because of the low completeness of the data-sets, all 1,2 and 1,3 distances were restrained to the values observed in the ambient pressure structure. Specifically, the applied restraints were as follows: distances (Å) S1-C1 1.818(20); C3-O2 1.267(20); C3-O1 1.245(20); C3-C2 1.538(20); C2-N1 1.480(20); C2-C1 1.523(20); angles (°) O1-C3-O2 125.73(100); O1-C3-C2 117.25(100); O2-C3-C2 117.01(100); N1-C2-C1 112.05(100); N1-C2-C3 109.67(100); C1-C2-C3 113.39(100). Hydrogen atoms attached to carbon and nitrogen were placed geometrically and not refined. The numbering scheme used is the same as CSD refcode LCYSTI14 (Dahaoui, *et. al.* 1999).

All non-hydrogen atoms were refined with anisotropic displacement parameters to 2.3 GPa. At 3.7 GPa only the sulfur atoms were refined anisotropically, while all other non-hydrogen atoms were refined with isotropic displacement parameters. This parameterisation strategy was dictated by the quality of the data collected: reflections broadened with increasing pressure, making indexing and integration increasingly difficult. Acceptable refinements could be obtained for the final 5.0 and 6.4 GPa data sets; unit cell dimensions at these pressures were a = 5.21970(10), c = 52.793(6) Å and a = 5.1852(3), c = 52.172(7) Å, respectively. The deterioration of the data quality was the result of increasing mosaic spread with increasing pressure, a frequent problem with crystallographic pressure studies on soft materials. Listings of crystal and refinement data are given in Table 4.1.

4.2.4 High Pressure Data Collection on Station 9.8, SRS, Daresbury Laboratory.

High-pressure single-crystal diffraction experiments may be carried out at SRS, Daresbury Laboratory on Stations 9.8 and 16.2SMX. Both facilities are equipped with Bruker D8 3-circle fixed-χ goniometers with APEXII detectors. On most currently-available models of home-laboratory X-ray diffractometer it is necessary to re-machine the collimator and beam-stop in order that full ϕ-rotations may be performed. This is not necessary on a synchrotron beam-line because the fixed distance constraints of tube to collimator housing are absent. In 'high-pressure mode' at the SRS the collimator is retracted towards the X-ray source by 30 mm into the space where the tube housing and

optics would usually sit. This increases the collimator to sample distance to allow full 360° rotation in ϕ; rotations in ω are restricted only by the position of the detector. The distance from sample to beam stop a custom beam was set at 70 mm. Alignment procedures follow Dawson *et al.* (2004). We have found that the ease and simplicity of setup combined with small beam divergence and high brightness allows high pressure to be a routine option for users of the facilities at the SRS.

4.2.5 Software for Structure Analysis

Crystal structures were visualized using the programs CAMERON Watkin *et al.*, 1993), DIAMOND (Crystal Impact, 2004), MERCURY (Bruno *et al.*, 2002) and XP (Sheldrick, 1997). Analyses were carried out using PLATON (Spek, 2004), as incorporated in the WIN-GX suite (Farrugia, 1999). Searches of the Cambridge Database (Allen, 2002; Allen & Motherwell, 2002) were performed with the program CONQUEST and version 5.26 of the database with updates up to November 2004.

Topological calculations of void distributions were carried out with TOPOS (Blatov *et al.*, 2000, Blaton & Shevchenko, A.P., 2003). Considerable simplification of the void distributions can be gained by clustering; voids were therefore clustered using what the program calls the 'floating' method with the 'size' parameter specified as 1.0.

Equation-of-state calculations were carried out with EOSFIT (Angel, 2002).

4.3 Results

4.3.1 The structure of hexagonal L-cystine at ambient pressure

L-cystine crystallises in two polymorphic forms: a tetragonal phase ($P4_1$) that was characterised by Chaney & Steinrauf (1974) and a hexagonal phase ($P6_122$) first investigated by Oughton & Harrison (1959) but more recently in a charge density study, by Dahaoui *et al.* (1999). We have re-determined the structure at room temperature (Figure 4.1) in order to be able to compare all structures obtained here under similar conditions of temperature. Though we quote our own room-temperature structural parameters, our interpretation of the structure owes much to the paper of Dahaoui *et al.* (1999), which, in addition to describing the structure of cystine at high-resolution, also contains a database survey of geometries and interactions of crystal structures containing –CSSC- moieties.

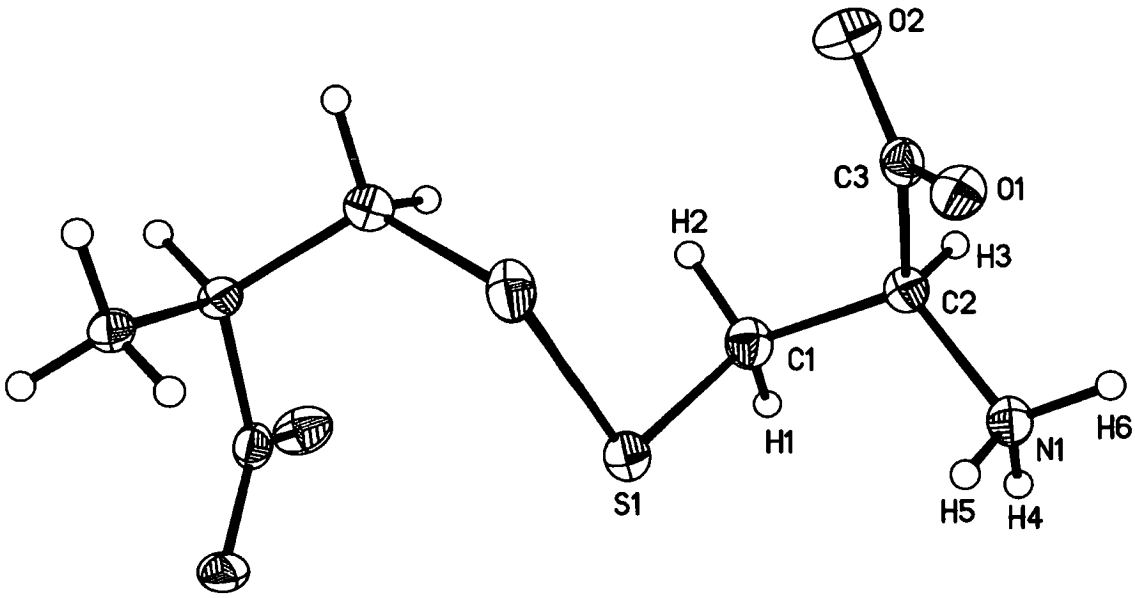

Figure 4.1: The molecular structure of L-cystine at ambient temperature and pressure showing atom labelling. Ellipsoids are drawn at the 30% probability level, and H-atoms are shown as spheres of arbitrary radius.

Both the tetragonal and hexagonal phases of L-cystine crystallise with the molecule in its zwitterionic form. The S-S bond distances in the two polymorphs [2.042(6) and 2.043(2) Å, respectively] do not differ significantly from the average for such bonds in the Cambridge Database [2.039(2) Å]. The same comment applies to the C-S-S-C torsion angle, which is positive in both forms [69.3(2)° and 75.18(5)°, respectively]. The hydrochloride and hydrobromide salts of L-cystine have both been structurally characterised in the anhydrous forms and as dehydrates; interestingly, these all have negative C-S-S-C torsion angles in the range -79° to -83°. The length of S-S bonds in compounds containing C-S-S-C moieties has been shown to be dependent on the torsion angle about the S-S bond: torsion angles which approach 90° result in short S-S bonds because π-interactions are optimised and repulsions between S-based lone-pairs are minimised (Dahaoui *et al.*, 1999).

In this study the effect of pressure on the crystal structure of the hexagonal phase was studied. The principal intermolecular interactions take the form of unusually short S...S contacts and NH...O hydrogen bonds, formed between the ammonium and carboxylate moieties. The NH...O H-bonds lead to the formation of layers which lie perpendicular to the *c*-axis. The layers can be considered to be formed from the intersection of two primary *C*(5) chain motifs (Bernstein *et al.*, 1995), one via N1-H4...O1 interactions, the other via N1-H5...O2 interactions (Figure 4.2*a*). The first of

these interactions is substantially bifurcated (Jeffrey & Maluszynska, 1982) with donor-to-acceptor distances (*i.e.* N...O) in N1-H4 ... O1/O2 measuring 2.792(5)/3.147 (5) Å.

The structure of the layers is strongly reminiscent of layers formed perpendicular to the *b*-axis in α-glycine (Figure 4.2*b*, Boldyreva *et al.*, 2003). In both cases intersection of the *C*(5) chains leads to formation of a secondary-level $R^4_4(16)$ ring motif. In the asymmetric unit of LCYSTI14, and all the structures reported here, the chains based on N1-H4 ... O1 and N1-H5 ... O2 interactions are respectively formed along lattice-repeats in the [010] and [110] directions, but these directions interchange for successive layers generated by the 6_1 screw axis. Head-to-tail NH...OOC motifs are often observed in amino acid structures and are usually associated with a cell dimension of *ca* 5.5Å. This is also observed in L-cystine with an *a*-axis length of 5.4203(5) Å.

The hydrogen bonded layers are linked to other such layers on one side by covalent S-S bridges and on the other by NH ... O hydrogen bonds (Figure 4.3). The latter are formed via N1-H6...O1 interactions, which connect pairs of molecules in successive layers, forming an $R^2_2(10)$ ring motif (Figure 4.4).

Weak CH...O hydrogen bonds are also present at ambient pressure and can play an important role in stabilising medium-strength hydrogen bonds e.g. NH...O (Desiraju & Steiner, 1999; Derewenda *et al*,. 1995). Under ambient pressure two such interactions are present, both of which occur within the glycine-like layers already described. The first of these, C1-H1...O2, runs approximately parallel to N1-H4...O1 and bisects the $R^4_4(16)$ ring motif described above, while the second, C2-H3...O1, runs in the same direction as N1-H5...O2. If all other hydrogen bonding interactions are ignored, these weak C-H...O interactions combine to produce an $R^4_4(16)$ ring motif of their own (Figure 4.2*c*).

At ambient pressure S...S intermolecular interactions are formed (Figure 4.3); the S ... S distance [3.444(4) Å] is much shorter than the sum of the van der Waals radii of the sulfur atoms (3.7Å). At 110 K this distance is 3.4264(4) Å (Dahaoui, *et. al.*,1999). These interactions run perpendicular to the *c*-axis direction, and the S...S contact is approximately co-linear with the S-S covalent bond. Trends in the geometries of such interactions have been shown to be consistent with donation of a lone-pair into an S-S-based σ* molecular orbital (Dahaoui *et al.*,1999).

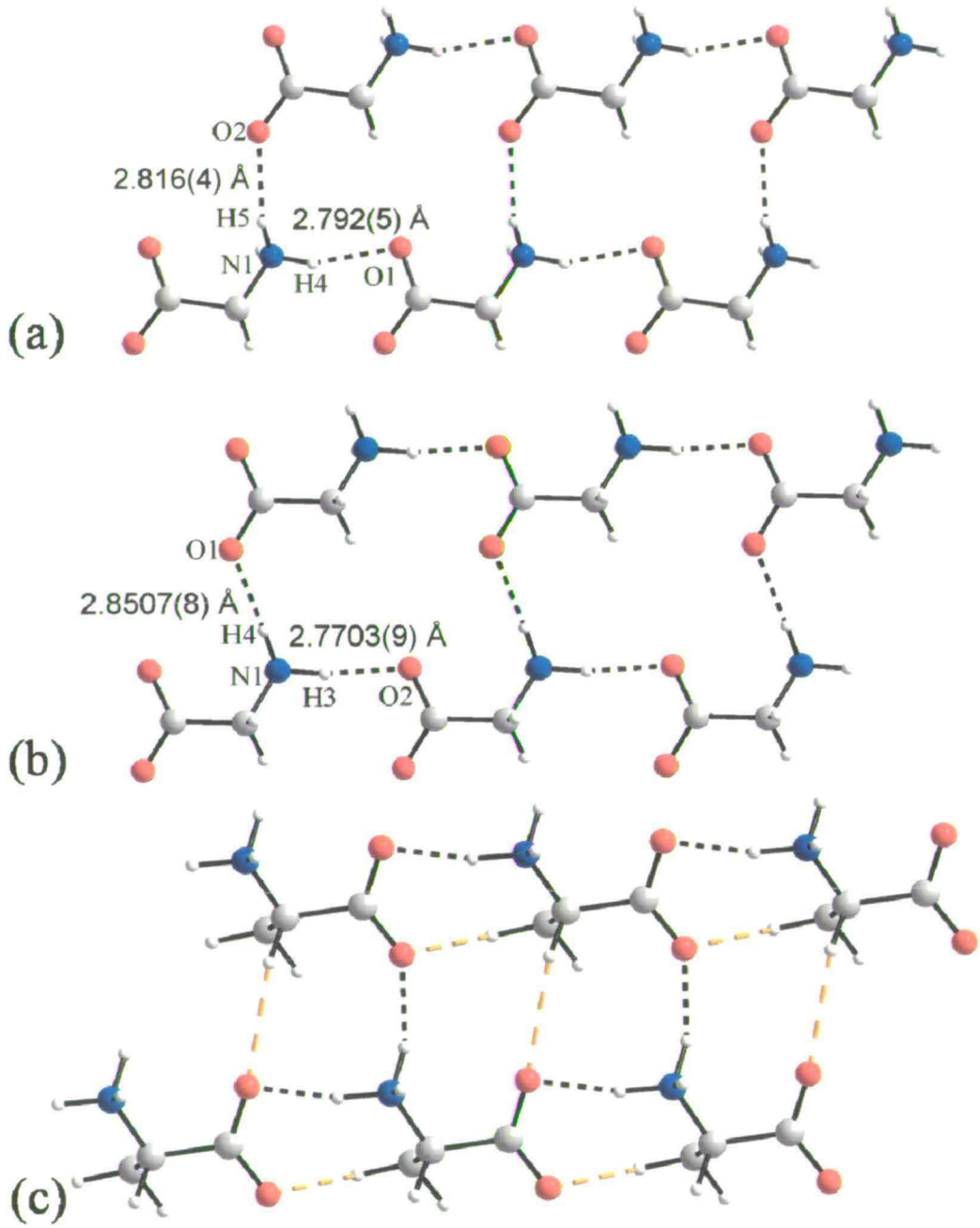

Figure 4.2: $R^4_4(16)$ ring motifs in (*a*) hexagonal L-cystine and (*b*) α-glycine, as viewed perpendicular to the *c* and *b*-axes, respectively; the figures correspond to N...O distances in N-H…O hydrogen bonds. (*c*) $R^4_4(16)$ ring motifs created by interlaced CH...O and NH...O interactions in cystine as viewed perpendicular to the *c*-axis. The black dotted lines represent the ring motif as created by NH...O hydrogen bonds [*cf* (*a*)], while the orange dotted lines, show the interlaced ring motif as created by CH...O interactions. In (*a*) and (*c*) only the basic α-amino acid unit involved within the ring-motif is shown for the sake of clarity. Colour scheme C grey, H white, O red and N blue.

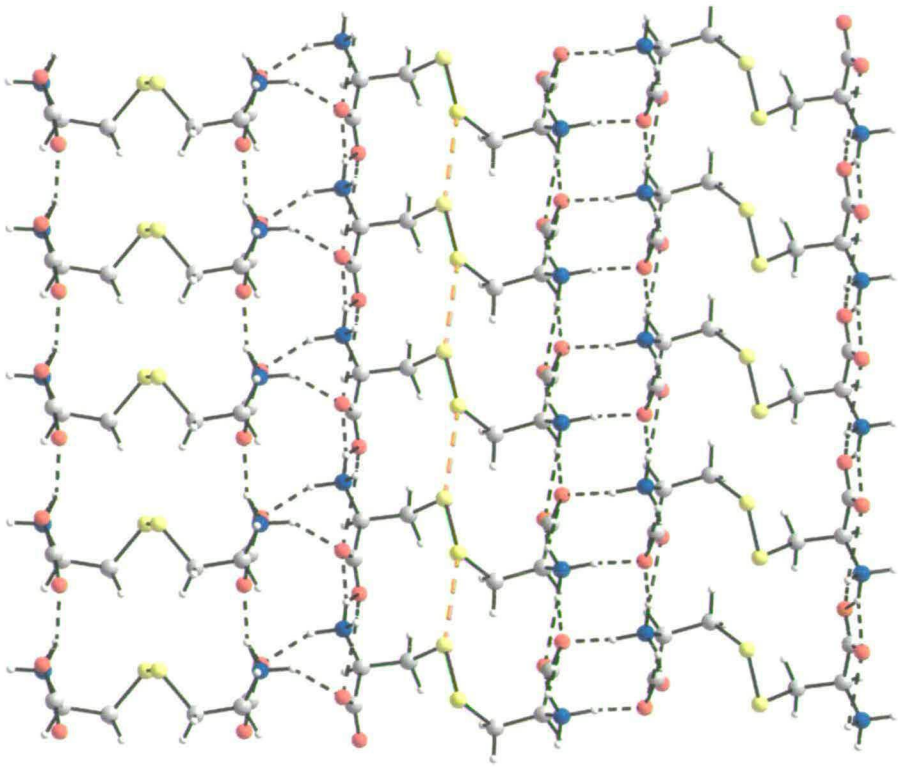

Figure 4.3: H-bonded glycine-like double layers linked down the *c*-axis by disulfide bridges. This view is along *a*, with the *c*-axis running from left to right. The dashed black lines correspond to N...O hydrogen bonds; the dashed orange lines are S…S contacts. Sulfur is shown in yellow, but otherwise the colour scheme is as Figure 4.2.

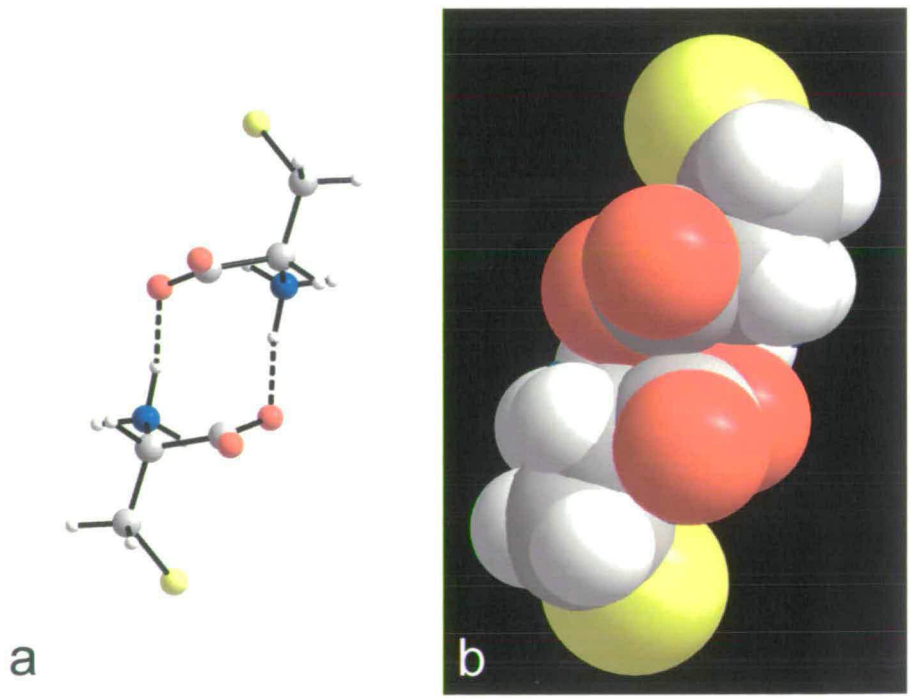

Figure 4.4: $R^2_2(10)$ ring-motif as viewed perpendicular to the *c*-axis. (*a*) is a standard ball-and-stick model and (b) represents the space filling model of (a) on the same scale. Half of each L-cystine molecule has been removed for clarity. Note the apparent lack of free space at the centre of the $R^2_2(10)$ ring.

4.3.2 *The response of hexagonal L-cystine to pressure up to 3.7 GPa*

Hexagonal L-cystine was found to be stable up to 6.4 GPa. However, no structural data could be extracted above 5.0 GPa, and even at this pressure the refined parameters are imprecise. Therefore only structural data to 3.7 GPa were used for comparison to the ambient pressure structure. The S-S distance appears to decrease from 2.043(2) to 2.038(5) Å, though this is not statistically significant. Other bond distances and angles were restrained during refinement to their ambient pressure values, and so no conclusions about their variation with pressure should be drawn from these data. Significant changes do occur in the torsion angles, however. The C-S-S-C torsion angle reduces from 75.20(7)° at ambient pressure, to 72.3(4)° at 3.7 GPa, while the N1-C2-C3-O2 torsion angle (also referred to as NCαCO or ψ in macromolecular crystallography) also reduces from 166.12(8)° to 164.1(7)°.

4.3.3 *Lattice Parameters*

The response of the lattice parameters of hexagonal L-cystine to pressure is anisotropic, with the principal component of the strain tensor acting in the *c*-axis direction. Between ambient pressure, and 6.4 GPa the *c*-axis reduces in length by 6.8%; the reduction in the *a*-axis length is 4.4%. The volume change in the initial 0.4 GPa range is approximately 1.0%, while from 0.4 to 6.4 GPa the volume changes by approximately 2.8% every 1.0 GPa until the sample became poly-crystalline.

Changes in unit-cell dimensions and volume as a function of pressure are plotted in Figure 4.5. The strain induced within molecular systems by pressure is usually anisotropic, and in layered structures the greatest direction of strain is often observed to be normal to the layers. Such behaviour has been observed, for example, in the monoclinic and orthorhombic polymorphs of paracetamol (Boldyreva *et al.*, 2000, 2002) and is also observed in L-cystine, where the direction of greatest compressibility is normal to the glycine-like layers formed within the structure.

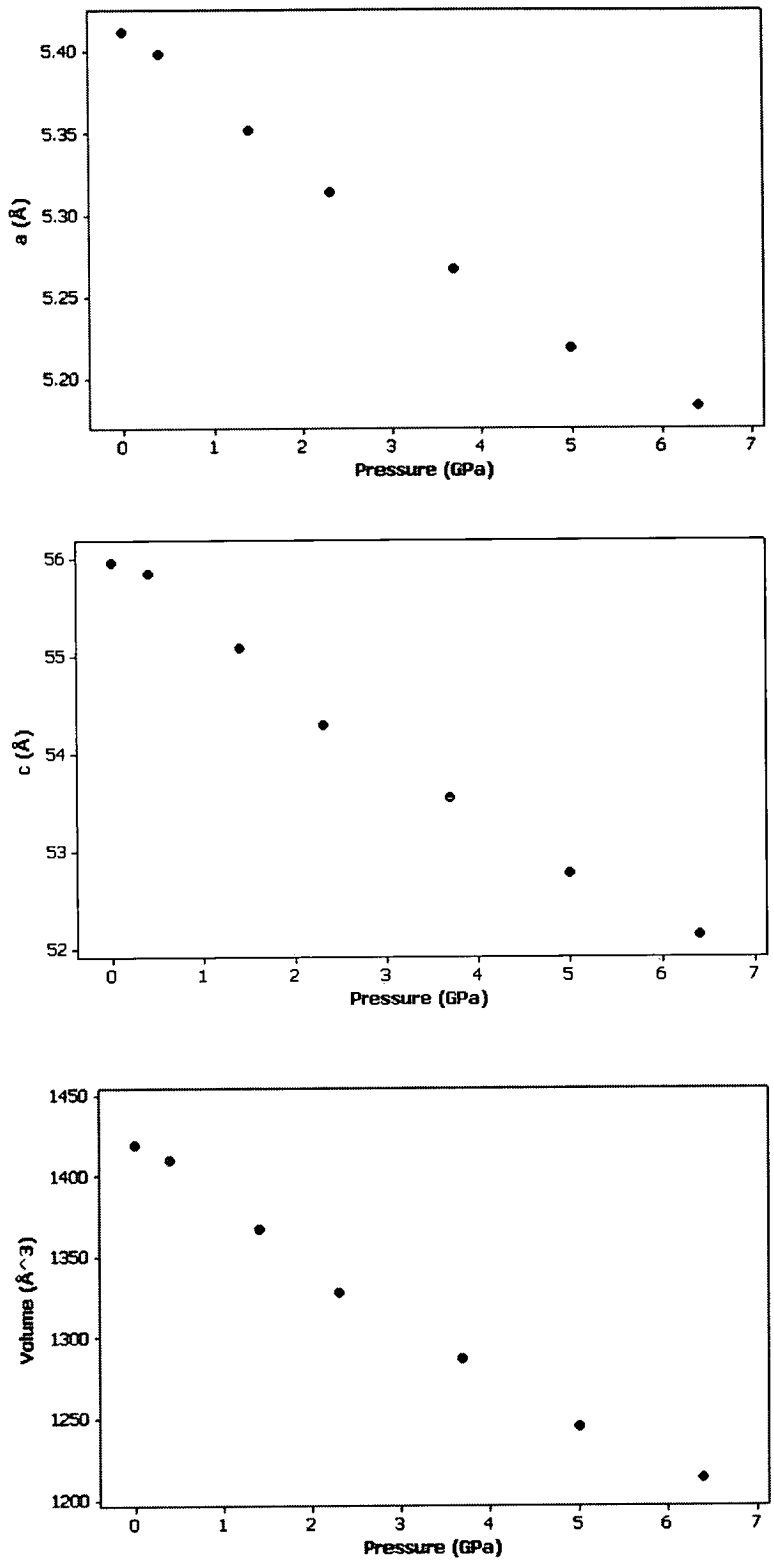

Figure 4.5: Variation of lattice parameters (*a*, *c*, Å) and volume (Å^3) of hexagonal L-cystine as a function of pressure (GPa).

The bulk modulus (B_0), refined for a Birch-Murnaghan equation-of-state (Birch, 1947; Angel, 2000) to second order, is 29.1(4) GPa. The data-set used to calculate this quantity is admittedly rather limited, and the values of V_0, B' and B'' were fixed at 1424.3 Å^3, 4 and -0.1337 GPa^{-1}, respectively. Molecular solids typically have B_0 < 30 GPa (Angel, 2004), and the value obtained for L-cystine-I is towards the high end of this range. Slebodnick *et al.* (2004) quote the following B_0 values which are useful for comparison: $Ru_3(CO)_{12}$ (6.6 GPa); NaCl (25 GPa), quartz (37 GPa), ceramics (50-300 GPa) and diamond (440 GPa).

4.3.4 NH...O Hydrogen Bonds

Variation in hydrogen bonding parameters between ambient and 3.7 GPa are given in Table 4.2. H-atoms were placed in idealised positions during refinement, and so we quantify hydrogen bonding with increasing pressure by using hydrogen bond donor-to-acceptor (N...O) distances, rather than H...O distances.

The most compressible of the NH...O hydrogen bonds was found to be the longer interaction in the bifurcated N1-H4...O1/O2 H-bond. Between 0 and 3.7 GPa N1...O2 shortens from 3.147(5) to 2.970(7) Å at 3.7 GPa. The shorter of the H-bonds, N1-H4...O1, also decreases in length from 2.792(5) Å to 2.643 (7) Å. This head-to-tail H-bonding interaction is also observed in α-glycine and serine, but in these structures it is less compressible than observed in this study, shortening from 2.7703(9) to 2.740(7) Å in α-glycine at 6.2 GPa, and from 2.871(3) to 2.775(13) Å in serine at 4.8 GPa.

The other hydrogen bond formed within the glycine-like layers, N1-H5...O2, decreases in length from 2.816(4) Å to 2.690(18) Å. A search of the Cambridge Database reveals that there are no ambient-pressure amino acid structures (out of 213 hits) with N-H...O interactions shorter than N1...O1 at 3.7 GPa, and only three amino acid structures shorter than N1...O2 at 3.7 GPa. The shortest interaction at ambient pressure [2.661(2) Å] was observed in L-arginine L-glutamate trihydrate (DUSMAF; Suresh *et al.*, 1986).

The fourth hydrogen bond, N1-H6...O1, which interacts between the layers to form an $R^2_2(10)$ ring motif, decreases in length from 2.842(4) Å to 2.786(14) Å at 3.7 GPa. The O...C contacts formed between the carboxyl groups across the rings are of a similar length at ambient pressure [3.243(1) Å] to those observed in dipolar C=O...C=O contacts (2.92 – 3.32 Å), though the geometry does not match any of the common types identified by Allen *et al.* (1998). These contacts also shorten only modestly to 3.200(14)

Å at 3.7 GPa. For comparison, the sheared-parallel C=O...C=O contacts formed in acetone at 0 and 1.5 GPa are 3.587(3) and 3.365(2) Å in acetone-II (Allan *et al.*, 1999).

This is the least compressible of the head-to-tail NH...OOC interactions even though it is formed in the same direction as the most compressible unit cell dimension, the *c*-axis.

Pressure/GPa	0	0.4	1.4	2.3	3.7
N1H4..O1[i] N1..O2	2.792(5)	2.777(2)	2.732(2)	2.693(4)	2.643(7)
N1H4..O2[i] N1..O2	3.147(5)	3.119(2)	3.071(3)	3.029(3)	2.970(7)
N1H5..O2[ii] N1..O2	2.816(4)	2.806(3)	2.769(3)	2.742(4)	2.703(8)
N1H6..O1[iii] N1..O1	2.842(4)	2.829(5)	2.815(5)	2.781(8)	2.786(14)
C1H1..O2[i] C1..O2	3.259(6)	3.235(3)	3.190(3)	3.153(5)	3.124(9)
C2H3..O1[iv] C3..O1	3.499(4)	3.480(2)	3.407(2)	3.355(3)	3.285(6)

Symmetry operators:

i	*x*,-1+*y*,*z*
ii	1+*x*,*y*,*z*
iii	1+*x*-*y*,2-*y*,-*z*
iv	-1+*x*,-1+*y*,*z*

Table 4.2: Hydrogen bonding parameters in hexagonal L-cystine. Distances are in Å, of which only D...A distances are given (see experimental).

4.3.5 CH...O Hydrogen Bonds

Within the glycine-like layers the compression of weak C-H...O interactions parallels the compression of the N-H...O interactions. The more compressible is C2-H3...O1, which shortens from C...O = 3.499(4) Å to 3.285(6) Å. This interaction runs

approximately parallel to the N1-H5...O2 hydrogen bond. C1-H1...O2 (formed in the same direction as the N1-H4...O1) shortens from 3.259(6) Å to 3.124(9) Å.

4.3.6 S...S Interactions

The structure of L-cystine is notable for the formation of S...S contacts which are substantially shorter [3.444(4) Å] than the sum of the van der Waals radii of the sulfur atoms (3.6 Å; Bondi, 1964). Under pressure, this contact shortens to 3.263(4) Å at 3.7 GPa. A search of the Cambridge Database reveals 19 entries containing a $C(sp^3)$-S-S-$C(sp^3)$ fragment in which an S...S contact is observed between 2.5 and 3.7 Å. All of these structures were determined at ambient pressure. The distribution is rather uniform in this distance range, but the shortest contact so-far observed (Refcode KOWMEO, Fujimura *et al.*, 1992) measures 3.31 Å. The application of pressure has therefore caused the S...S interaction to reduce in length close to below the lower distance-limit observed under ambient pressure conditions.

4.4 Discussion

4.4.1 Anisotropic compression of L-cystine

In pressure studies of α-glycine and L-serine-I we have ascribed trends in the relative compressibilities of C-H...O and N-H...O hydrogen bonds to the closing-up of voids existing in the structure at ambient pressure. At pressure these voids contract with the shortening of N-H...O and C-H...O interactions. Similar conclusions on the importance of void-closure were drawn in a study of $Ru_3(CO)_{12}$. Recent work by Blatov & Shevchenko (2003) makes it possible to analyse the sizes and distributions of voids in crystal structures using the Voronoi-Dirichlet formalism.

The environment of an atom in a crystal structure can be visualised using a Voronoi-Dirichlet polyhedron or VDP (Peresypkina & Blatov, 2000*a* and 2000*b*). Voronoi-Dirichlet analysis is a method for partitioning space amongst points which occupy that space. A point is separated from a neighbouring point by a plane which bisects the vector between them. This construction is repeated for every pair of points to yield a subdivision of the space into cells which each contain one point. VDP analysis carried out using individual atoms to define the points leads to a *molecular* VDP, and these correspond to a complete partitioning of space in a crystal structure. Interatomic interactions occur at the points in the structure where faces of VDPs meet, whereas the

topological definition of a void is a point at which the vertices of VDPs meet (Blatov & Shevchenko, 2003).

Figure 4.6*a* shows the distribution of voids in the crystal structure of L-cystine at ambient pressure. The largest void conglomerate in the structure occurs in the vicinity of the sulfur atoms; this is labelled '1' in Figure 4.6*a*. These voids straddle the short intermolecular S...S contact of 3.444(4) Å, and the contraction of this distance to 3.263(4) Å at 3.7 GPa is consistent with the orientation of the void-conglomerates in this region of the structure.

Figure 4.6*b* shows the distribution of voids in the region of the $R^4_4(16)$ rings formed in the glycine-like layers; this region is labeled '2' in Figure 4.6*a*. Figure 4.7 illustrates the sizes of the voids in cystine at ambient pressure; the close correspondence between the positions of the voids in Figure 4.7*a* and the largest void positions in Figure 4.6*b* is readily apparent. On compression to 3.7 GPa the sizes of the voids in the $R^4_4(16)$ ring are reduced, leading to the observed shortening in the CH...O and NH...O hydrogen bonds which form within these layers. It is notable that the S...S interaction is approximately parallel to the N1-H4...O1 $C(5)$ chains, and the change of -0.18 Å in the former is reflected in the -0.15 Å change in the latter.

There is a collection of voids between the glycine-like sheets in the region labeled '3' in Figure 4.6*a*. Voids are less evident within the $R^2_2(10)$ ring motifs which connect pairs of glycine-like layers, than in the $R^4_4(16)$ rings formed within the layers (see also Figure 4.4). This may explain why the N1-H6...O1 hydrogen bond is the least compressible of the N-H...O interactions in the system. Larger voids do exist elsewhere in region '3', though, as shown in Figure 4.6*a*. There is a marked contraction of the void between the two oxygen atoms labeled O2 in Figure 4.8, with the O...O distance reducing from 3.643(4) to 3.350(15) Å, between ambient pressure and 3.7 GPa. The reduction of the N1-C2-C3-O2 torsion angle from 166.12(8)° to 164.1(7)° may also be associated with the void closure in this region of the structure. Overall the distance between the planes containing the C2 (or C_α) atoms in neighbouring glycine-like layers (labelled A in Figure 4.9) reduces from 3.729(2) Å at ambient pressure to 3.539(21) Å at 3.7 GPa.

The final conglomerate of voids (4) occurs in the region formed by the NH_3-CH-CH_2-S moieties. The C-S-S-C torsion angle reduces from 75.27(18)° at ambient pressure, to 72.3(4)° at 3.7 GPa. Since the S-S bond is approximately perpendicular to the *c*-axis.

The conformational change reduces the height of the molecule in the *c*-direction, and the distance between the planes containing the C_α atoms either side of the disulfide bridges (labelled 'B' in Figure 4.9) reduces from 5.597(2)Å at ambient pressure to 5.386(22) Å at 3.7 GPa. The twisting action of the L-cystine molecules could be described as a molecular 'spring', whose action allows the compression of the structure along the *c*-axis direction.

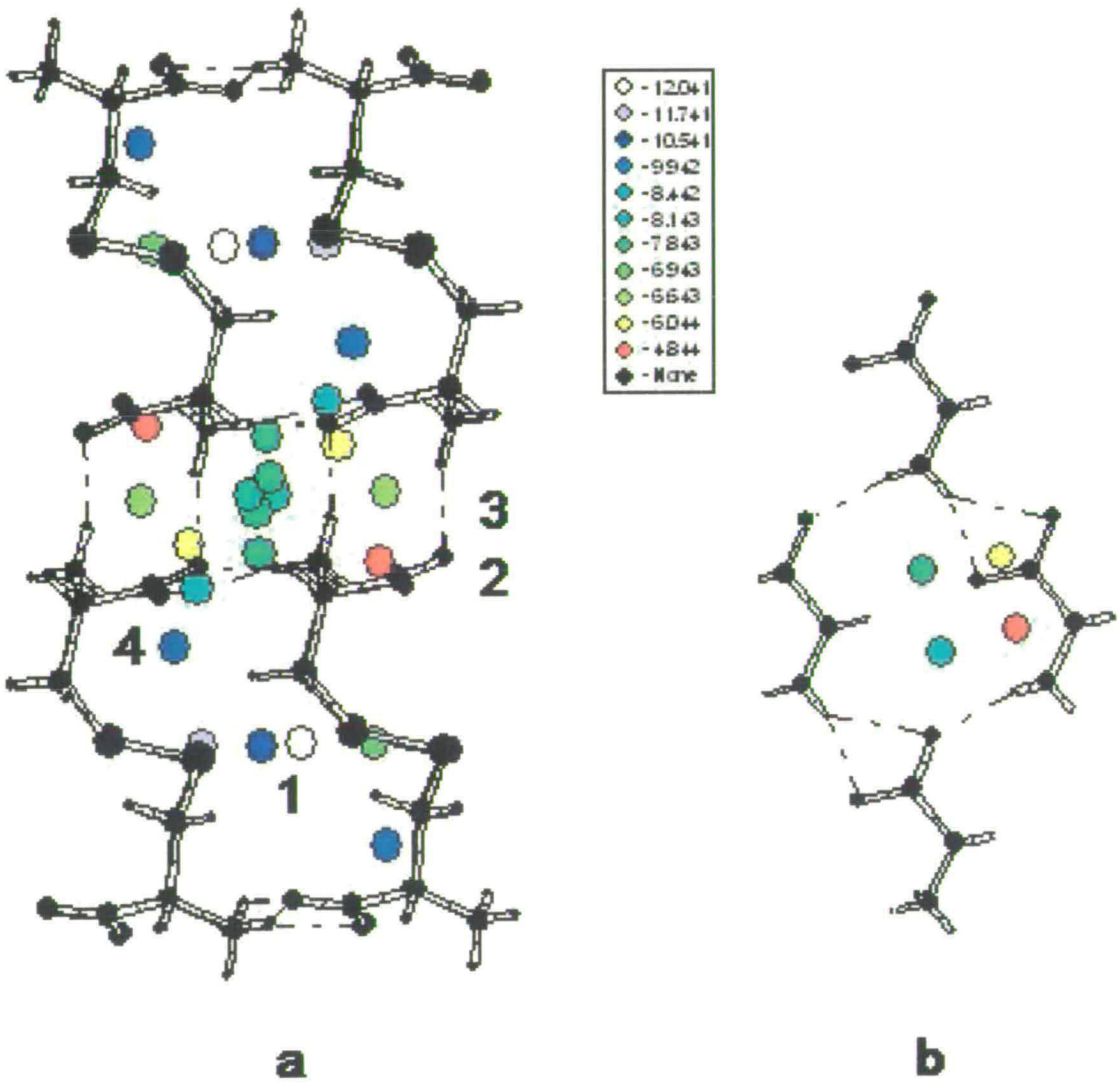

Figure 4.6: (*a*) The distribution of voids in cystine under ambient conditions, viewed with the *c*-axis vertical. The numbers 1-4 refer to regions of the structure, as discussed in the text. (*b*) Voids in the glycine-like $R^4_4(16)$ layers under ambient conditions. The colour scheme represents the volumes of the VDPs of the voids (in $Å^3$) as discussed by Blatov; the largest void is shown in white, voids then progressively decrease in volume from blue to red; precise values are given in the legend.

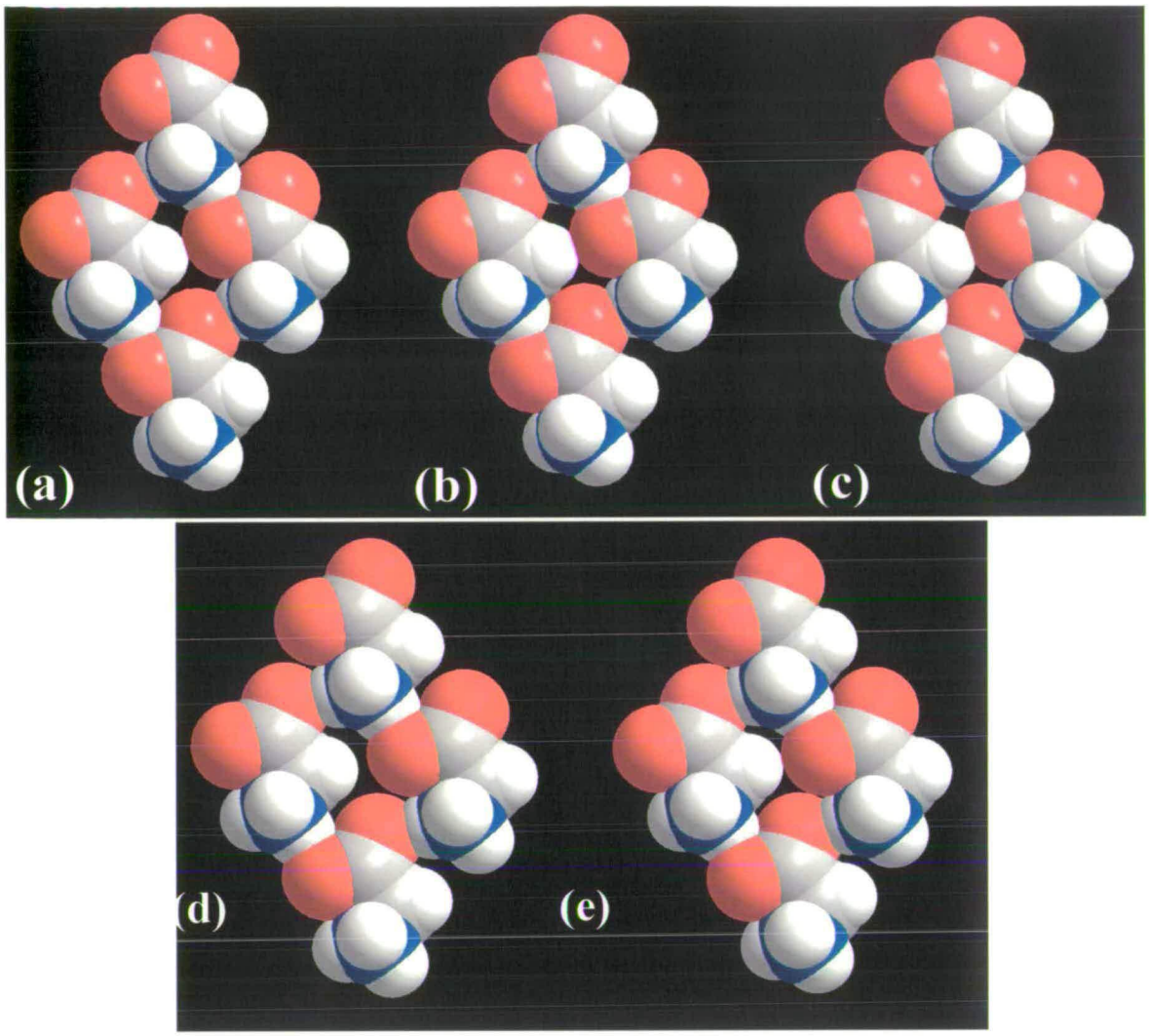

Figure 4.7: Space-filling plots showing $R^4_4(16)$ ring-motifs in L-cystine at ambient temperature and pressure (*a*), 2.3 GPa (*b*) and 3.7 GPa (*c*) and α-glycine at ambient temperature and pressure (*d*) and at 2 GPa (*e*). Notice the reduction in the sizes of the voids in the middle of the ring motifs with increasing pressure.

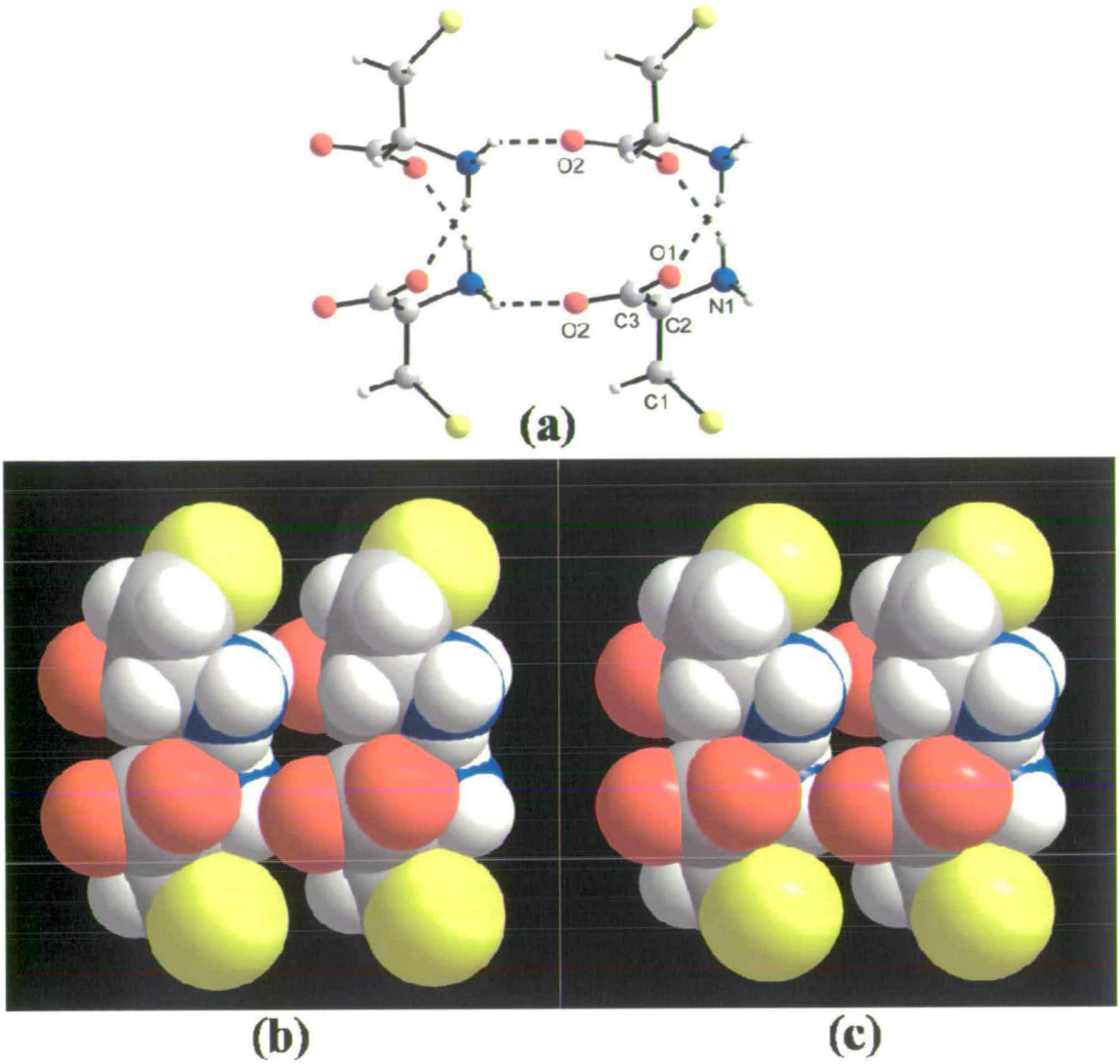

Figure 4.8: Voids formed between glycine-like layers at ambient pressure [(*a*) and (*b*)] and at 3.7 GPa (*c*). Notice the reduction in the sizes of the voids in (*b*) and (*c*) with increasing pressure.

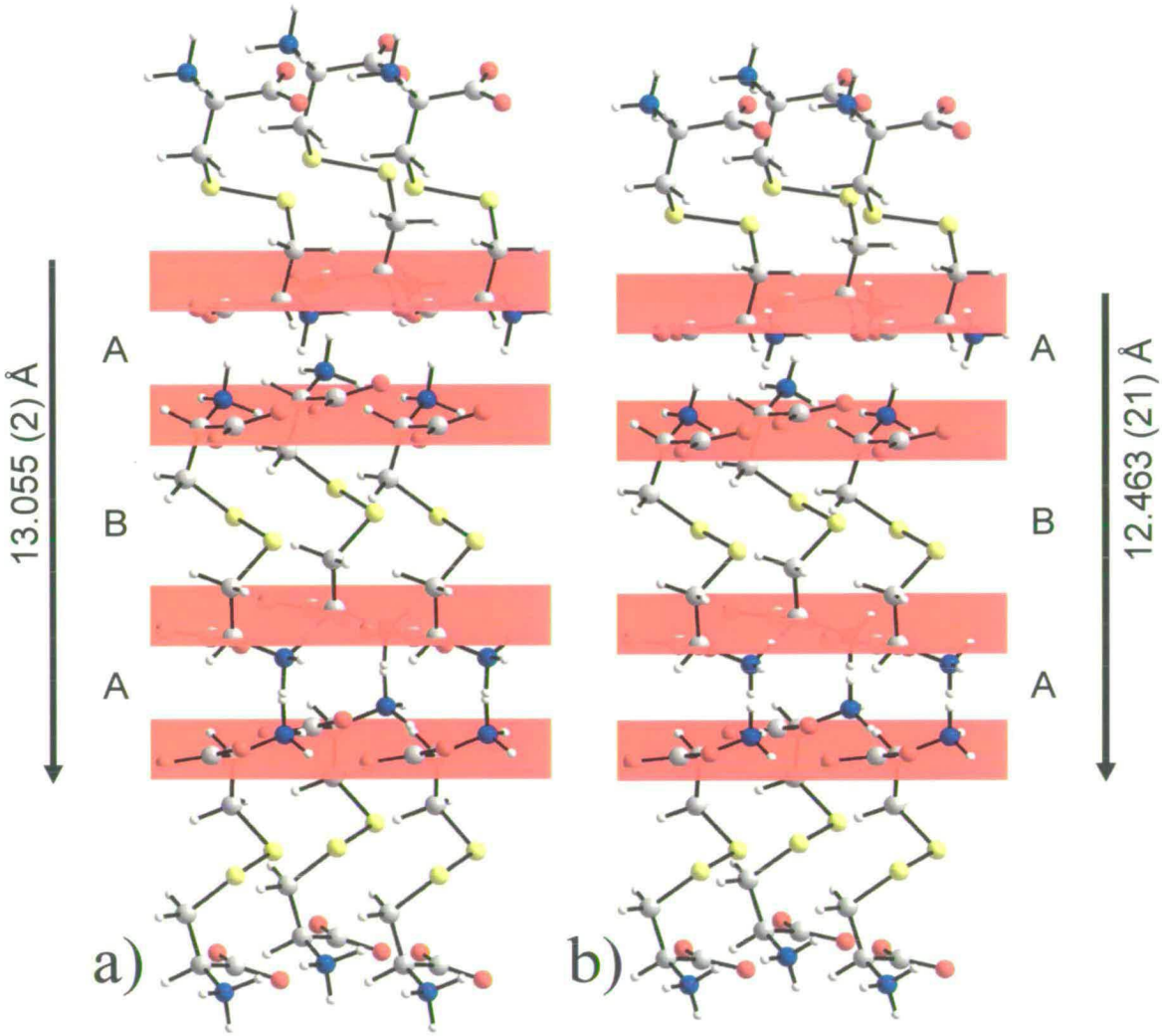

Figure 4.9: Ball-and-stick models of L-cystine at (*a*) ambient pressure and (*b*) 3.7 GPa as viewed down (0 1 -2). The red planes are through the Cα carbons in each glycine-like layer running perpendicular to the *c*-axes of each plot. The overall compression of L-cystine caused *via* the 'twisting' of the molecules can be seen in compression between the layers (A), and between pairs of layers (B). The distance between layers (A) and (B) reduces from 3.729(2) to 3.539(21) Å, and 5.597(2) to 5.386(22) Å from ambient to 3.7 GPa, respectively. The distance between the first and last adjacent-pairs of layers for both the ambient and 3.7 GPa data sets is shown.

4.4.2 *Comparison of compression in α-glycine and L-cystine.*

We have previously determined the crystal structure of α-glycine at 2.0 GPa (Dawson *et al.*, 2005), and in this paper we report the crystal structure of L-cystine at 2.3 GPa. Given the similarity in the layer structures of L-cystine and α-glycine it is interesting to compare the effect of pressures around 2 GPa on this part of the two crystal structures. Figure 4.7 compares the voids in the two structures as a function of pressure.

α-Glycine is the more compressible of the two structures and at 2 GPa its unit cell volume is 90% of its ambient pressure value; the corresponding figure of cystine is 93%. Comparison of Figures 4.7 *a* and *d* suggests that the voids in the centres of the $R^4_4(16)$ rings are slightly larger in α-glycine than in cystine, and this observation can be quantified by comparison of the respective areas of the *ac* and *ab* unit cell faces in the two structures.[1] At ambient pressure these areas are 25.904(2) Å^2 for glycine and 25.444(3) Å^2 for cystine. At 2 GPa the areas are remarkably similar: 24.429(8) Å^2 for glycine and 24.446(1) Å^2 for cystine.

The overall similarity of the structures of the glycine-like layers is reflected in the similarity of the mean values of the principal components of the strain tensor which reside in the layers in both structures, *viz.* -0.03 for glycine and -0.02 for cystine. That the value for glycine is slightly higher than for cystine is presumably ascribable to the more efficient packing in cystine at ambient pressure.

Compression in the *ab*-plane of cystine is constrained by the crystal symmetry to be isotropic, and this is reflected in the similar responses of the N1-H4...O1 and N1-H5...O2 H-bond distances to pressure (Table 4.2), which shorten by 0.10 and 0.08 Å, respectively. In α-glycine (which is monoclinic with the *b*-direction perpendicular to the view shown in Figures 4.7*d* and *e*) the strain is markedly anisotropic. The largest strain component (-0.06) acts to close up the voids in the structure by forming a CH...O interaction as shown in Figures 4.7*d* and *e*. The N-H...O H-bond which forms parallel to this C-H...O interaction shortens by 0.10 Å, whereas the other barely changes in length at all.

[1] The unit cell data for α-glycine at ambient pressure [2.0 GPa] are: monoclinic, a = 5.1047(3) [4.9669(9)], b = 11.9720(14) [11.459(4)], c = 5.4631(3) [5.4231(12)] Å, β = 111.740(5)° [114.916(15)°]. All data were measured at room temperature. Refs: Boldyreva *et al.* (2003) and Dawson *et al.* (2005).

4.5 Conclusions

We have described the effect of pressure on the structure of hexagonal L-cystine at room temperature up to 3.7 GPa, with data on unit cell dimensions reported up to 6.4 GPa. The structure can be described as being composed of pairs of glycine-like layers which lie in the *ab*-plane. Each layer is composed of head-to-tail NH...OOC hydrogen bonds which combine to produce an $R^4_4(16)$ ring motif. Another NH...OOC hydrogen bonding interaction then links the layers together in pairs via a $R^2_2(10)$ ring motif perpendicular to the *c*-axis. Paired layers then repeat down the *c*-axis separated by disulfide bridges about the 6_1-screw axes.

Under pressure, the structure undergoes anisotropic compression with the direction of greatest strain acting in the *c*-axis direction. This direction is normal to the glycine-like layers within the structure, which up to 3.7 GPa are pushed closer together along the *c*-axis direction. This compression occurs with the closing-up of voids which are distributed along the *c*-direction (in regions 3 and 4 in Figure 4.6). As this closure proceeds, two intramolecular torsion angles decrease, C1-S1-S1'-C1' and N1-C2-C3-O2. Compression in the *ab* planes is constrained to be isotropic by symmetry and acts to decrease an already short S...S interaction and to close up voids within the $R^4_4(16)$ rings with a shortening of both N-H...O and C-H...O distances.

4.6 References

Allan, D.R., Parsons, S. & Teat, S.J. (2001). *J. Synchrotron Rad.*, **8**, 10-17.

Allan, D. R., Clark, S. J., Ibberson, R. M., Parsons, S., Pulham, C. R. & Sawyer, L. (1999). *Chem Commun.* 751-752.

Allen, F.H. (2002). *Acta Cryst. B***58**, 380-388.

Allen, F. H., Baalham, C. A., Lommerse, J. P. M. & Raithby, P. R. (1998). *Acta Cryst. B***54**, 320-329.

Allen, F. H. & Motherwell, W. D. S. (2002). *Acta Cryst. B***58**, 407-422.

Angel, R. (2002). *Rev. Mineralogy & Geochemistry*, **41**, 35-59.

Angel, R. (2002). EOSFIT version 5.2. Virginia Tech., Blackburg, VA, USA.

Angel, R. (2004). In *High Pressure Crystallography*. NATO Science Series II. Editors A. Katrusiak & P. McMillan. pp 21-36.

Berman, H. M., Westbrook, J., Feng, Z., Gilliland, G., Bhat, T. N., Weissig, H., Shindyalov, I. N. & Bourne, P. E. (2000) *Nucleic Acid Res.* **28**, 235-242.

Bernstein, J., Davis, R.E., Shimoni, L. & Chang, N-L. (1995). *Angew. Chem. Int. Ed. Engl.*, **34**, 1555-1573.

Betteridge, P.W., Carruthers, J.R., Cooper, R.I., Prout, K. & Watkin, D.J. (2003). *J. Appl. Cryst.*, **36**, 1487.

Bhattacharaya, R., Pal, D. & Chakrabarti, P. (2004) *Prot. Eng. Des. Select.* **17**, 795, 808.

Birch, F. (1947). *Phys. Rev.* **71**, 809-824.

Blatov, V.A., Shevchenko, A.P. & Serezhkin, V. N. (2000). *J. Appl. Cryst.* **33**, 1193.

Blatov, V.A. & Shevchenko, A.P. (2003). *Acta Cryst. A***59**, 34-44.

Boldyreva, E.V. (2004*a*). *J. Mol. Struct.*, **700**, 151-155.

Boldyreva, E.V. (2004*b*). *Crystal Engineering*, **6**, 235-254.

Boldyreva, E. V., Ahsbahs, H. & Weber, H.-P. (2003). *Z. Kristallogr.*, **218**, 231-236.

Boldyreva, E. V., Shakhtshneider, T. P., Ahsbahs, H., Sowa, H. & Uchtmann, H. Journal of Thermal Analysis and Calorimetry (2002), 68(2), 437-452.

Boldyreva, E. V., Shakhtshneider, T. P., Vasilchenko, M. A., Ahsbahs, H., & Uchtmann, H. *Acta Cryst.* (2000). B**56**, 299-309

Bondi, A. (1964). *J. Phys. Chem.* **68**, 441-451.

Bruker-AXS (2003). SAINT version 7. Bruker-AXS, Madison, Wisconsin, USA.

Bruno, I.J., Cole, J.C., Edgington, P.R., Kessler, M., Macrae, C.F., McCabe, P. Pearson, J. & Taylor, R. (2002). *Acta Cryst. B***58**, 389-397.

Cernik, R. J., Clegg, W., Catlow, C. R. A., Bushnell-Wye, G., Flaherty, J. V.; Greaves, G. N., Burrows, I., Taylor, D. J., Teat, S. J. & Hamichi, M. (1997). *J. Synchrotron Rad.*, **4**, 279-286.

Chaney, M.O. & Steinrauf, L.K. (1974). *Acta Cryst. B***30**, 711-716.

Crystal Impact (2004). DIAMOND. Version 3.0. Crystal Impact GbR, Postfach 1251, 53002 Bonn, Germany. (URL: http://www.crystalimpact.com/diamond.)

Dahaoui, S., Pichon-Pesme, V., Howard, J. A. K. & Lecomte, C. (1999). *J. Phys. Chem. A*, **103**, 6240-6250.

Dawson, A., Allan, D.R., Belmonte, S.A., Clark, S.J., David, W.I.F., McGregor, P.A., Parsons, S., Pulham, C.R. & Sawyer, L. (2005). *Cryst. Growth Des.* In press.

Dawson, A., Allan, D.R., Clark, S.J., Parsons, S. & Ruf, M. (2004). *J. Appl. Cryst.*, **37**, 410-416.

Derewenda, Z.S., Lee, L. & Derewenda, U. (1995). *J. Mol. Biol.*, **252**, 248-262.

Desiraju, G.R. & Steiner, T. (1999). *The Weak Hydrogen Bond.* IUCr Monographs on Crystallography No. 9. Oxford University Press, Oxford, UK.

Farrugia, L. J. (1999). *J. Appl. Cryst.* **32**, 837-838.

Fujimura, K., Ito, S., Suhara, H. & Kawashima, Y. (1992). *J.Chem.Res.*, 88-89.

Jeffrey, G.A. & Maluszynska, H. (1982). *Int. J. Biol. Macromol.*, **4**, 173-185.

Merrill, L. & Bassett, W.A. (1974). *Rev. Sci. Instrum.*, **45**, 290-294.

Moggach, S.A., Allan, D.R. Morrison, C.A., Parsons, S. & Sawyer L. (2005). *Acta Cryst. B***61**, 58-68.
Morris, A. L., MacArthur, M. W., Hutchinson, E. G. & Thornton, J. M. (1992) *Proteins: Struct. Funct. Genet.* **12**, 345-364.

Oswald, I. D. H., Allan, D. R., Motherwell, W. S. D. & Parsons. S. (2005). *Acta Cryst. B***61**, 69-79.

Oswald, I. D. H., Allan, D. R., Day, G.M., Motherwell, W. S. D. & Parsons. S. (2005). *Cryst. Growth Des.*, **5**, in press.

Oughton, B.M. & Harrison, P.M. (1959). *Acta Cryst.* **12**, 396-404.

Parsons, S. (2004). *SHADE*. Program for empirical absorption corrections to high pressure data. The University of Edinburgh, Scotland.

Peresypkina, E.V. & Blatov, V.A. (2000*a*). *Acta Cryst.* B**56**, 501-511.

Peresypkina, E.V. & Blatov, V.A. (2000*b*). *Acta Cryst.* B**56**, 1035-1045.

Piermarini, G. J., Block, S., Barnett, J. D. & Forman, R. A. (1975). *J. Appl. Phys.* **46**, 2774-2780.

Richardson, J.S. (1981) *Adv. Prot. Chem.* **34**, 167-339.

Sheldrick, G. M. (1997). *XP.* University of Göttingen, Germany.

Sheldrick, G. M. (2004). *SADABS.* University of Göttingen, Germany..

Slebodnick, C., Zhao, J., Angel, R., Hanson, B. E., Song, Y., Liu, Z. & Hemley, R. J. (2004). *Inorg. Chem.* **43**, 5245-5252.

Spek, A. L. (2004). *PLATON- A Multipurpose Crystallographic Tool*, Utrecht University, Utrecht, The Netherlands.

Suresh, C.G., Ramaswamy, J. & Vijayan, M. (1986). *Acta Cryst. B***42**, 473-478.

Thornton, J.M. (1081) *J. Mol. Biol.* **151**, 261-287

Watkin, D. J., Pearce, L. & Prout, C. K. (1993). *CAMERON - A Molecular Graphics Package.* Chemical Crystallography Laboratory, University of Oxford, England.

Wunschel, M., Dinnebier, R. E., Carlson, S., Bernatowicz. P. & van Smaalen, S. (2003). *Acta Cryst. B***59**, 60-71.

Chapter 5

High Pressure polymorphism in L-Cysteine: The Crystal Structures of L-Cysteine-III and L-Cysteine-IV.[iv]

[iv] Moggach, S. A., Allan, D. R., Clark, S. J., Gutmann, M. J., Parsons, S., Pulham, C. R. & Sawyer, L. (2005). *In press.*

5.1 Synopsis

Compression of orthorhombic L-cysteine-I, which contains molecules in the g^+ conformation, leads to the formation of a new orthorhombic phase (L-cysteine-III) with the molecules in the g^- conformation. Decompression of L-cysteine-III ultimately leads to L-cysteine-I, but this proceeds through an intermediate phase, L-cysteine-IV, which contains molecules in both g^+ and g^- conformations.

5.2 Introduction

The response of crystalline molecular solids to high hydrostatic pressure is a rapidly advancing area of interest in small-molecule crystallography. The extent to which the anisotropy of compressibility can be explained, and how far a structure can be compressed before it undergoes a phase transition, are key issues of current interest. This area has been the subject of a number of recent reviews, for example Boldyreva (2003, 2004a, 2004b), Katrusiak (2004) and Hemley & Dera (2000).

Within the field of organic crystal chemistry a number of monofunctional alcohols (*e.g.* Allan *et al.*, 2001; McGregor *et al.*, 2005; Moggach *et al.* 2005a), phenols (*e.g.* (Oswald *et al.*, 2005), ketones (Allan *et al.*, 1999), carboxylic acids (*e.g.* Allan & Clark, 1999) and amines (Lozano-Casal *et al.*, 2005) have been investigated and shown to be polymorphic at high pressure when crystals are grown by application of pressure to pure liquids. In polyfunctional systems, polymorphs of pharmaceutical compounds have been produced when crystals are grown by careful application of pressure to a concentrated solution (Fabbiani *et al.*, 2003, 2004, 2005*a*, 2005*b*). We have recently described the effect of compression of the three solid forms of glycine (Dawson *et al.*, 2005). Though α-glycine is stable to 23 GPa (Murli *et al.*, 2003), the β- and γ-polymorphs respectively transform to the high-pressure δ- and ε- polymorphs on compression of the solids. L-serine-I transforms to a high pressure polymorph (L-serine-II) at 4.8 GPa (Moggach *et al.*, 2005b).

While compression of a single crystal of γ-glycine yields the ε-phase as a polycrystalline solid, both β-glycine and L-serine-I undergo single-crystal to single-crystal phase transitions to high-pressure polymorphs. The transition from one single-crystalline form to another depends on the similarity of the topology and orientations of the molecules in the two phases. The β-to-δ-glycine transition is accomplished by a quite

modest conformational change of the glycine molecules; the L-serine-I to L-serine-II transition is characterised by a change in the H-O-C-C torsion angle and a small shift of the molecules relative to each other. In the γ-to-ε-glycine transition a more substantial reorientation of the molecules occurs, leading to break-up of the crystal.

The relative compressibility of crystals of serine and glycine, as well as cystine and several other amino acids, along different crystallographic directions could all be rationalised in terms of the distributions and shapes of intermolecular voids.

Cysteine is an important amino acid in biology. Although the average amount present in proteins is less than 2%, the properties of its side-chain thiol suit it to metal-binding both intra-and extra-cellularly. Generally, within the reducing environment of the cell, it exists as cysteine while its oxidation to cystine provides a covalent cross-link in many secreted proteins like insulin and trypsin. Mercury, lead and other heavy metals tend to displace metal ions like copper and zinc with concomitant modification to the biological properties. With increased pressure, proteins tend to unfold, water being forced into their interior (Hummer *et al.*, 1998), at relatively modest pressures (0.3-0.8 GPa) and to date, it is unclear how the effects of pressure are related to the amino-acid composition. As a prelude to answering this question, we are examining the effects of pressure on the individual amino-acids and we now describe the effect of pressure (up to 4.3 GPa) on the crystal structure of the orthorhombic phase of L-cysteine.

Prior to this work, L-cysteine (Figure 5.1*a*) was known to crystallise in two forms, an orthorhombic phase, ($P2_12_12_1$, Z' = 1) and a monoclinic phase, ($P2_1$, Z' = 2). We refer to these phases as L-cysteine-I and L-cysteine-II, respectively. The crystal structure of the orthorhombic form, L-cysteine-I, was determined by Kerr & Ashmore (1973) by X-ray diffraction and then again by Kerr *et al.* (1975) by neutron diffraction. We have also recently determined the structure at 30 K (Moggach *et al.*, 2005d). L-cysteine-II was characterised at ambient temperature by Harding & Long (1968) and later by Görbitz & Dalhus (1996) at 120 K; both of these determinations employed X-ray diffraction. The structure of the racemate, D,L-cysteine, was determined by Luger & Weber (1999).

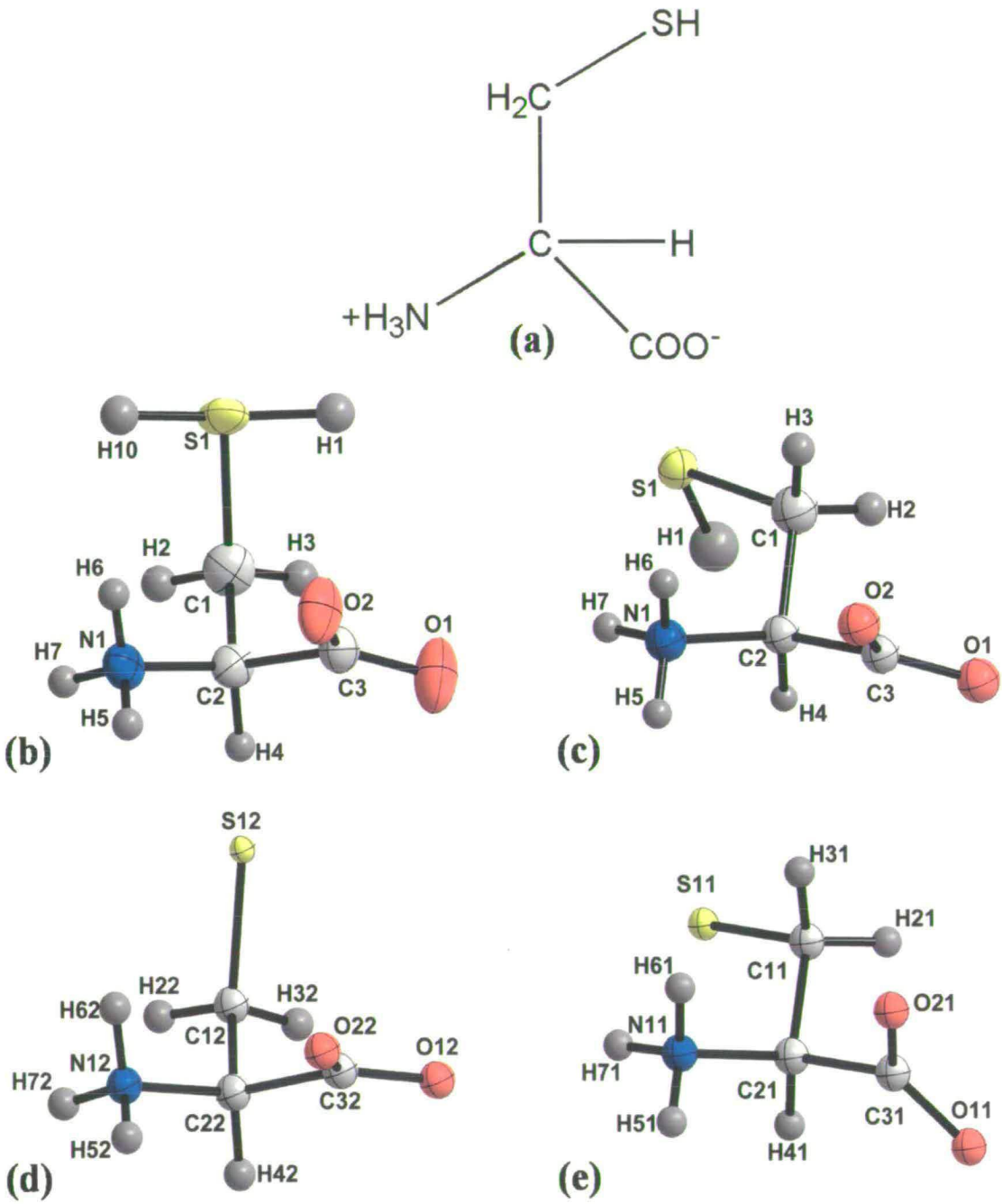

Figure 5.1: (*a*) The chemical structure of L-cysteine in its zwitterionic form. Thermal ellipsoid plots showing numbering schemes for (*b*) L-cysteine-I (at ambient pressure and ambient temperature), (*c*) L-cysteine-III and (*d*/*e*) L-cysteine-IV. All thermal ellipsoids are drawn at 30% probability. Note (*d*) and (*e*) are referred to in the text as molecules 1 and 2 respectively.

5.3 *Experimental*

5.3.1 *General Procedures*

Crystals of orthorhombic L-cysteine (hereafter referred to as L-cysteine-I) obtained from Sigma (99%, catalogue number G, 1002) were used as received.

High-pressure experiments were carried out using a Merrill-Bassett diamond anvil cell (half-opening angle 40°), equipped with 600μm culets and a tungsten gasket (Merrill & Bassett, 1974). A small ruby chip was also loaded into the cell as a pressure calibrant, with the ruby-fluorescence method being used to measure the pressure (Piermarini *et al.*, 1975).

5.3.2 *Diffraction Data Collection and Processing*

In all except one case (see below) diffraction data were collected at room temperature on a Bruker Smart APEX diffractometer (Bruker, 2002) with graphite-monochromated Mo-Kα radiation (λ = 0.71073 Å). High-pressure data-collection and processing procedures were as described by Dawson *et al.* (2004). Integrations were carried out using the program SAINT (Bruker, 2004). Absorption corrections were applied in a two-stage procedure with the programs SHADE (Parsons, 2004) and SADABS (Sheldrick, 2004a) for the high pressure data sets, or with SADABS alone for ambient pressure data.

5.3.3 *L-Cysteine-I at ambient pressure and temperature*

A sphere of data was collected on a crystal of L-cysteine-I at ambient temperature and pressure in order to provide data for comparison with the high pressure studies. Refinement was carried out against $|F|^2$ using all data (CRYSTALS; Betteridge *et al.*, 2003) starting from the ambient pressure coordinates of Kerr *et al.*, (1975). The thiol H-atom is disordered over two sites, and these sites were both located in a slant-plane difference map [Marching Cubes; Hušák, & Kratochvila, (2003)]; the positions and occupancies were refined subject to the restraint that the S-H distances were 1.34(1) Å; all other H-atoms were placed geometrically. The final conventional *R*-factor was 0.0343 for 1197 data. Listings of crystal and refinement data are given in Table 5.1; the structure is depicted in Figure 5.1*b*.

The numbering schemes (Figure 5.1) used in all polymorphs of L-cysteine described here are the same as CSD refcode LCYSTN12 (Kerr *et al.* 1975). The settings of the structures reported here are also the same as those used in LCYSTN12.

Pressure (GPa)	0^{I}	1.8^{I}	2.6^{III}	4.2^{III}	1.7^{IV}
Crystal data					
Chemical formula	$C_3H_7NO_2S$	$C_3H_7NO_2S$	$C_3H_7NO_2S$	$C_3H_7NO_2S$	$C_3H_7NO_2S$
M_r	121.16	121.16	121.16	121.16	121.16
Cell setting, space group	Orthorhombic, $P2_12_12_1$	Orthorhombic, $P2_12_12_1$	Orthorhombic, $P2_12_12_1$	Orthorhombic, $P2_12_12_1$	Monoclinic, $P2_1$
a, b, c (Å)	8.1109 (10), 12.1621 (15), 5.4210 (7)	7.4146 (19), 12.000 (3), 5.3318 (9)	8.0558 (10), 10.4883 (19), 5.3471 (5)	7.9981 (8), 10.2976 (15), 5.2840 (3)	8.105 (3), 5.4420 (8), 10.916 (4)
α, β, γ (°)	90, 90, 90	90, 90, 90	90, 90, 90	90, 90, 90	90, 94.897 (19), 90
V (Å^3)	534.76 (12)	474.4 (2)	451.79 (11)	435.20 (8)	479.7 (2)
Z	4	4	4	4	4
D_x (Mg m^{-3})	1.505	1.696	1.781	1.849	1.677
Radiation type	Mo $K\alpha$	Mo $K\alpha$	Mo $K\alpha$	Mo $K\alpha$	Mo $K\alpha$
No. of reflections for cell parameters	2797	376	388	736	337
θ range (°) for unit cell determination	6–56	6–45	8–39	6–46	8–37
μ (mm^{-1})	0.49	0.55	0.58	0.60	0.55
Temperature (K)	293	293	293	293	293
Crystal form, colour	Block, colourless	Block, colourless	Block, colourless	Block, colourless	Block, colourless
Crystal size (mm)	0.43 × 0.22 × 0.18	0.20 × 0.20 × 0.20	0.20 × 0.20 × 0.10	0.20 × 0.20 × 0.10	0.20 × 0.20 × 0.10

Table 5.1: Crystallographic data for L-cysteine at ambient temperature and pressure, and at increasing pressures. Phase of L-cysteine present is indicated by Roman numerals in superscript.

Pressure (GPa)	0[I]	1.8[I]	2.6[III]	4.2[III]	1.7[IV]
Data collection					
Diffractometer	Bruker SMART	Bruker SMART	Bruker SMART	Bruker SMART	Bruker SMART
Data collection method	ω	ω	ω	ω	ω
Absorption correction	Multi-scan	Multi-scan	Multi-scan	Multi-scan	Multi-scan
T_{min}	0.82	0.59	0.46	0.82	0.01[1]
T_{max}	0.92	0.90	0.94	0.94	0.95
No. of measured, independent and observed reflections	4806, 1311, 1197	1309, 402, 266	1290, 370, 287	1240, 367, 335	937, 613, 395
Criterion for observed reflections	$I > 2.00\sigma(I)$	$I > 2.00\sigma(I)$	$I > 2.00\sigma(I)$	$I > 2.00\sigma(I)$	$I > 2.00\sigma(I)$
Completeness (%)	100	55.9	56.3	57.0	42.7
R_{int}	0.053	0.107	0.083	0.038	0.147
θ_{max} (°) for structure analysis	28.9	23.3	23.1	23.2	23.2
Range of h, k, l	$-10 \rightarrow h \rightarrow 10$	$-7 \rightarrow h \rightarrow 7$	$-8 \rightarrow h \rightarrow 8$	$-8 \rightarrow h \rightarrow 8$	$-7 \rightarrow h \rightarrow 7$
	$-15 \rightarrow k \rightarrow 15$	$-10 \rightarrow k \rightarrow 10$	$-7 \rightarrow k \rightarrow 7$	$-8 \rightarrow k \rightarrow 8$	$-6 \rightarrow k \rightarrow 6$
	$-7 \rightarrow l \rightarrow 7$	$-5 \rightarrow l \rightarrow 5$	$-5 \rightarrow l \rightarrow 5$	$-5 \rightarrow l \rightarrow 5$	$0 \rightarrow l \rightarrow 8$
Refinement					
Refinement on	F^2	F^2	F^2	F^2	F
$R[F^2 > 2\sigma(F^2)]$, $wR(F^2)$, S	0.034, 0.088, 1.03	0.057, 0.123, 1.02	0.057, 0.117, 1.07	0.040, 0.098, 1.09	0.144, 0.162, 1.15
No. of reflections used	1309	391	368	367	395
No. of parameters	72	34	38	38	47
Weighting scheme	Calculated $w = 1/[\sigma^2(F^2) + (0.06P)^2 + 0.01P]$ where $P = (\max(F_o^2,0) + 2F_c^2)/3$	Calculated $w = 1/[\sigma^2(F^2) + (0.04P)^2 + 1.09P]$ where $P = (\max(F_o^2,0) + 2F_c^2)/3$	Calculated $w = 1/[\sigma^2(F^2) + (0.04P)^2 + 0.56P]$ where $P = (\max(F_o^2,0) + 2F_c^2)/3$	Calculated $w = 1/[\sigma^2(F^2) + (0.06P)^2 + 0.57P]$ where $P = (\max(F_o^2,0) + 2F_c^2)/3$	Calculated Method: Chebychev polynomial with coefficients 2.10 0.669 and 1.21, with a robust-resistant modifier. (Watkin, 1994, Prince, 1982)
$(\Delta/\sigma)_{max}$	<0.0001	<0.0001	<0.0001	<0.0001	<0.0001
$\Delta\rho_{max}$, $\Delta\rho_{min}$ (e Å^{-3})	0.31, –0.22	0.40, –0.43	0.36, –0.44	0.26, –0.24	1.19, –0.99

Table 5.1 (cont'd): Crystallographic data for L-cysteine at ambient temperature and pressure, and at increasing pressures. Phase of L-cysteine present is indicated by Roman numerals in superscript.

5.3.4 *Compression of L-cysteine-I Studied by Single Crystal X-ray Diffraction*

In order to ensure that the pressure applied to a crystal held in a diamond anvil cell is uniform, it is necessary to immerse the sample in a medium which displays hydrostatic behaviour throughout the pressure range of interest. Two media used commonly in high-pressure work are a 1:1 mixture of pentane and isopentane and a 4:1 mixture of methanol and ethanol. Compression studies were carried out with both of these media, but slightly different results were obtained.

5.3.5 *Compression using pentane/isopentane as a hydrostatic medium*

Compression data were collected using a block-shaped crystal of L-cysteine-I, loaded with a 1:1 mixture of pentane and isopentane as the hydrostatic medium. Pressure was increased in approximately 0.9 GPa steps from 0.1 GPa with X-ray diffraction data being collected at each stage. Above 1.8 GPa the sample became polycrystalline. Other experiments in which the pressure was increased in small steps, with intensity data collection at each stage gave similar results, with sample deterioration occurring in every case.

A crystal of L-cysteine-I was loaded and compressed in approximately 1.5 GPa steps in quick succession from 0.3 GPa to 4.2 GPa. Raman spectra were acquired at each stage, and the pressure increase from 0.3 to 4.2 GPa occurred over *ca* 90 minutes, *i.e.* much more quickly than when the effect of pressure was monitored using X-ray diffraction. At 4.2 GPa the Raman spectrum, (Figure 5.2), and determination of the unit cell dimensions, showed that a single-crystal to single-crystal phase transition had taken place to give a previously uncharacterised phase of L-cysteine which we have designated L-cysteine-III. Single crystal X-ray diffraction data were collected, with the results shown in Table 5.1.

The sample was then decompressed to 2.6 GPa, and then further to 1.7 GPa. Diffraction data collected at 1.7 GPa showed that another single-crystal to single-crystal phase transition had taken place to another previously uncharacterised monoclinic phase, which we have designated L-cysteine-IV (Table 5.1).

The sample became polycrystalline on further decompression, and no further structural data could be extracted.

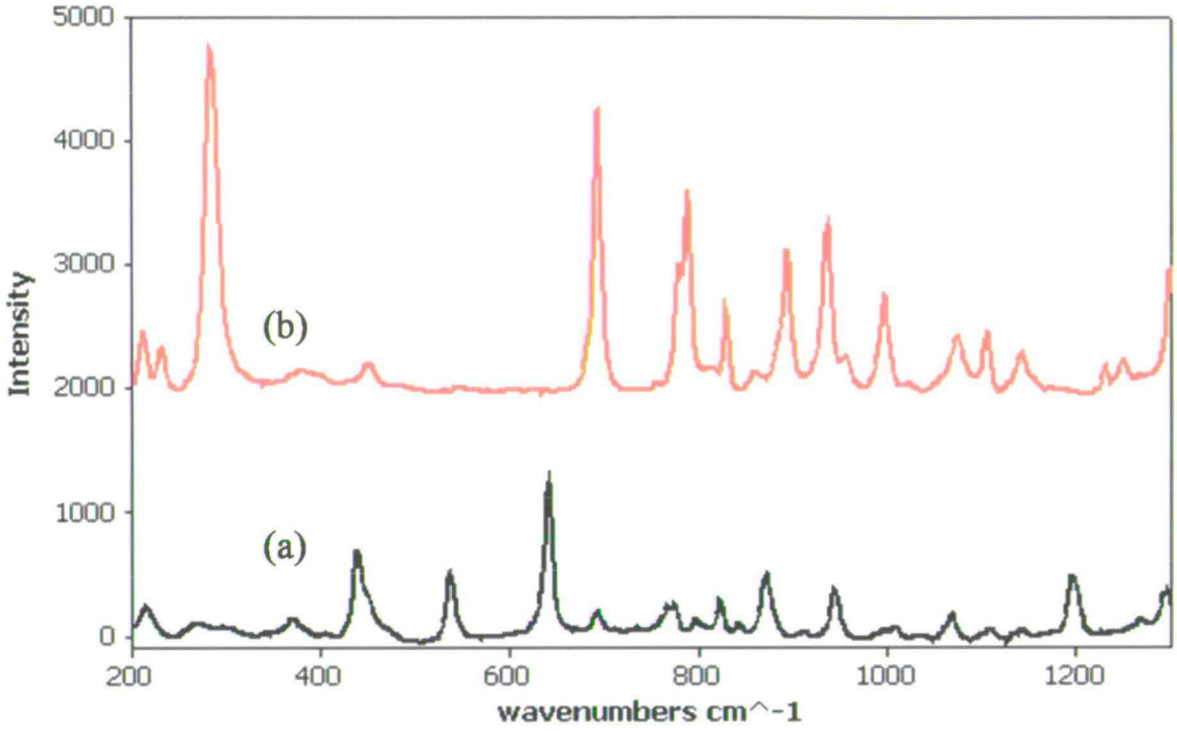

Figure 5.2: Raman spectra of (a) L-cysteine-I at 0.3 GPa and (b) L-cysteine-III at 4.2 GPa (also shown in red) between 0 and 1300 cm^{-1}.

5.3.6 Compression using methanol/ethanol as a hydrostatic medium

Compression data were collected on L-cysteine-I in approximately 0.7 GPa steps starting at 0.7 GPa using a 4:1 mixture of methanol and ethanol as the hydrostatic fluid; X-ray diffraction data were collected at each stage. A phase transition from phase-I to phase-III occurred *during* data collection; the pressure at the beginning of data collection was 1.7 GPa, but after data collection the pressure was found to have increased to 2.1 GPa. Changes in pressure can often fluctuate due to changes in temperature, however, the change in pressure here was thought to change due to the cell still equilibrating during data collection. The time taken for this to occur can vary, as this process is highly dependant on the time taken for the gasket to protrude inwards providing the hydrostatic environment, a process which is difficult to quantify as deformation of the gasket on increasing pressure can not be measured. Pressures are measured before and after each diffraction experiment, where the pressure is usually found to vary only slightly *ca* 0.1 GPa. This was the case for L-cysteine for all but this particular data collection, with the effect proving fortuitous on this occasion. Further data were collected on L-cysteine-III on increasing pressure further to 2.6 and 3.2 GPa.

Data were then collected on backing down in pressure at 2.5 and 1.8 GPa. At 1.8 GPa the sample broke-up, but it was nevertheless possible to determine the unit cell dimensions by indexing spots from one of the larger crystallites [a = 8.08(3) Å, b = 5.442(11) Å, c = 10.63(4) Å, β = 93.7(3)°]. This showed that the sample was L-cysteine-IV. The sample was then removed from the cell, and a small crystallite (crystal dimensions measuring 37.5 x 12.5 x 12.5μm) from the now, polycrystalline sample was taken to the SRS Daresbury Laboratory. Single crystal diffraction data were collected at room temperature with synchrotron radiation (λ = 0.6778 Å) on a Bruker APEX-II diffractometer installed on Station 9.8. This experiment showed that on downloading, the sample had returned to phase-I.

Data for L-cysteine-I at ambient pressure and 1.8 GPa (medium pentane/isopentane), L-cysteine-III at 2.6 GPa (methanol/ethanol) and 4.2 GPa (pentane/isopentane), and L-cysteine-IV at 1.7 GPa (pentane/isopentane) are included in Table 5.1.

5.3.7 *Refinement of the crystal structure of L-cysteine-I at 1.8 GPa*

The data-set used here was that obtained during the increasing-pressure phase of the experiments carried-out with pentane/isopentane as the hydrostatic medium. Refinements were carried out against $|F|^2$ using all data (CRYSTALS) starting from the coordinates of Kerr *et al.* (1975). Because of the low completeness of the data-set (57.5%), all 1, 2 and 1, 3 distances were restrained to the values observed in the ambient-pressure structure. Only the S-atom was refined with anisotropic displacement parameters, while all other non-hydrogen atoms were refined isotropically. All H-atoms attached to N or C were placed geometrically and not refined; the thiol H-atom was not placed. Listings of crystal and refinement data are given in Table 5.1.

5.3.8 *Solution and Refinement of L-cysteine-III at 2.6 GPa*

The data-set used here was that obtained during the increasing-pressure phase of the experiments carried-out with methanol/ethanol as the hydrostatic medium. We have chosen to discuss these data in detail because they were obtained under the conditions which were closest to those of the highest pressure study on phase-I.

The structure of L-cysteine-III was solved by direct methods (SIR92; Altomare *et al.*, 1994). The setting used was chosen to facilitate comparisons with L-cysteine-I.

Refinement procedures were the same as those described for L-cysteine-I at 1.8 GPa. All H-atoms attached to N or C were placed geometrically and not refined.

The position of H1, the H-atom attached to sulfur, was located in a difference map based on phases calculated using refined positions for all other atoms in the structure. The highest electron density difference peak was 1.49 Å from S1 in a staggered position between H2 and C2. Assignment of this peak as H1, followed by free refinement yielded d(S1-H1) = 1.24 Å, <(C10S1-H1) = 93° and U_{iso}(H1) = 0.08 Å^2, while reducing $R1$ by 0.2%. The S-H distance was restrained to 1.33(1) Å in subsequent cycles of least-squares. The two possible alternative positions for H1, staggered between H2 and H3 or C2 and H3, make contacts of 1.6 and 1.7 Å to H-atoms in neighbouring molecules, therefore making these choices for the position of H1 unfavourable.

Listings of crystal and refinement data are given in Table 5.1.

5.3.9 Solution and Refinement of L-cysteine-IV at 1.7 GPa

The data-set used here was that obtained during the decreasing-pressure phase of the experiments carried-out with pentane/isopentane as the hydrostatic medium. The data set was of poor quality with broad, irregular reflection peak shapes; indexing was achieved after manual selection of diffraction spots. After integration R_{int} was 0.166 in point group 2, and, in spite of numerous attempts, this is the best data set that we ever obtained. L-cysteine-IV is monoclinic $P2_1$ with a volume implying Z' = 2. Structure solution was attempted using direct methods, Patterson methods and global optimisation, but all failed to yield a recognisable structure.

The unit cell dimensions of L-cysteine-IV are a = 8.13 , b = 5.44, c = 10.91 Å and β = 95°; corresponding (transformed) values for L-cysteine-I are rather similar at 8.11, 5.42 and 12.16 Å, β = 90°, and it seemed probable that the two structures were similar. A model of structure of the L-cysteine-IV was prepared from the coordinates of L-cysteine-I; the space group was changed to $P2_1$ with two previously symmetry equivalent molecules comprising the asymmetric unit. The S-atoms were deleted and then re-located in a difference synthesis calculated on the phases based on the C, N and O-positions.

The molecules were initially treated as rigid groups during refinement, but these constraints were later relaxed, and 1, 2 and 1, 3 distances were restrained to values in L-cysteine-I. The program ROTAX (Cooper *et al.*, 2002) indicated that the sample was non-merohedrally twinned via an approximate 2-fold about [100]; twinning was

anticipated because the crystal had been formed in a phase transition from the higher-symmetry phase-III. The twin law matrix was,

$$\begin{pmatrix} 1 & 0 & 0 \\ 0 & -1 & 0 \\ -0.23 & 0 & -1 \end{pmatrix}.$$

The data were then reintegrated with both twin components simultaneously using the program SAINT, and an absorption correction applied with SHADE and TWINABS (Sheldrick, 2004b).

Restrained refinement was carried out against F using data with $F > 4\sigma(F)$. Common isotropic displacement parameters were refined for the C, N and O atoms in each of the two molecules in the asymmetric unit; isotropic displacement parameters were also refined for each of the two S-atoms. H-atoms attached to C and N were placed geometrically and not refined. H-atoms attached to both sulfur atoms were not placed as these H-atoms could not be located in a difference map. The twin scale factor refined to 0.476(11). Though it is commensurate with R_{int}, the R factor is high at 14%, and the solution we present here should be regarded as rather tentative.

Listings of crystal and refinement data are given in Table 5.1.

5.3.10 L-cysteine-I at 0.5 GPa studied by single crystal neutron diffraction

Note: Data collection and processing of these data were carried out by Dr Matthias Gutman (beamline scientist on the SXD single-crystal beamline at ISIS), Dr Colin R. Pulham and Dr Dave Allan (The University of Edinburgh).

We show in the *Results Section* that one effect of compression of L-Cysteine-I is a substantial shortening of S...S distances. Neutron diffraction data were collected with the aim of characterising the behaviour of the thiol H-atom.

Neutron diffraction data were collected on Station SXD (Keen *et al.*, 2005) at the ISIS neutron spallation source, Didcot, UK. Three crystals were fixed at random orientations on Al tape and mounted inside a null-scattering Ti/Zr cell. The assembly was pressurised to 0.5 GPa using He gas resulting in a uniform, hydrostatic pressure. Data were collected at room temperature at three orientations whereby the cell/crystal assembly was rotated successively by 30 degrees around the vertical axis. Data from the three

crystals were processed using locally available software (SXD2001, Gutmann *et al.*, 2005) and corrected for absorption within the same program.

A difference synthesis was calculated using phases based on all atoms except for the thiol H-atom, the model being taken from Kerr *et al.* (1975). Amongst the most prominent features in the map were two holes (depths -0.91 and -0.67 fm $Å^{-3}$) located either side of the S-atom at a distance of *ca* 1.3 Å. These were included in the model as two part-weight H-atoms. The S-H distances were restrained to be 1.33(1) Å, and a common isotropic displacement parameter was refined for the two atoms. When at site H1 the H-atom forms an SH...S contact; when in site H10 it forms a contact to a neighbouring O-atom (see below). The occupancies were also refined. Anisotropic displacement parameters were refined for all non-H atoms using global rigid bond and rigid body restraints; the NH_3^+, CH and CH_2 moieties were treated as variable metric rigid groups with common isotropic displacement parameters. The occupancies of H1 and H10 refined to 0.53(4) and 0.47(4), and the final *R* factor based on 213/341 unique data to 0.8 Å with $F > 4\sigma(F)$ was 0.0786. The sulfur atom adopts a somewhat prolate adp (principal values: 0.1097, 0.0535 and 0.0135); this was interpreted by Kerr *et al.* (1975) as indicative of disorder in the S-position, induced by the H-atom disorder. No attempt was made to model disorder here though. All calculations were carried out using the program SHELXL97 (Sheldrick, 2001).

5.3.11 Structure Analysis and Visualisation Software

Crystal structures were visualised using the programs CAMERON Watkin *et al.*, 1993), DIAMOND (Crystal Impact, 2004), MERCURY (Bruno *et al.*, 2002) and XP (Sheldrick, 1997). Analyses were carried out using PLATON (Spek, 2003), as incorporated in the WIN-GX suite (Farrugia, 1999). Searches of the Cambridge Database (Allen, 2002; Allen & Motherwell, 2002) were performed with the program CONQUEST and version 5.26 of the database with updates up to August 2005.

5.3.12 Ab-Initio Calculations

Ab initio calculations were performed with the plane-wave pseudopotential implementation of density functional theory (DFT) using the CASTEP code (Segall *et al.*, 2002), with the aim of further characterising the behaviour of the thiol H-atom in L-cysteine-I. Plane wave basis sets have many benefits compared to conventionally used

quantum chemistry basis sets; in particular, there exists a simple parameter, the cut-off energy, to determine the completeness of the basis. This gives us confidence that the wave function can describe any properties without bias towards any other particular result (Clark *et al.*, 1998). In our calculations, the many-body exchange and correlation interactions are described using the generalized gradient approximation (Perdew & Wang, 1992). Such calculations are capable of giving accurate and reliable structural and electronic information. Ultrasoft pseudopotentials (Vanderbilt, 1990) are used to describe the electron-ion interactions. A cut-off energy of 380 eV is used which converged the total energy of the system to 1.0 meV/molecule. The Monkhorst-Pack *k*-point sampling scheme (Monkhorst & Pack, 1976) was used to perform the integrations in *k*-space over the first Brillouin zone with the grids for each cell chosen to be dense enough to also converge the total energy to 1.0 meV/molecule. For each structure considered the geometry (atomic position and unit cell parameters) were optimised using a conjugate gradient algorithm. The tolerances used give energy differences between structures accurate to better then 1.0 meV.

5.4 *Results*

5.4.1 *Structure of L-cysteine-I at ambient pressure and temperature.*

Our motive for discussing the structure of L-cysteine-I here is to highlight structural features that become relevant when analysing the effects of high pressure. The cysteine molecule is in its zwitterionic tautomer. In principle the N1-C2-C1-S1 torsion angle (χ1) can adopt values of *ca.* 60° (*gauche*-+ or g^+), -60° (g^-), and 180° (*trans* or *t*), though in small molecules there is a strong preference for the g^+ conformation (Görbitz. 1990). In L-cysteine-I, χ1 = 65.32(13)° (g^+, Figure 5.1*b*, Table 5.2); in L-cysteine-II χ1 = 74.40(12)° (g^+) in one molecule and -170.16(8)° (*t*) in the other.

Pressure (GPa)	0	1.8	2.6	4.2	1.7	1.7
Phase	I	I	III	III	IV(1)	IV(2)
N1-C2-C1-S1	65.32(13)	57.2(7)	-56.6(7)	-57.3(5)	71.3(18)	-67(2)
N1-C2-C3-O2	-16.96(19)	-23.6(10)	-26.6(10)	-20.6(8)	1(4)	-45(3)

Table 5.2: Torsion angles (°) in L-cysteine as a function of pressure. For L-cysteine-IV, (1) and (2) refers to each symmetry independent molecule as referred to in the text.

The shortest H-bond (Table 5.3), N1H7...O2, lies along **c** to form a primary-level $C(5)$ chain (Figure 5.3*a*). The second shortest H-bond, N1H5...O1, links molecules into primary-level $C(5)$ chains which run perpendicular to the $C(5)$ chains formed by the N1H7...O2 H-bonds. The combination of these two $C(5)$ chains yields a layer composed of $R^4_4(16)$ ring motifs (Figure 5.3*a*). The layer is parallel to the *ac* plane, having a sinusoidal appearance when viewed in projection down **c** (Figure 5.4*a*; the layers in this Figure are indicated with block-arrows). The last of the NH...O interactions, N1H6...O2, links the layers together along the *b*-direction. Pairs of N1H6...O2 contacts form a secondary-level $R^2_3(9)$ ring motif (Figure 5.5*a*).

In L-cysteine-I the thiol H atom is disordered over two sites, forming either SH...S or SH...O contacts. The former is slightly preferred (Kerr *et al.*, 1975), and the SH-group becomes ordered in this orientation at 30 K (Moggach *et al.*, 2005d). The S-H...S interactions form an infinite H-bonded chain which zigzags along **c** (Figure 5.4*a*), supporting the $R^2_3(9)$ ring motifs in connecting the sinusoidal layers. The SH...O interaction forms a discrete contact to the carboxylate oxygen (O2) atom involved in the $R^2_3(9)$ ring motif.

Under ambient conditions only two CH...O interactions are present: C1H2...O1, which forms a primary $C(6)$ H-bonded chain that runs along the *c*-axis direction, and C1H3...O1 which runs parallel with N1H5...O1. Both of these combine to produce an $R^4_4(14)$ ring that intertwines within the $R^4_4(16)$ ring formed by the NH...O H-bonds (Figure 5.3*a*). A similar motif has been observed in L-cystine (Moggach *et al.*, 2005c).

Orthorhombic L-cysteine-I undergoes a phase transition above 1.8 GPa.

X-H...Y	Pressure (GPa)					
	0	1.8	2.6	4.2	1.7	1.7
Phase	I	I	III	III	IV(1)	IV(2)
N1-H5...O1[i]						
N1...O1	2.787(2)	2.721(9)	2.724(9)	2.716(6)	2.85(4)	2.69(4)
N1-H6...O2[ii]						
N1...O2	3.017(2)	2.863(11)	2.837(11)	2.817(8)	2.89(5)	2.99(5)
N1-H7...O2[iii]						
N1...O2	2.7600(16)	2.715(8)	2.708(8)	2.699(6)	2.73(3)	2.80(3)
C1-H2...O1[iv]						
C1...O1	3.289(2)	3.241(9)	-	-	-	3.26(3)
C1-H3...O1[v]						
C1...O1	3.839(2)	3.450(10)	-	-	-	3.39(3)
C2-H4...O2[vi]						
C2...O2	-	-	3.325(9)	3.220(7)	3.17(3)	-
C1-H3...O2[vii]						
C1...O2	-	-	-	-	3.10(4)	3.43(4)
S1-H10...O2[viii]						
S1...O2	3.3788(15)	3.275(7)				
H10...O2	2.17(3)	-	-	-	-	-
∠S1H10O2	148(3)	-				
S1-H1...S1[ix]						
S1...S1	3.8457(10)	3.450(4)				
H1...S1	2.81(4)	-				
∠S1H1S1	133(2)	-	-	-	-	-
S1-H1...O1[x]						
S1...O1			3.432(7)	3.373(5)		
H1...O1			2.49(10)	2.50(8)		
∠S1H1O1	-	-	125(5)	120(4)	-	-

Symmetry codes-L-cysteine-I & III: (i) 1/2+x,3/2-y,1-z; (ii) 3/2-x,2-y,1/2+z; (iii) x,y,1+z; (v) 1-x,-1/2+y,3/2-z; (vi) 1-x,-1/2+y,3/2-z; (viii) 3/2-x,2-y,1/2+z; (ix) 1/2-x,2-y,-1/2+z; (x) (-1/2+x,3/2-y,1-z. L-cysteine-IV, molecule 1: (i) 1-x,1/2+y,1-z; (ii) 1-x,-1/2+y,1-z; (iii) x,-1+y,z; (vi) -x,1/2+y,1-z; (vii) 1-x,-1/2+y,1-z. L-cysteine-IV, molecule 2: (i) -x,-1/2+y,1-z; (ii) -x,1/2+y,2-z; (iii) x,1+y,z; (iv) x,1+y,z; (v) 1-x,-1/2+y,1-z; (vii) 1-x,-1/2+y,1-z.

Table 5.3: H-bonding parameters (Å, °) in L-cysteine-I, III and IV. In L-cysteine-IV, (1) and (2) refer to the symmetry independent molecules.

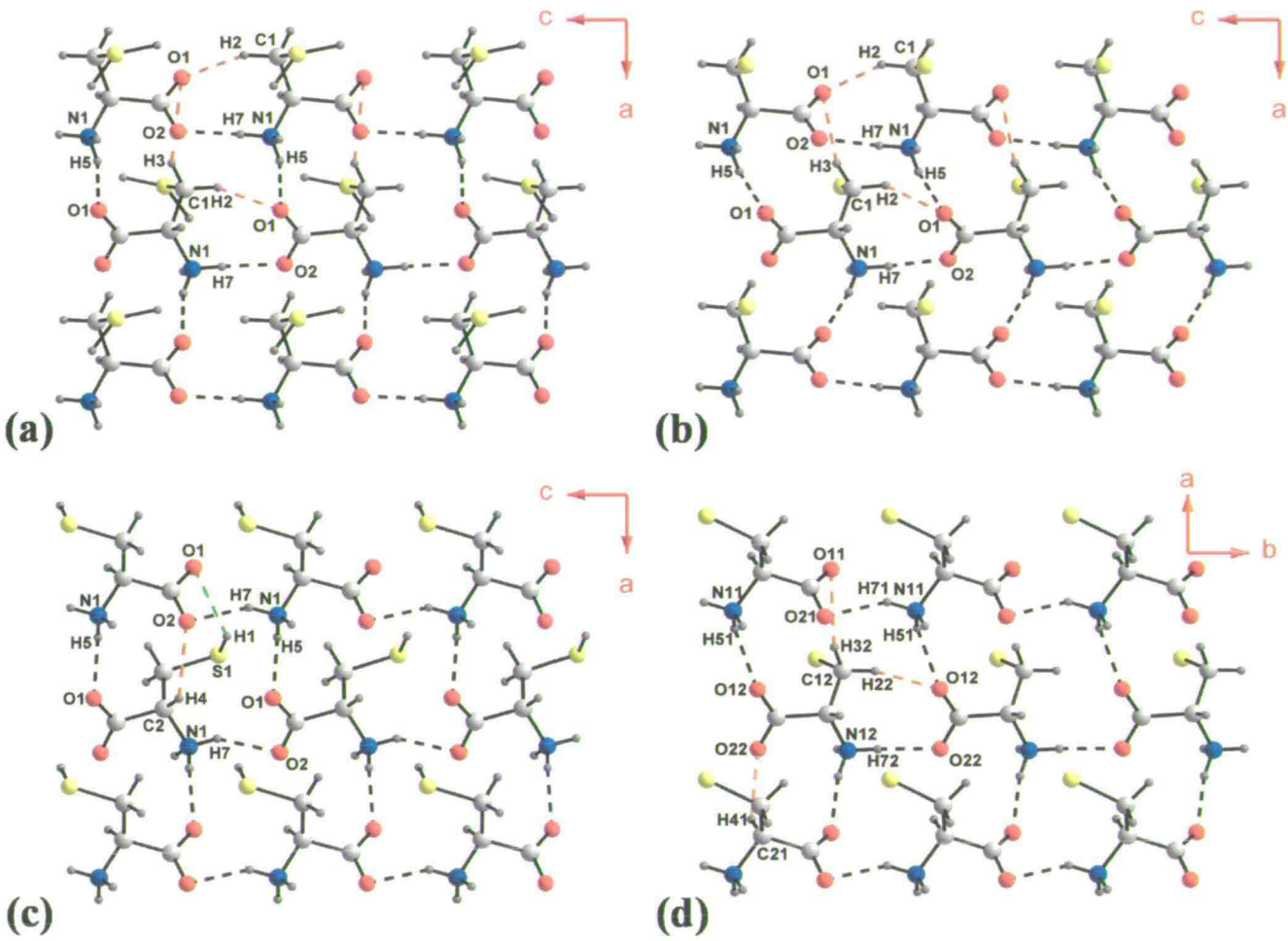

Figure 5.3: $R^4_4(16)$ ring motifs in (*a*) L-cysteine-I at ambient pressure, (*b*) L-cysteine-I at 1.8 GPa, (*c*) L-cysteine-III at 2.6 GPa and (*d*) L-cysteine-IV at 1.7 GPa. Figures (*a-c*) are viewed along **b**, while (*d*) is viewed along **c**. N-H...O and C-H...O H-bonds are drawn as black and orange dotted lines, respectively, while S-H...O interactions in L-cysteine-III, are depicted as green dotted lines. For clarity, all C-H...O and S...O interactions are drawn only in the top left quadrant. Colour scheme yellow S, green N, red O, grey C and dark grey H.

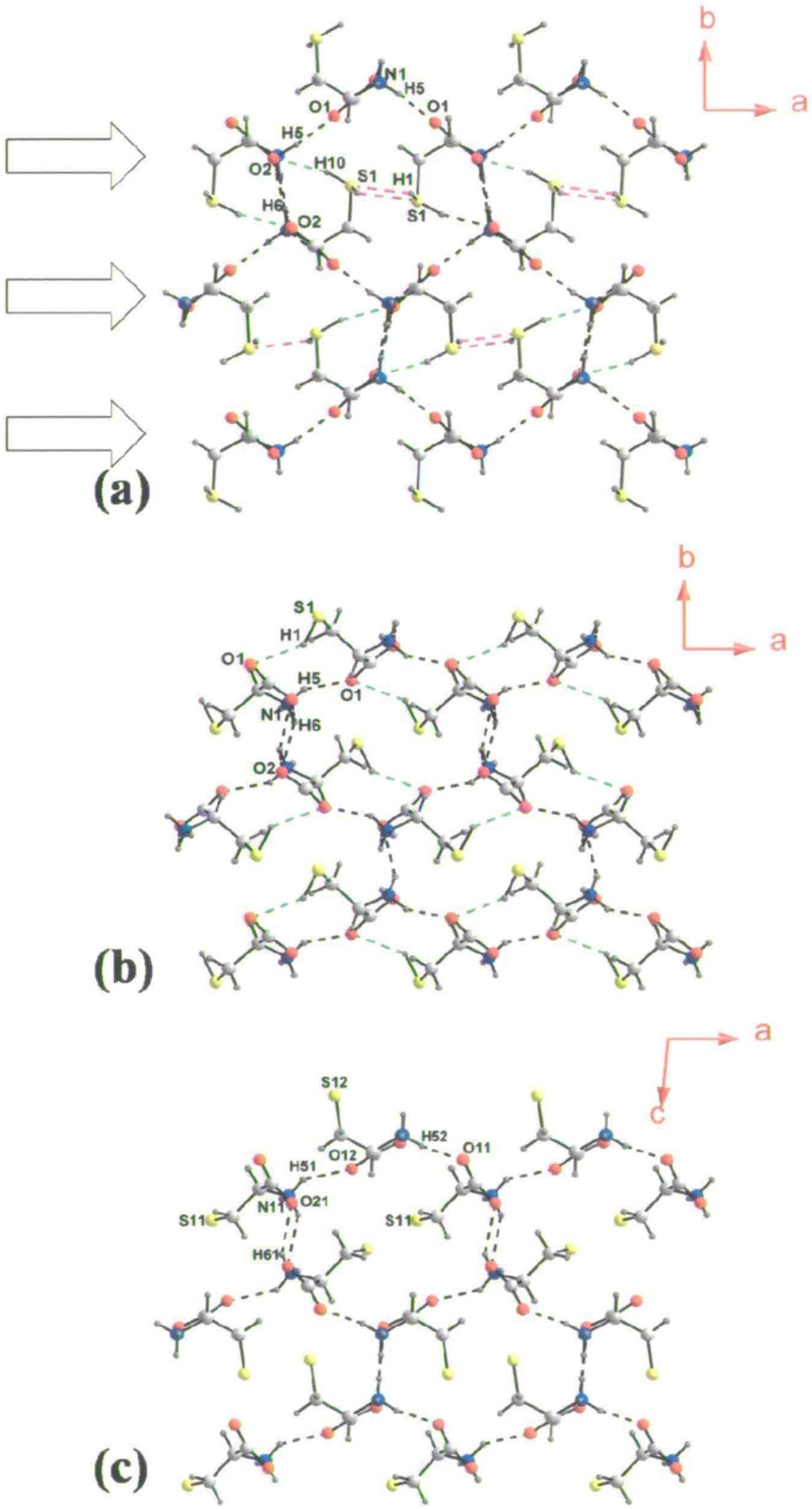

Figure 5.4: Unit cell packing motifs in (*a*) L-cysteine-I at ambient pressure, (*b*) L-cysteine-III at 2.6 GPa and (*c*) L-cysteine-IV at 1.7 GPa. Both (*a*) and (*b*) are viewed along **c**, while (*c*) is viewed along **b**. Note the sinusoidal appearance of $R^4_4(16)$ ring motifs along **a** as indicated by arrows in (*a*). NH...O, SH...S and SH...O H-bonds are depicted as black, pink, and green dotted lines, respectively.

5.4.2 *Lattice parameters of L-cysteine-I up to 1.8 GPa.*

The response of the unit cell dimensions to pressure is anisotropic, with the most compressible lattice parameter between ambient pressure and 1.8 GPa being the *a*-axis, which decreases in length by 8.6%, with the *b* and *c*-axes shortening by 1.3% and 1.6%, respectively. Because the system is orthorhombic, the principal component of the strain tensor is also along the *a*-axis.

5.4.3 *Intramolecular Geometry in L-cysteine-I at 1.8 GPa*

Bond distances and angles were restrained during refinement to their ambient pressure values, and so no conclusions about their variation with pressure should be drawn from the data reported here. Significant changes do occur in the torsion angles (Table 5.2), however. Between ambient pressure and 1.8 GPa the NCCS and NCCO torsion angles reduce from 65.32(13) to 57.2(7)° and -16.96(19) to -23.6(10)°, respectively. It seems likely that these changes occur in order to accommodate the changes in the intermolecular interactions described below.

5.4.4 *H-Bonds in L-cysteine-I at 1.8 GPa*

Variation in H-bonding parameters between ambient and 1.8 GPa are given in Table 5.3. H-atoms were placed in idealised positions during refinement and so donor to acceptor distances (N...O) rather than H...O have been used to quantify the relative compressibility of the H-bonds.

The data in Table 5.3 (columns 1 and 2) can be summarised as follows; Δ refers to the N or C...O distance at ambient pressure minus the corresponding distance at 1.8 GPa. The most compressible of the NH...O H-bonds, N1H6...O2, is also the longest (Δ = 0.15 Å). This H-bond is involved in the $R^2_3(9)$ motifs that links the sinusoidal layers described above (Figure 5.5*a*). The other H-bond involved in this motif is N1H7...O2, which is the least compressible of the NH...O H-bonds (Δ = 0.05 Å). The last of the NH...O H-bonds, N1H5...O1, is involved in the $R^4_4(16)$ ring motifs (Figure 5.3*a* and *b*); the decrease in the length is only slightly greater than in N1H7...O2 (Δ = 0.07 Å). We note that of the three NH...O H-bonding interactions, N1H5...O1 makes the smallest angle with the *a*-axis (the most compressible crystallographic direction); however, this interaction is not the most

compressible NH...O H-bond. The compression in C1H3...O1 is substantially greater (Δ = 0.39 Å) than in the NH...O H-bonds, but the reduction in the length of C1H2...O1 is more similar (Δ = 0.05 Å).

Under ambient conditions the thiol H-atom is disordered over SH…S and SH…O contacts (see above), and it has not been placed in the high pressure structures reported here. While the S...O distance reduces in length by 0.10 Å, the S…S contact is much more compressible, decreasing in length by 0.40 Å. This is one of the most compressible interactions in the structure decreasing in length by 8.70%. At 1.8 GPa the S…S distance is 3.450(4) Å, well within twice the van der Waals radius of S [3.6 Å (Bondi, 1964)].

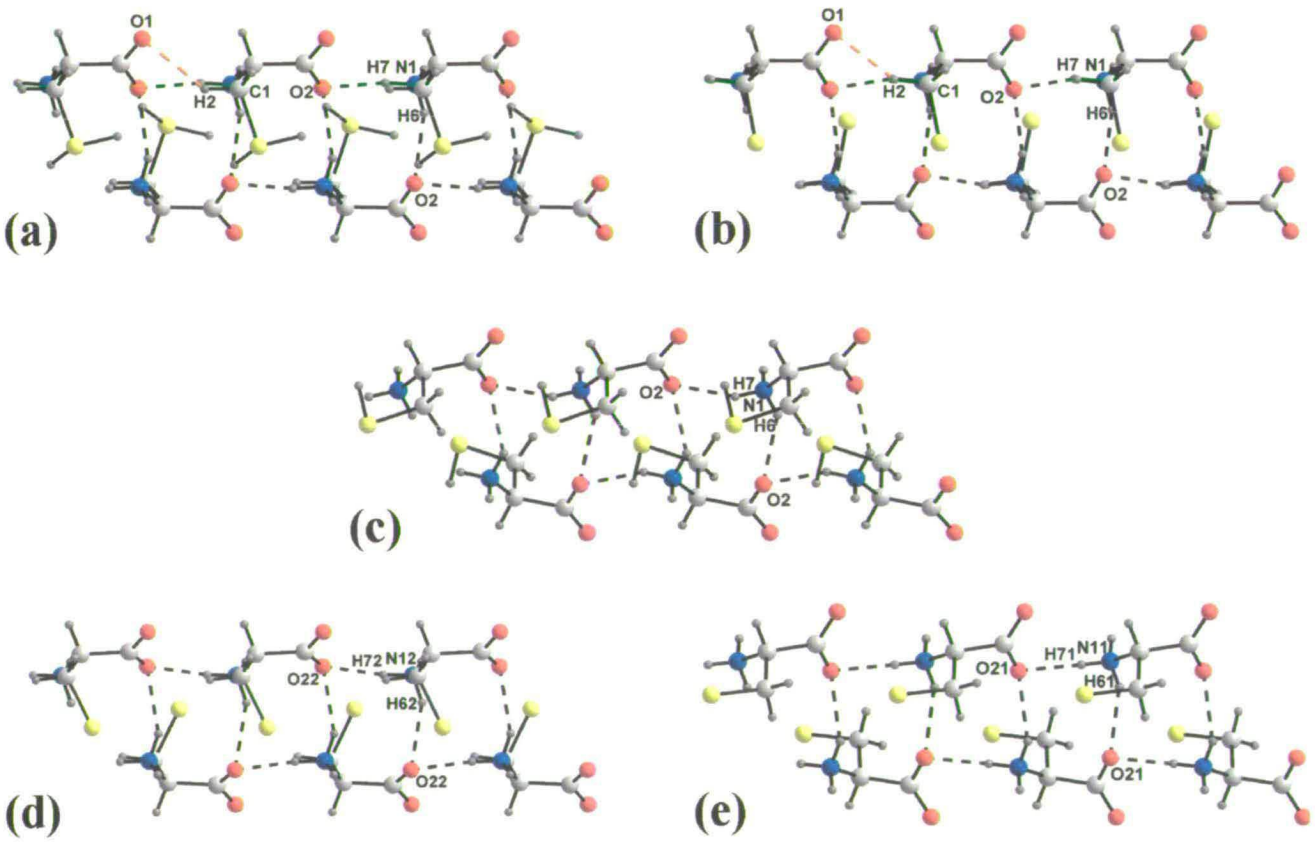

Figure 5.5: $R^2_3(9)$ ring motifs in (a) L-cysteine-I at ambient pressure, (b) L-cysteine-I at 1.8 GPa, (c) L-cysteine-III at 2.6 GPa and (d,e) L-cysteine-IV at 1.7 GPa. H-bonds and colour scheme as in Figure 5.3.

5.4.5 L-cysteine-I at 0.5 GPa as studied by single crystal neutron diffraction.

The changes in the geometry about the sulfur atom led us to speculate that the thiol H-atom may become ordered at elevated pressures. Neutron diffraction data were collected using a gas pressure cell on station SXD at ISIS; the maximum operating pressure of this cell is 0.5 GPa. It was clear that at 0.5 GPa the H-atom is still disordered;

the occupancies of both SH...S and SH...O H-atoms refined to 0.53(4) and 0.47(4), respectively (Figure 5.1*b*).

5.4.6 L-cysteine-III at 2.6 GPa.

The transition from L-cysteine-I to L-cysteine-III occurs at above 1.8 GPa. The effect of the transition on the sample depended on the hydrostatic medium being used. In 4:1 methanol-ethanol the transition proceeded smoothly during data collection from one well-formed crystalline form to another. In pentane-isopentane incremental increase of pressure caused the sample to break-up or develop high mosaic spread; this could be avoided by increasing the pressure more rapidly in larger steps to *ca* 4 GPa. Here we discuss the data obtained for L-cysteine-III at 2.6 GPa derived from data obtained using methanol-ethanol; intermolecular contact data are collected in Table 5.3.

There is a significant conformational difference between the cysteine molecules in phases I and III (Figure 5.1*b*, *c*). In phase-I the molecules adopt g^+ conformation, with τ(N1-C2-C1-S1) = 57.2(7)° at 1.8 GPa. In phase-III the molecules adopt the much less common g^- conformation, with a corresponding torsion of -56.6(7)° at 2.6 GPa (Table 5.2). The N1-C2-C3-O2 torsion changes slightly from -24.9(10)° in phase-I at 1.8 GPa to -26.6(10)° in phase-III at 2.6 GPa. Interestingly, on increasing pressure further to 4.2 GPa, the trend is reversed with the torsion angle adopting a value of -20.6(8)°. The thiol H-atom is ordered at 2.6 GPa, with τ(C2-C1-S1-H1) = -66(3)°.

The fact that the phase-I to III transition proceeds from one single crystal form to another indicates that the topology of the two forms is likely to be very similar. This proves to be the case, and much of the description given above for L-cysteine-I also applies to L-cysteine-III. The structure consists of rows of molecules linked into *C*(5) chains along **c** by N1-H7...O2 H-bonds. These chains are linked into a layer by N1-H5...O1 H-bonds, the two types of H-bond combining to form a secondary-level $R^4_4(16)$ motif (Figure 5.3*c*). The layers are less sinusoidal in cross-section than in phase-I, but they are still connected along the *b*-direction by N1-H6...O2 H-bonds, which combine with N1-H7...O2 H-bonds to form $R^2_3(9)$ rings (Figure 5.5*c*).

Whereas in L-cysteine-I SH...O and SH...S interactions connected the layers, in phase-III S1H1...O1 interactions are formed across the $R^4_4(16)$ rings (Figure 5.3*c*). At 3.433(7) Å the S...O distance is longer than the SH...O contact observed in L-cystine-I at 1.8 GPa. C2H4...O2 contacts are also formed across the $R^4_4(16)$ rings to the same

carboxylate group as is involved in the SH...O interaction. In phase-I H4 was not involved in H-bonding interactions, even though this α-H atom is often regarded as being activated towards H-bonding by the neighbouring ammonium and carboxylate groups (Derewenda *et al.*, 1995). The final weak interaction worthy of comment is C1H2...S1, which supports the N1H6...O2 H-bonds which connect the layers along the *b*-direction. There are no S...S contact distances within 3.6 Å.

5.4.7 L-cysteine-IV at 1.7 GPa.

L-cysteine-IV, which crystallises in the monoclinic space group $P2_1$, was formed in a single-crystal to single-crystal phase transition on decompression of phase-III. The diffraction data were of low quality, and the transition from orthorhombic to monoclinic symmetry resulted in twinning. Nevertheless the broad structural characteristics of this phase can be discerned, albeit with some disclaimers: caution should be exercised because the data were poor and the *R*-factor high. There are two molecules in the asymmetric unit. Molecule 1, containing S11 *etc.*, adopts an N11-C21-C11-S11 torsion angle of -67(2)°, while in molecule 2 the corresponding angle is 71.0(18)°. The first of these corresponds to the conformation observed in L-cysteine-III, and the second to that found in L-cysteine-I. The N1C2C3O2 torsion angles also differ in the two molecules, adopting values of -45(3)° and 1(4)° in molecules 1 and 2, respectively, and these compare with values of -26.5(10)° and -23.6(10)° in phases III at 2.6 GPa and I at 1.8 GPa, respectively.

The crystal structure contains rows of molecules related by lattice repeats along **b** (Figure 5.3*d*). Alternate rows contain molecules 1 or 2, connected by N11H71...O21 or N12H72...O22 H-bonds. These rows are connected into a layer by N11H51...O12 and N12H52...O11 H-bonds, forming $R^4_4(16)$ rings. The layers are connected by pairs of N11H61...O21 or N12H62...O22 H-bonds which form $R^2_3(9)$ motifs (Figures 5.5*d* and 5.5*e*). Packing between the layers connected by N11H61...O21 bonds strongly resembles that in L-cysteine-III (*cf* Figures 5.4*c* and 5.4*b*), while packing between the layers connected by N12H62...O22 H-bonds resembles that in L-cysteine-I (*cf* Figures 5.4*c* and 5.4*a*).

On further decrease in pressure the sample became polycrystalline and no structural data could be extracted. The sample was downloaded from the high-pressure cell, and diffraction data collected with synchrotron radiation using a small crystallite from the now polycrystalline sample. Determination of the unit cell dimensions and

structure solution confirmed that the sample had returned to the ambient pressure L-cysteine-I phase.

5.5 *Discussion*

5.5.1 Anisotropic Compression of L-cysteine-I at 1.8 GPa.

In previous studies of L-serine, L-cystine and α-glycine, we have ascribed the compressibility of intermolecular interactions to closing up of voids which exist, for example, at the centres of *R*-type H-bond motifs. In L-cysteine-I the relative compressibility of intermolecular interactions can also be analysed in this way.

Comparison of space-filling plots of $R^4_4(16)$ ring motifs at ambient pressure and 1.8 GPa clearly illustrate the closing-up of holes within these motifs (Figures 5.6*a* and 5.6*b*).

The secondary-level $R^4_4(16)$ rings comprise two rows of molecules, consisting of primary-level *C*(5) chains built by N1H7...O2 H-bonds formed along the *c*-axis direction (Figure 5.3*a*). Under pressure, alternate rows shift along the positive and negative *c*-directions (*cf* Figures 5.3*a* and *b*, Figure 5.7). This sliding movement enables the voids to close-up perpendicular to the *c*-direction. A similar effect was observed in L-serine, though in that case the sliding of the rows occurred abruptly and resulted in a phase transition.

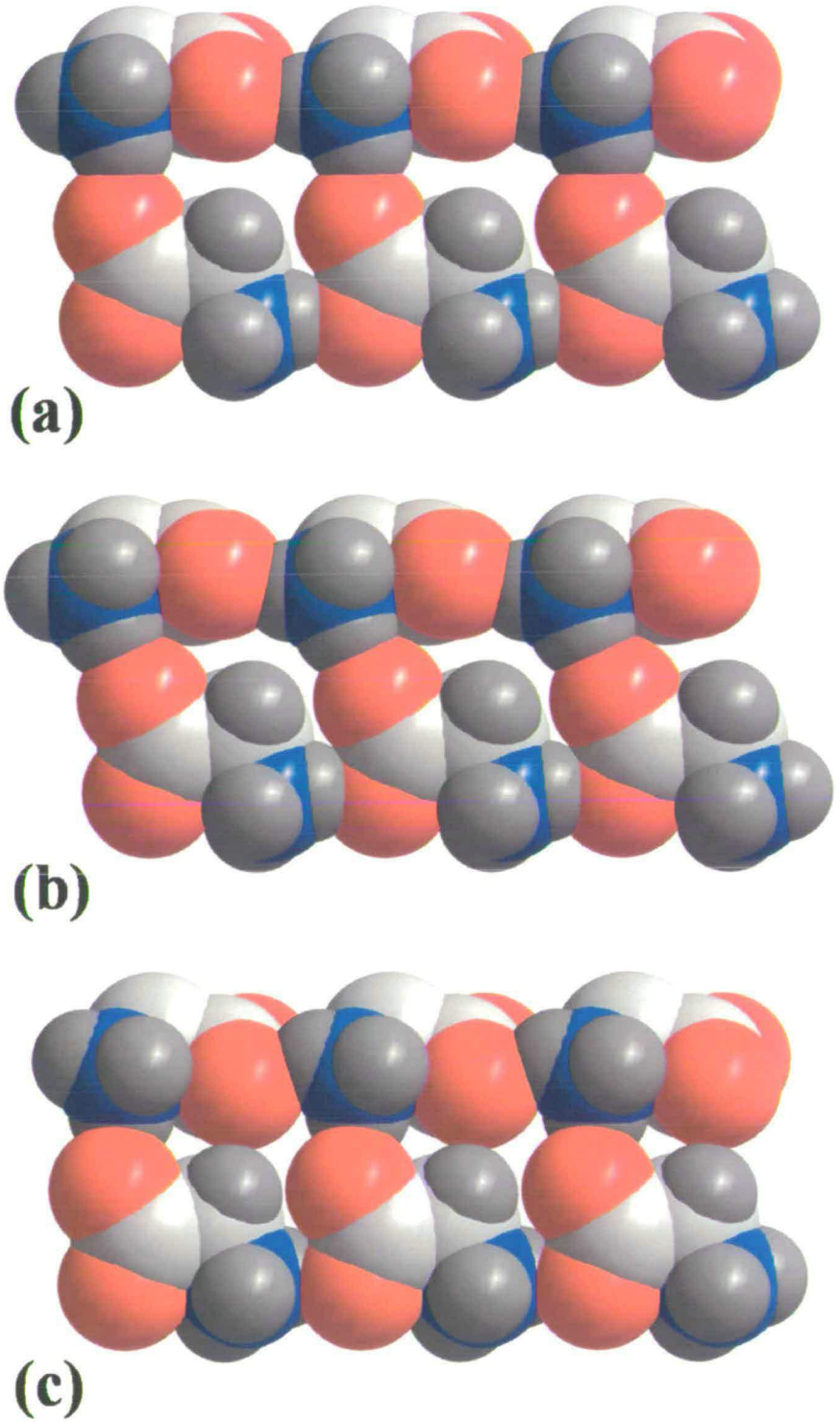

Figure 5.6: Space-filling plots showing $R^4_4(16)$ ring motifs of (a) L-cysteine-I at ambient pressure, (b) L-cysteine-I at 1.8 GPa and (c) L-cysteine-III at 2.6 GPa. Note the hole in the middle of the ring gets progressively smaller on going from (a) to (c). In all three diagrams, the -CH_2SH group has been removed for clarity. Colour scheme as in Figure 5.3.

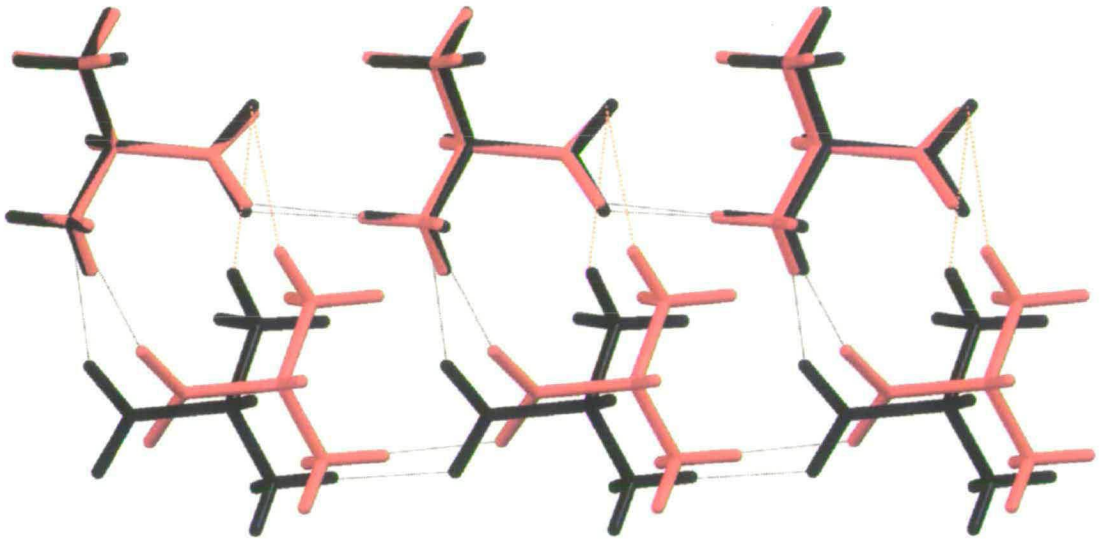

Figure 5.7: Superposition of the $R^4_4(16)$ ring motifs of L-cysteine-I at ambient pressure (black) and 1.8 GPa (red). N-H...O H-bonds are drawn as black dotted lines. Note the sliding movement of the layers that comprise the ring motifs over each other, and a shortening of the C1-H3...O1 contact (orange dotted line) on increasing pressure as a result.

Although the sliding of the rows of molecules contracts the voids in the $R^4_4(16)$ rings, the N-H…O interactions around the perimeter of the rings are not greatly affected, and N…O separations in N1H5...O1 and N1H7...O2 decrease by only 0.06 and 0.05 Å, respectively. We note in passing that the head-to-tail N1H7…O2 interaction is characteristic of many amino acid structures; we have studied its response to pressure in L-serine, L-cystine and α-glycine, and it is always amongst the least compressible of the NH...O H-bonds.

C1H2...O1, which, like N1H7...O2, is formed approximately along the *c*-direction, reduces in length by 0.05 Å. The C1H3...O1 contact, by contrast, becomes shorter by a much greater amount (0.39 Å), and this can be traced to the direction in which this contact is formed relative to the direction in which the void closes. (Figures 5.3*a*, 5.3*b* and 5.7).

A space-filling plot of the $R^2_3(9)$ ring motifs in L-cysteine-I at ambient pressure (Figure 5.8*a*) shows that, though voids are present at the centres of these rings, they are substantially smaller than those which exist in the $R^4_4(16)$ rings (Figure 5.6*a*). Some modest compression of these voids occurs at 1.8 GPa, largely through shortening of the N1H6...O2 H-bonds. With an N…O separation of 3.017(2) Å at ambient pressure these H-bonds are the longest such interactions in L-cysteine-I, and relatively long by the

standards of amino acids in general. It is, perhaps, not surprising that N1H6...O2 H-bonds are the most compressible of this type of interaction, reducing in length by 0.15 Å.

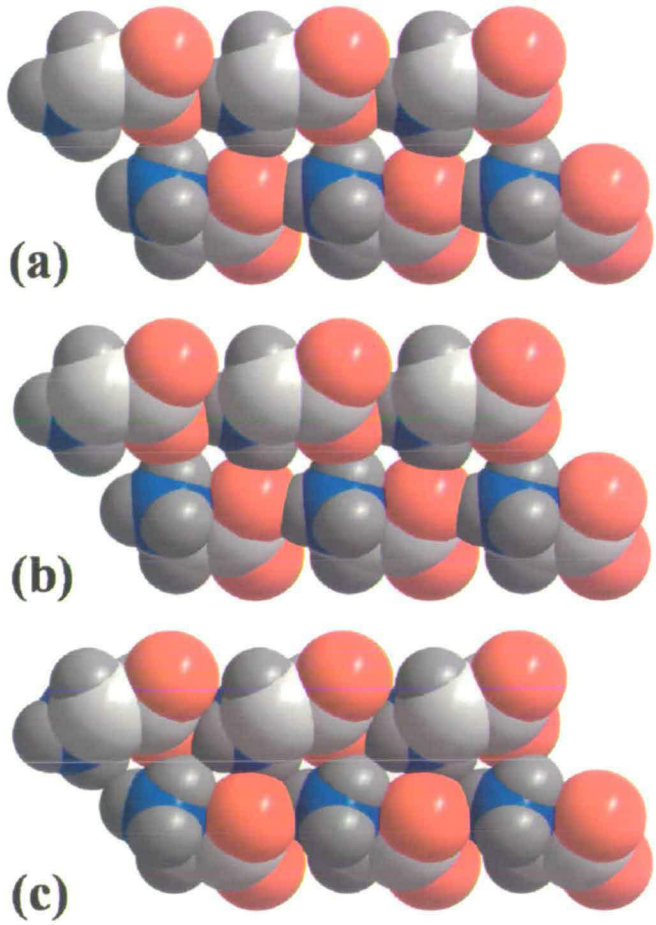

Figure 5.8: Space-filling plots showing $R^2_3(9)$ ring motifs of (a) L-cysteine-I at ambient pressure, (b) L-cysteine-I at 1.8 GPa and (c) L-cysteine-III at 2.6 GPa all viewed perpendicular to the *a*-axis. Note the hole in the middle of the ring motifs get progressively smaller on going from (a) to (c). In all three diagrams, the -CH_2SH group has been removed for clarity. Colour scheme as in Figure 5.3.

The thiol group is disordered in the crystal structure of L-cysteine-I at RT. Different components of the disorder lead to formation of SH...O and SH...S H-bonds, but the latter is marginally favoured. This result is consistent with the results of DFT calculations, which place the SH...S structure 4.11 kJ/mol lower in energy. The shortening of the contacts made around the sulfur atom might imply that ordering of this site occurs. At 1.0 GPa, however, the difference in energy between S1H1...S1 and S1H1...O2 models decreases to 3.94 $kJmol^{-1}$. Moreover, single-crystal neutron diffraction data at 0.5 GPa show that the disorder of the thiol H-atom is not significantly different to that observed at

ambient pressure. Such information as we have available therefore tends to support retention of disorder in L-cysteine-I at elevated pressure.

Interpretation of the changes in contacts involving the S-atoms is difficult because of the disorder of the H-site in the thiol group. For example, analysis of the structure in terms of void-distributions is not possible unless all atomic positions have been modelled. It is possible, though, to draw some conclusions on the basis of the S...O and S...S distances.

In L-cysteine-II at 120 K the thiol group is ordered, with one molecule forming an SH...O H-bond with d(S...O) = 3.404(1) Å, while the other is involved in an SH...S interaction with d(S...S) = 4.080(1) Å. More generally, though data are rather sparse, S...O distances in SH...O H-bonds typically fall into the range 3.3-3.6 Å, whereas S...S distances in SH...S H-bonds are usually *ca* 4 Å (Desiraju & Steiner, 1999).

Even at ambient pressure the S...O and S...S distances, 3.3788(15) and 3.8457(10) Å, are quite short (particularly the latter). At 1.8 GPa the S...O distance [3.280(6) Å] approaches the lower limit for SH...O interactions determined at ambient pressure. The S...S distance becomes very short indeed [3.451(4) Å] by comparison with other SH...S H-bonds. By contrast, a search of the Cambridge Database shows that the shortest N...O and C...O distances observed under ambient conditions in amino acids are 2.6 Å and 3.0 Å; none of the distances N...O or C...O observed at 1.8 GPa in L-cysteine-I approach these values.

We have observed that on increasing pressure to *ca* 2 GPa, a single-crystal to single-crystal phase transition occurs to a hitherto uncharacterised phase of L-cysteine, which we have designated L-cysteine-III. The shortness of the contacts made around the S-atom at 1.8 GPa implies that the system has become quite strained, and it seems plausible to suggest that the phase transition is driven by the need to relieve strain around the S-atom.

5.5.2 L-cysteine-III

The transition from L-cysteine-I to L-cysteine-III was observed during data collection at between 1.7 and 2.1 GPa. This observation is significant because it shows that on compression phase I transforms directly to phase-III without going via an intermediate phase; the reverse statement does not apply on decompression (see below).

There are numerous similarities between L-cysteine-III and L-cysteine-I: for example both contain $R^4_4(16)$ ring motifs arranged in layers which are linked by $R^2_3(9)$ rings. The change from the g^+ to the g^- conformation during the transition is accompanied by an alteration in the pattern of weaker SH...O and CH...O contacts. The strained environment about the S-atom of phase-I at 1.8 GPa (noted above) appears to have been relieved, and though the pressure is higher, the distances involving S are all longer in phase-III.

Space-filling plots of the $R^4_4(16)$ and $R^2_3(9)$ ring motifs in L-cysteine-I and III are compared in Figures 5.6 and 5.8, and it is clear that the voids at the centres of these motifs have closed up significantly in the course of the phase transition. Between ambient pressure and 1.8 GPa the $R^4_4(16)$ and $R^2_3(9)$ rings both contract, but these contractions also act to decrease the length of the S...S interactions. The short interactions about the sulfur atoms in phase I thus act as an effective brake to further closing up of the voids, and the change in conformation which occurs in the phase transition alleviates the steric hindrance between neighbouring CH2-SH groups.

Paradoxically, the data in Table 5.3 show that the lengths of the NH...O H-bonds either stay much the same or actually get longer in passing from phase I to III, while the angles subtended at H in the NH...O H-bonds are somewhat smaller than in the corresponding interactions at ambient pressure. This departure for ideal H-bonding geometry presumably reflects the compromise that needs to be reached between more effective packing and the geometry of specific intermolecular contacts as pressure is increased.

The resistance to compression of the head-to-tail N1H7...O2 H-bonds has been referred to above; this interaction is formed along **c** in both phases I and III, and the *c*-axes are the same length in both phases. The *a*-axis in L-cysteine-III at 2.6 GPa is longer by *ca* 0.5 Å than that in L-cysteine-I at 1.8 GPa. This is related to the smaller amplitude in phase-III of the sinusoidal conformation of the layers formed by the $R^4_4(16)$ rings. This can be quantified by comparing the angle between planes formed by N1 and O1 atoms in the $R^4_4(16)$ rings, which decreases from 72.8(3)° to 41.6(3)° in L-cysteine-I at 1.8 GPa and L-cysteine-III at 2.6 GPa, respectively (Figure 5.9).

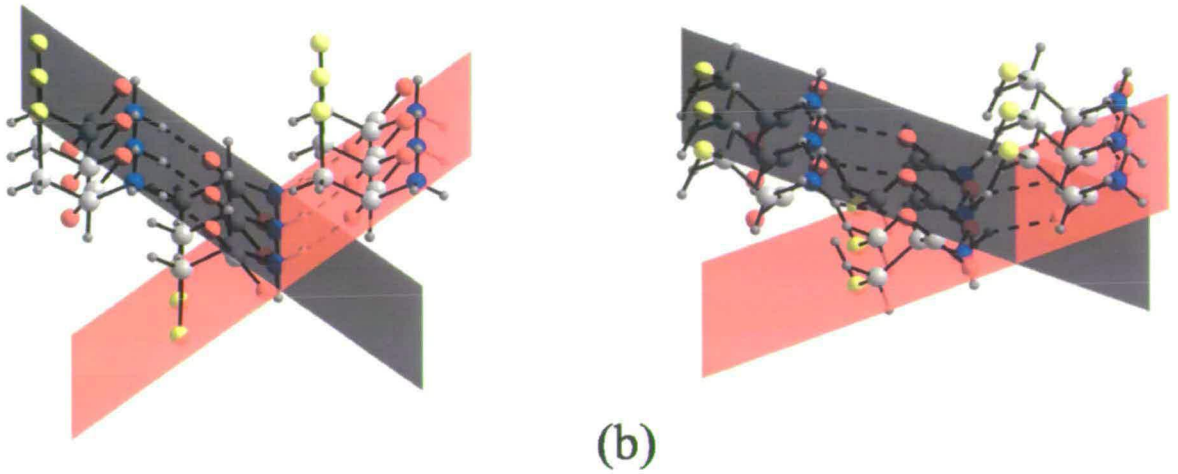

Figure 5.9: Staggered $R^4_4(16)$ ring motifs in (a) L-cysteine-I at 1.8 GPa, and (b) L-cysteine-III at 2.6 GPa. Red and black planes represent the best plane through N1...O1 atoms in adjacent $R^4_4(16)$ ring motifs. Note the reduction in angle between the planes from 72.8(3)° in (a), to 41.6(3)° in (b). Colour scheme as in Figure 5.3.

The cell-dimension that exhibits the largest change during the phase transition is *b*, which reduces from 12.000(3) Å at 1.8 GPa, to 10.4883(19) Å at 2.6 GPa. The reduction is related to the flattening of the layers described above, but also to the conformational change in the cysteine molecules, which makes the -CH_2-SH groups rotate, allowing the layers to move closer together.

5.5.3 L-Cysteine-IV

L-cysteine-III is stable to at least 4.2 GPa. Similar cell dimensions were observed for phase-III at similar pressures during the compression and decompression phases of experiments. This has been a consistent feature of compression studies of other amino acids, which tend to be quite elastic. However on decreasing the pressure to 1.8 GPa L-cysteine-III converts not to L-cysteine-I, but instead to another, previously unobserved, phase of cysteine, L-cysteine-IV. Like the I-to-III transition, this phase change occurs from one single crystal form to another. In most experiments the transition resulted in such a marked increase in mosaic spread that, though unit cell dimensions could be determined, intensity data were of very low quality. Many attempts were made to obtain a better sample suitable for structure determination, with the best data obtained in a study using pentane-isopentane; the pressure on a crystal of L-cysteine-I was increased rapidly in 1.5 GPa steps in quick succession from 0.3 GPa, to a final pressure of 4.2 GPa

(formation of phase-III being confirmed by single crystal diffraction), and then reduced back down to 1.7 GPa.

L-cysteine-IV is an intermediate in the phase transition between L-cysteine-III and L-cysteine-I. The structure of L-cysteine-IV contains elements of both phases I and III, with the two molecules that comprise the asymmetric unit in the g^+ and g^- conformations found in I and III, respectively. It was noted above that the geometric parameters which characterise the H-bonds in L-cysteine-III show some departure from ideal values. Molecule 1 in L-cysteine-IV is in the same conformation as the molecules in L-cysteine-III, and the geometries of its intermolecular interactions are also similar to those observed in phase-III. That this phase should be unstable as the pressure is reduced is therefore understandable, and on further reduction of pressure it transforms completely to L-cysteine-I.

While formation of intermediate phases is uncommon in molecular systems, it has been observed in some 'inorganic' systems. $CsCuCl_3$, for example exhibits related dynamically and statically disordered phases (Christy *et al.*, 1994). The low-pressure, low-temperature phases of anorthite and clinopyroxene are formed by zone-boundary transitions from the high-pressure or high-temperature structures, and have structures that are made up of the alternation of portions of the high-pressure and high-temperature structures (Christy & Angel, 1996). Additionally, lithium transforms between two cubic phases via an intermediate rhombohedral phase, while in PbTe transformation from a NaCl to a CsCl structure occurs via an intermediate orthorhombic phase (Rousse *et al.*, 2005).

5.6 Conclusions

We have described the effect of pressure on the crystal structure of L-cysteine-I to 1.8 GPa. The structure can be considered to consist of layers that lie within the *ac*-plane constructed from $R^4_4(16)$ ring motifs that in projection, have a sinusoidal appearance. These layers are then linked along the *b*-direction by $R^3_3(9)$ ring motifs. The main response of L-cysteine-I to pressure is ascribed to the closing up of voids within these ring motifs. At 1.8 GPa the N...O distances fall into the range 2.7-2.9 Å, which is quite normal for such interactions even at ambient pressure. However, the S...S distances are very short [3.450(4) Å], and beyond 1.8 GPa a phase transition occurs to L-cysteine-III.

As was described in the introduction section, this behaviour is consistent with the behaviour of other amino acids under pressure.

The phase change from L-cysteine-I to L-cysteine-III is accomplished by a change in the NCCS torsion angle, and small positional displacements with no major changes in the orientations of the molecules. The transition from one single-crystal to another is therefore not surprising. Like L-cysteine-I, the structure of L-cysteine-III comprises $R^4_4(16)$ and $R^2_3(9)$ ring motifs; the torsion twist about NCCS alleviates the close S...S contact formed at 1.8 GPa, and allows voids within these ring motifs to be compressed further.

L-cysteine-III was found to be stable to at least 4.2 GPa. On decompression to 1.7 GPa, another single-crystal to single-crystal phase transition was observed to L-cysteine-IV, a transition that is not observed on increasing pressure. The structure consists of two crystallographically independent cysteine molecules in the same conformations as those found in L-cysteine-I and L-cysteine-III. The structure separates into zones which are alternately phase-I-like and phase-III-like. L-cysteine-IV and can therefore be thought of as an unusual example of an intermediate phase. On further decompression to ambient pressure, diffraction data collected on a small crystallite from the now polycrystalline sample confirmed return to the ambient pressure, L-cysteine-I phase.

5.7 *References*

Allan, D. R. & Clark, S. J. (1999). *Phys. Rev. Lett.*, **82**, 3464-3467.

Allan, D.R., Clark, S. J., Ibberson, R. M., Parsons, S., Pulham, C. R. & Sawyer, L. (1999) *Chem. Comm.*, 751-752.

Allan, D. R., Parsons, S. & Teat, S. J. (2001). *J. Synchrotron Rad.*, **8**, 10-17.

Allen, F. H. (2002). *Acta Cryst. B***58**, 380-388.

Allen, F. H. & Motherwell, W. D. S. (2002). *Acta Cryst. B***58**, 407-422.

Altomare, A., Cascarano, G., Giacovazzo G., Guagliardi A., Burla M. C., Polidori, G. & Camalli, M. (1994). *J. Appl. Cryst.* **27**, 435-435.

Betteridge, P. W., Carruthers, J. R., Cooper, R. I., Prout, K., & Watkin, D. J. (2003). *J. Appl. Cryst.* **36**, 1487.

Boldyreva, E. V. (2003). *J. Mol. Struct.* **647**, 159-179.

Boldyreva, E. V. (2004a). *J. Mol. Struct.* **700**, 151-155.

Boldyreva, E. V. (2004b). *NATO Science Series, II: Mathematics, Physics & Chemistry*, edited by A. Katrusiak & P. F. McMillan, Vol. 140, pp. 495-512. Dordrecht: Kluwer Academic Publishers.

Bondi, A. (1964). *J. Phys. Chem.* **68**, 441-451.

Bruker (2002). SMART. Area-Detector Software Package, Madison, Wisconsin, USA.

Bruker (2004). SAINT, Version V7.12A. Area-Detector Integration Software, Madison, Wisconsin, USA.

Bruno, I. J., Cole, J. C., Edgington, P. R., Kessler, M., Macrae, C. F., McCabe, P., Pearson, J. & Taylor, R. (2002). *Acta Cryst. B***58**, 389-397.

Christy, A. G. & Angel, R. J. (1996). *Phys. Chem. Min.* **22**, 129-134.

Christy, A. G., Angel, R. J., Haines, J. & Clark, S. M. (1994). *J. Phys.: Condensed Matter,* **6**, 3125-36.

Clark, S. J., Ackland, G. J. & Crain, J. (1998). *Europhys. Lett.* **44**, 578-584.

Cooper, R.I., Gould, R.O., Parsons, S. & Watkin, D.J. (2002). *J. Appl. Cryst.*, **35**, 168-174.

Crystal Impact (2004). *DIAMOND*. Version 3.0. Crystal Impact GbR, Postfach 1251, 53002 Bonn, Germany. http://www.crystalimpact.com/diamond.

Dawson, A., Allan, D. R., Belmonte, S. A., Clark, S. J., David,W. I. F., McGregor, P. A., Parsons, S., Pulham, C. R. & Sawyer, L. (2005). *Cryst. Growth Des.* **5**, 1415-1427.

Dawson, A., Allan, D. R., Clark, S. J., Parsons, S. & Ruf, M. (2004). *J. Appl. Cryst.* **37**, 410-416.

Derewenda, Z. S., Lee, L. & Derewenda, U. (1995). *J. Mol. Biol.* **252**, 248-262.

Desiraju, G. R. & Steiner, T. (1999). *The Weak Hydrogen Bond in Structural Chemistry and Biology. IUCr Monographs on Crystallography No. 9*. Oxford Univerity Press, Oxford.

Fabbiani, F. P. A., Allan, D. R., David, W. I. F., Moggach, S. A., Parsons, S. & Pulham, C. R. (2004). *CrystEngComm.*, **6**, 504-511.

Fabbiani, F. P. A., Allan, D. R., Dawson, A., David, W. I. F., McGregor, P. A., Oswald, I. D. H., Parsons, S. & Pulham, C. R. (2003). *Chem. Comm.*, 3004-3005.

Fabbiani, F. P. A.., Allan, D. R., Marshall, W. G., Parsons, S., Pulham, C. R.. & Smith, R. I. (2005a). *J. Cryst. Growth*, **275**, 185-192.

Fabbiani, F. P. A., Allan, D. R., Parsons, S. & Pulham, C. R. (2005b) *CrystEngComm*, **7**, 179-186.

Farrugia, L. J. (1999). *J. Appl. Cryst.* **32**, 837-838.

Görbitz, C. H. (1990). *Acta Chem. Scand.* **44**, 584-590.

Görbitz, C. H. & Dalhus, B. (1996). *Acta Cryst. C***52**, 1756-1759.

Gutmann, M. J. (2005). SXD2001. ISIS, Faciltiy, Rutherford-Appleton Laboratory, Oxfordshire, England.

Harding, M. M., Long H.A. (1968). *Acta Cryst. B***24**, 1096-1102.

Hemley, R. J. & Dera, P. (2000). *Rev. Mineral. Geochem.* **41**, 335-419.

Hummer, G., Garde, S., Garcia, A.E., Paulaitis, M. E. & Pratt, L.R. (1998). *Proc. Nat. Acad. Sci. USA*, **95**, 1552-1555.

Hušák, M. & Kratochvila, B. (2003). *J. Appl. Cryst.* **36**, 1104.

Katrusiak, A. (2004). *NATO Science Series, II: Mathematics, Physics and Chemistry*, edited by A. Katrusiak & P. F. McMillan, Vol. 140, pp. 513-520. Dordrecht: Kluwer Academic Publishers.

Keen, D. A., Wilson, C. C. & Gutmann, M. J. (2005) *Manuscript in preparation.*

Kerr, K. A. & Ashmore, J. P. (1973). *Acta Cryst. B***29**, 2124-2127.

Kerr, K. A., Ashmore, J. P. & Koetzle, T. F. (1975). *Acta Cryst. B***31**, 2022-2026.

Lozano-Casal, P., Allan, D. R., & Parsons, S. (2005). *Acta Cryst. B***61**. In press.

Luger, P. & Weber, M. (1999). *Acta Cryst. C***55**, 1882-1885.

McGregor, P. A., Allan, D. R., Parsons, S. & Pulham, C. R. (2005). *Acta Cryst. B***61**, 449-454.

Merrill, L. & Bassett, W.A. (1974). *Rev. Sci. Instrum.*, **45**, 290-294.

Moggach, S. A., Allan, D. R., Lozano-Casal, P. & Parsons, S. (2005a). *J. Synchrotron Rad.*, **12**, 590-597.

Moggach, S. A., Allan, D. R., Morrison, C. A., Parsons, S. & Sawyer, L. (2005b). *Acta Cryst. B***61**, 58–68.

Moggach, S. A., Allan, D. R., Parsons, S., Sawyer, L. & Warren, J. E. (2005c). *J. Synchrotron Rad.* **12**, 598–607.

Moggach, S. A., Clark, S. J. & Parsons, S. (2005d). *Acta Cryst. E***61**, 2739-2742.

Monkhorst, H. J. & Pack, J.D. (1976). *Phys. Rev. B***13**, 5188-5192.

Murli, C., Sharma, S. M, Karmakar, S. and Sikka, S. K. (2003) *Physica B, 339*, 23-30.

Oswald, I. D. H., Allan, D. R., Day, G. M., Motherwell, W. S. D. & Parsons, S. (2005). *Cryst. Growth Des.* **5**. 1055–1071.

Parsons, S. (2004). *SHADE*. The University of Edinburgh, Scotland.

Perdew, J.P. & Wang, Y. (1992). *Phys.Rev.* B**46**, 12947-12954.

Piermarini, G. J., Block, S., Barnett, J. D. & Forman, R. A. (1975). *J. Appl. Phys.* **46**, 2774-2780.

Prince, E. (1982). *Mathematical Techniques in Crystallography and Materials Science.* Springer-Verlag, New York.

Rousse, G., Klotz, S., Saitta, A. M., Rodriguez-Carvajal, J. McMahon, M. I. Couzinet, B. & Mezouar. M. (2005). *Phys. Rev. B***71**, 2241161-2241166.

Segall, M. D., Lindan, P. J. D., Probert, M. J., Pickard, C. J., Hasnip, P. J., Clark, S. J. & Payne, M. C. (2002). *J. Phys. Condens. Matter*, **14**, 2717-2744.

Sheldrick, G. M. (2001). *SHELXL97*. University of Göttingen, Germany.

Sheldrick, G. M. (2004a). *SADABS*. University of Göttingen, Germany.

Sheldrick, G. M. (2004b). *TWINABS*. University of Göttingen, Germany.

Sheldrick, G. M. (1997). *XP*. University of Göttingen, Germany.

Spek, A. L. (2003). *J. Appl. Cryst.* **36**, 7-13.

Vanderbilt, D. (1990). *Phys. Rev. B***41**, 7892-7895.

Watkin D.J. (1994). *Acta Cryst., A***50**, 411-437

Watkin, D. J., Prout, C. K. & Pearce, L. J. (1996). *CAMERON*. Chemical Crystallography Laboratory, Oxford, UK.

Chapter 6

The Effect of Pressure on the Crystal Structure of α-glycylglycine to 4.7 GPa; application of Hirshfeld surfaces to analyse contacts on increasing pressure.[v]

[v] Moggach, S. A., Allan, D. R., Parsons, S. & Sawyer, L. (2005). *Submitted for publication.*

6.1 *Synopsis*

The effect of pressure to 4.7 GPa on the crystal structure of the simplest dipeptide, glycylglycine, has been investigated. The structure is built of layers resembling the β-sheets of proteins. These layers are quite robust, with the main structural effect of pressure being to compress layers together.

6.2 *Introduction*

Glycylglycine (GLYGLY) is the simplest dipeptide. It is composed of two glycine residues, and in the solid state it exists in three different polymorphic forms. These polymorphs were designated α-, β- and γ- by Bernal *et al.*, (1931). The α- and β-polymorphs crystallise in the monoclinic space groups $P2_1/c$ and $A2/a$, respectively, while the γ-polymorph crystallises in the orthorhombic space group $Pbc2_1$. A preliminary investigation made by Bernal *et al.*, (1931) found that all three polymorphs could be grown simultaneously from the same mother liquor by slow evaporation from concentrated mixtures in *n*-propyl alcohol and water. It was found in this study that the plate-like α-form predominates, with numerous recrystallisations required to obtain crystals of the β- and γ-polymorphs. The β- and γ- forms can also be converted to the α-form upon heating at 105° for 24 hours (Hughes *et al.*, 1949). No report of the γ-polymorph has appeared since Bernal's publication in 1931, while no report of the β polymorph has appeared since Hughes *et al.*, (1949). The α-GLYGLY polymorph, however, has been studied more recently by both neutron and X-ray diffraction, the most recent of which was reported by Kvick *et al.*, (1979) in a deformation electron density study.

The response of crystal structures of several amino acids to high hydrostatic pressure have been described recently (Dawson *et al.*, 2005; Moggach *et al* 2005a; Moggach *et al* 2005b; Moggach *et al* 2005c, Boldyreva *et al.*, 2004, Boldyreva *et al.*, 2005). The behaviour of the distances characterising intermolecular interactions was rationalised by studying the way in which interstitial voids deform under pressure. It was notable that compression continued until the minimum distance as observed for a specific interaction (*e.g.* the N...O distance in an N-H...O hydrogen bond) under ambient pressure has been reached (*i.e.* super-short H-bonds are apparently not formed up to about 10 GPa), and it was at this point that a phase transition occurred. However, the extent to

which our observations have any generality still needs to be established, and we now extend this work to the α-polymorph of GLYGLY. Although some studies have appeared recently on the behaviour of proteins under non ambient pressure conditions, for example on cubic Cowpea mosaic virus crystals (Girard *et. al.*, 2005), this is the first study in which the crystal structure of a dipeptide has been examined at high pressure.

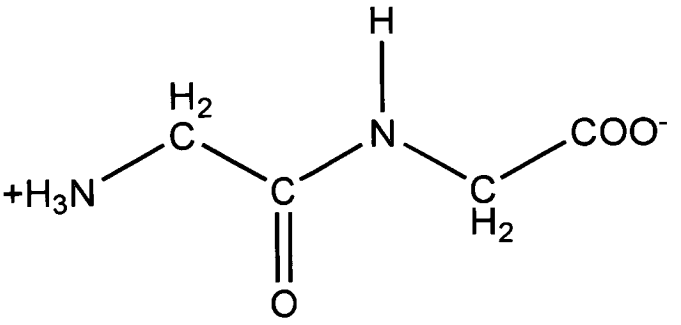

GLYGLY

6.3 *Experimental*

6.3.1 Crystal growth and high-pressure crystallography

Crystals of α-GLYGLY were grown by slow diffusion of ethanol into a concentrated aqueous solution of GLYGLY (99%) obtained from Sigma (catalogue number G, 1002). One block shaped crystal of dimensions 0.1 × 0.2 × 0.2 mm^3 was selected and loaded into a Merrill-Bassett diamond anvil cell (Merrill & Bassett, 1974). The cell had a half-opening angle of 40° and was equipped with 600μm culets and a tungsten gasket. A 4:1 mixture of methanol and ethanol was used as a hydrostatic medium. A small ruby chip was also loaded into the cell as the pressure calibrant, with the ruby fluorescence method used to measure the pressure (Piermarini *et al.*, 1975).

6.3.2 Data collection, reduction and refinement.

A hemisphere of reflections was collected at ambient temperature and pressure in order to provide a comparison with data collected at increasing pressures during the pressure study, all of which were also collected at ambient temperature (see below). Diffraction data were collected (Bruker-Nonius, 2002) on a Bruker SMART APEX diffractometer with graphite-monochromated Mo-Kα radiation (λ = 0.71073 Å). These data were integrated using the program SAINT (Bruker-Nonius, 2004a), and an absorption correction was performed with the program SADABS (Sheldrick, 2004). The α-GLYGLY coordinates of Kvick *et al.*, (1979) were refined against these data to yield a conventional *R*-factor of 0.0488 for 1164 data with $I > 2\sigma(I)$. A listing of crystal and

refinement data is given in Table 6.1. The molecular structure and numbering scheme used is shown in Figure 6.1.

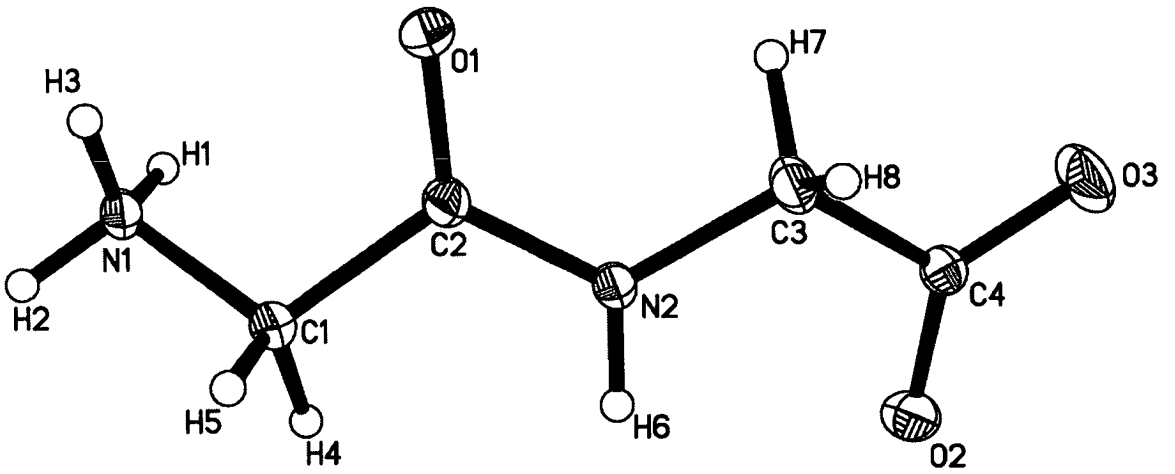

Figure 6.1: The molecular structure of GLYGLY at ambient temperature and pressure showing atom labelling. Ellipsoids are drawn at the 30% probability level, H-atoms are drawn as spheres of arbitrary radius.

High-pressure diffraction data were collected on a kappa-geometry, Bruker APEX II diffractometer with graphite-monochromated Mo-Kα radiation (λ = 0.71073 Å) (Bruker-Nonius, 2004b). Data collection procedures followed those of Dawson *et al.* (2004). Integrations were carried out using the program SAINT, and absorption corrections in a two stage process with the programs SHADE (Parsons, 2004) and SADABS. Data collections were taken in approximately 1.0 GPa steps from 1.4 GPa up to a final pressure of 5.3 GPa.

Refinements were carried out starting from the coordinates determined at ambient pressure. Minimisation was against $|F|^2$ using all data (CRYSTALS, Betteridge *et al.*, 2004). Because of the low completeness of the data-sets, all 1,2 and 1,3 distances were restrained to values observed in the ambient pressure structure, specifically, the restraints were as follows: distances (Å) N1-C1 1.473(5); C1-C2 1.511(5); C2-O1 1.238(5); C2-N2 1.330(5); N2-C3 1.450(5); C3-C4 1.513(5); C4-O3 1.240(5); C4-O2 1.255(5); angles (°) N1-C1-C2 109(1); C1-C2-O1 120(1); O1-C2-N2 123(1); N2-C2-C1 116(1); C4-C3-N2 112(1); C3-C4-O3 115(1); C3-C4-O2 118(1); O2-C4-O3 126(1); C2-N2-C3 121(1). All non-hydrogen atoms were refined with isotropic displacement parameters. Due to the poor quality of the data set collected at 5.4 GPa, only those data collected to 4.7 GPa are

used for structural comparison to the ambient temperature and pressure structure. Listings of crystal and refinement data are given in Table 6.1.

Crystal structures were visualized using the programs DIAMOND (Crystal Impact, 2004) and XP (Sheldrick, 1997). Analyses were carried out using PLATON (Spek, 2003), as incorporated in the WIN-GX suite (Farrugia, 1999). Searches of the Cambridge Database (Allen, 2002; Allen & Motherwell, 2002) were performed with the program CONQUEST and version 5.26 of the database with updates up to August 2005. Hirshfeld surface analysis was performed using the program CrystalExplorer (Wolff *et al.*, 2005).

	Pressure (GPa)				
	0	**1.4**	**3.0**	**3.7**	**4.7**
Crystal data					
Chemical formula	$C_4H_8N_2O_3$	$C_4H_8N_2O_3$	$C_4H_8N_2O_3$	$C_4H_8N_2O_3$	$C_4H_8N_2O_3$
M_r	132.12	132.12	132.12	132.12	132.12
Cell setting, space group	Monoclinic, $P2_1/c$	Monoclinic, $P2_1/c$	Monoclinic, $P2_1/c$	Monoclinic, $P2_1/c$	Monoclinic, $P2_1/c$
a, b, c (Å)	8.1233 (18), 9.554 (2), 7.8224 (17)	7.6428 (3), 9.3800 (4), 7.6505 (5)	7.4304 (4), 9.2896 (7), 7.5943 (9)	7.3100 (15), 9.232 (2), 7.550 (3)	7.2437 (8), 9.2083 (13), 7.5328 (17)
β (°)	107.596 (4)	103.882 (4)	102.465 (7)	101.51 (3)	101.214 (14)
V (Å^3)	578.7 (2)	532.44 (5)	511.84 (8)	499.3 (3)	492.86 (14)
Z	4	4	4	4	4
D_x (Mg m^{-3})	1.516	1.648	1.714	1.758	1.780
Radiation type	Mo $K\alpha$	Mo $K\alpha$	Mo $K\alpha$	Mo $K\alpha$	Mo $K\alpha$
No. of reflections for cell parameters	1501	1234	1235	1211	1070
θ range (°)	5–56	5–52	6–53	6–53	6–52
μ (mm^{-1})	0.13	0.14	0.15	0.15	0.15
Temperature (K)	293	293	293	293	293
Crystal form, colour	Block, colourless	Block, colourless	Block, colourless	Block, colourless	Block, colourless
Crystal size (mm)	0.60 × 0.36 × 0.12	0.20 × 0.20 × 0.10	0.20 × 0.20 × 0.10	0.20 × 0.20 × 0.10	0.20 × 0.20 × 0.10

Table 6.1: Crystallographic data for α-GLYGLY at ambient temperature and pressure and increasing pressures.

	Pressure (GPa)				
	0	**1.4**	**3.0**	**3.7**	**4.7**
Data collection					
Diffractometer	Bruker APEX	Bruker APEX II	Bruker APEX II	Bruker APEX II	Bruker APEX II
Data collection method	ω	ω	ω	ω	ω
Absorption correction	Multi-scan	Multi-scan	Multi-scan	Multi-scan	Multi-scan
T_{min}	0.86	0.85	0.86	0.84	0.75
T_{max}	0.98	0.99	0.99	0.99	0.98
No. of measured, independent and observed parameters	3696, 1390, 1164	2911, 471, 360	2733, 451, 348	2678, 435, 332	2669, 437, 318
Criterion for observed reflections	$I > 2.00u(I)$	$I > 2.00u(I)$	$I > 2.00u(I)$	$I > 2.00u(I)$	$I > 2.00u(I)$
Completeness (%)	99.8	45.4	45.2	45.8	45.8
R_{int}	0.027	0.052	0.048	0.048	0.052
θ_{max} (°)	28.7	27.2	26.8	26.9	27.2
Range of h, k, l	$-10 \rightarrow h \rightarrow 6$	$-9 \rightarrow h \rightarrow 9$	$-9 \rightarrow h \rightarrow 8$	$-9 \rightarrow h \rightarrow 8$	$-9 \rightarrow h \rightarrow 8$
	$-11 \rightarrow k \rightarrow 12$	$-11 \rightarrow k \rightarrow 11$	$-10 \rightarrow k \rightarrow 10$	$-10 \rightarrow k \rightarrow 10$	$-10 \rightarrow k \rightarrow 10$
	$-10 \rightarrow l \rightarrow 10$	$-5 \rightarrow l \rightarrow 5$	$-5 \rightarrow l \rightarrow 5$	$-5 \rightarrow l \rightarrow 5$	$-5 \rightarrow l \rightarrow 5$
Refinement					
Refinement on	F^2	F^2	F^2	F^2	F^2
$R[F^2 > 2\sigma(F^2)]$, $wR(F^2)$, S	0.049, 0.140, 1.01	0.076, 0.198, 1.05	0.075, 0.189, 1.03	0.068, 0.163, 1.04	0.072, 0.187, 1.03
No. of relections	1385 reflections	455 reflections	434 reflections	419 reflections	422 reflections
No. of parameters	82	37	37	37	37
H-atom treatment	Not refined	Not refined	Not refined	Not refined	Not refined
Weighting scheme	Calculated $w = 1/[\sigma^2(F^2) + (0.08P)^2 + 0.11P]$ where $P = (\max(F_o^2,0) + 2F_c^2)/3$	Calculated $w = 1/[\sigma^2(F^2) + (0.08P)^2 + 2.28P]$ where $P = (\max(F_o^2,0) + 2F_c^2)/3$	Calculated $w = 1/[\sigma^2(F^2) + (0.08P)^2 + 1.99P]$ where $P = (\max(F_o^2,0) + 2F_c^2)/3$	Calculated $w = 1/[\sigma^2(F^2) + (0.05P)^2 + 2.18P]$ where $P = (\max(F_o^2,0) + 2F_c^2)/3$	Calculated $w = 1/[\sigma^2(F^2) + (0.08P)^2 + 2.23P]$ where $P = (\max(F_o^2,0) + 2F_c^2)/3$
$(\Delta/\sigma)_{max}$	<0.0001	<0.0001	<0.0001	<0.0001	<0.0001
$\Delta\rho_{max}$, $\Delta\rho_{min}$ (e Å^{-3})	0.28, –0.35	0.40, –0.38	0.38, –0.35	0.31, –0.30	0.35, –0.33

Table 6.1 (cont'd): Crystallographic data for α-GLYGLY at ambient temperature and pressure and increasing pressures.

6.4 Results

6.4.1 *The structure of α-GLYGLY at ambient temperature and pressure.*

Like all amino acids, in the solid state α-GLYGLY crystallises in its zwitterionic tautomer, with charged carboxyl and ammonium moieties. The structure is dominated by the formation of NH...O H-bonds, with five such interactions formed under ambient temperature and pressure conditions. The H-bond N2H6...O1, is formed between the N-H and C=O moieties of neighbouring peptide groups and together with N1H3...O2 form an $R^2_2(10)$ ring motif (Figure 6.2a, Bernstein *et al.*, 1995). Both of these H-bonds are also involved in the formation of a larger $R^4_4(18)$ ring motif created with another of the NH...O H-bonds, N1H2...O3. The alternating pattern of $R^2_2(10)$ and $R^4_4(18)$ rings builds-up layers of GLYGLY molecules which lie parallel to the (1 0 -1) plane. The layers are reminiscent of anti-parallel β-sheets observed in protein structures (*cf* Figures 6.2a and b).

A bifurcated interaction, N1H1...O2/O3, connects the layers into a three-dimensional H-bonded array interacting between the layers (Figure 6.3a). The shorter of the bifurcated H-bonds, N1H1...O2, forms an $R^4_4(12)$ ring motif with N1H2...O3, the H-bond involved in the formation of the $R^4_4(18)$ ring motifs. Pairs of centrosymmetrically-related N1H1...O2 bonds also form $R^2_2(16)$ rings between the layers (Figure 6.4a). The longer component of the bifurcated interaction, N1H1...O3, is quite long at ambient pressure [3.196(3) Å], though it decreases in length on compression (see below). This bifurcated interaction, together with N1H2...O3 and N1H3...O2 forms an $R^2_3(6)$ ring motif which, like both the $R^2_2(16)$ and $R^4_4(12)$ ring motifs interacts between the layers (Figure 6.3a).

To summarise, the three dimensional H-bonding network within α-GLYGLY can be described by reference to five *R*-type ring motifs. $R^2_2(10)$ and $R^4_4(18)$ ring motifs form layers, reminiscent of anti-parallel β-sheet motifs in protein structures and lie parallel to the (1 0 -1) planes, while $R^4_4(12)$, $R^2_2(16)$ and $R^2_3(6)$ ring motifs connect these layers into a three-dimensional H-bonded network

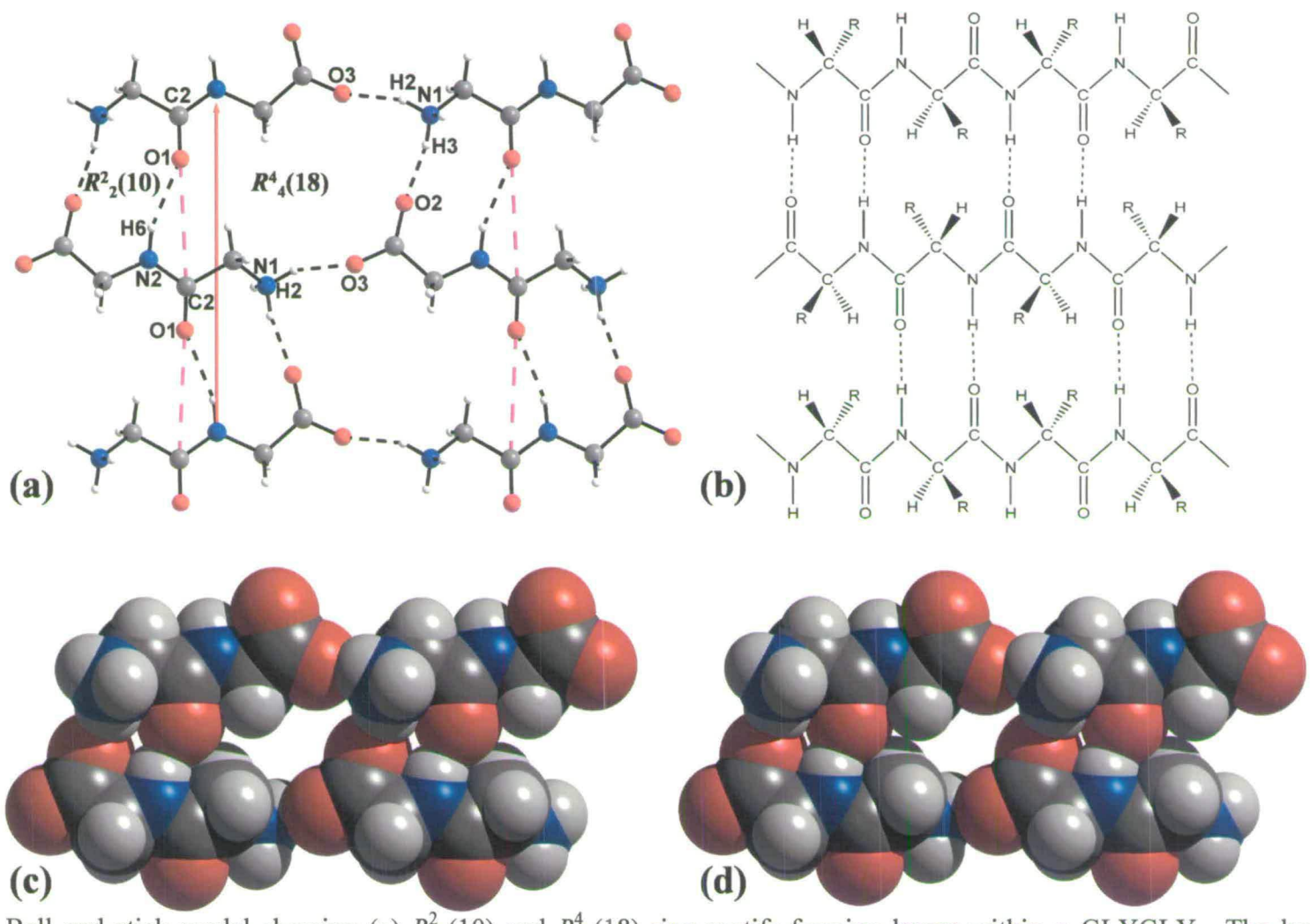

Figure 6.2: Ball and stick model showing (a) $R^2_2(10)$ and $R^4_4(18)$ ring motifs forming layers within α-GLYGLY. The layers formed within the structure are also reminiscent to that of an anti-parallel β-sheet motif (b). Hydrogen bonds are drawn as black dotted lines, while weak C=O…C=O interactions are shown, only in (a), as pink dotted lines. The second largest component of the strain tensor is drawn as a red arrow in (a). Space-filling plots for (c) α-GLYGLY at ambient pressure, and (d), at 4.7 GPa are shown. (a-c) are viewed perpendicular to the (1 0 -1) plane. Note that voids in $R^4_4(18)$ and $R^2_2(10)$ ring motifs close up on increasing pressure. Colour scheme N blue, C grey, O red and H white.

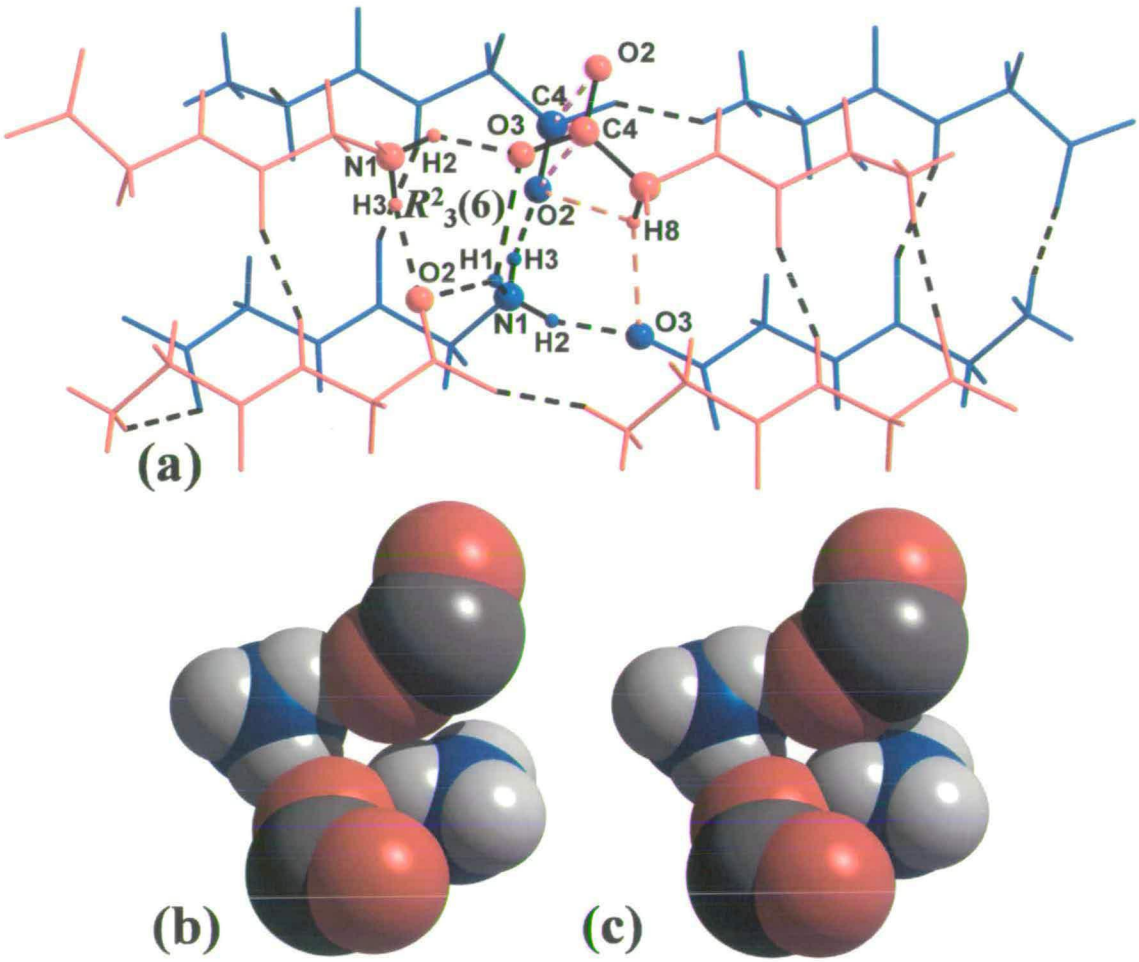

Figure 6.3: Ball and stick/wire model showing interactions between layers of GLYGLY molecules as viewed (a) perpendicular to the (1 0 -1) plane. Molecules in upper and lower layers are coloured red and blue respectively. $R^2_3(6)$ ring motifs between layers of GLYGLY molecules are shown. Black and orange dotted lines represent NH...O and CH...O H-bonds, respectively, while pink dotted lines represent weak C=O…C=O interactions. Space filling plots of $R^2_3(6)$ ring motifs at (b) ambient pressure and (c) 4.7 GPa are shown, drawn at the same scale and direction with only the ammonium and carboxyl groups involved in the formation of the rings shown. Colour scheme is the same as that in Figure 6.2.

In amino acid structures the presence of other interactions, particularly weaker CH...O interactions are thought to be important for supporting moderate strength NH...O H-bonds (Desiraju & Steiner, 1999; Derewenda *et al.*, 1995). We have discussed this recently in high-pressure studies of the crystal structures of polymorphs of glycine (Dawson *et al.*, 2005) and serine (Moggach *et al.*, 2005b). In α-GLYGLY, four CH....O interactions exist at ambient pressure and temperature. A pair of these, C3H8...O2/O3, constitutes a bifurcated H-bond which interacts between the layers to the carboxyl oxygen

atoms involved in the formation of the $R^4_4(18)$ ring motifs previously described (Figure 6.3a). The third CH...O interaction, C1H5...O1, is H-bonded to the peptide carbonyl oxygen and also interacts between the layers. The final CH...O H-bond, C1H4...O1, like C1H5...O1 is also H-bonded to the carbonyl oxygen, however, unlike C1H5...O1, this H-bond interacts within the layers. The combination of both C1H4...O1 and C1H5...O1 produces an $R^2_4(8)$ ring motif between the layers (Figure 6.5a). C1H4...O1 is of particular interest, as it has been shown to have preferred directionality and length in parallel and anti-parallel β-sheets with typical C...O distances of 3.31 and 3.27 Å respectively.

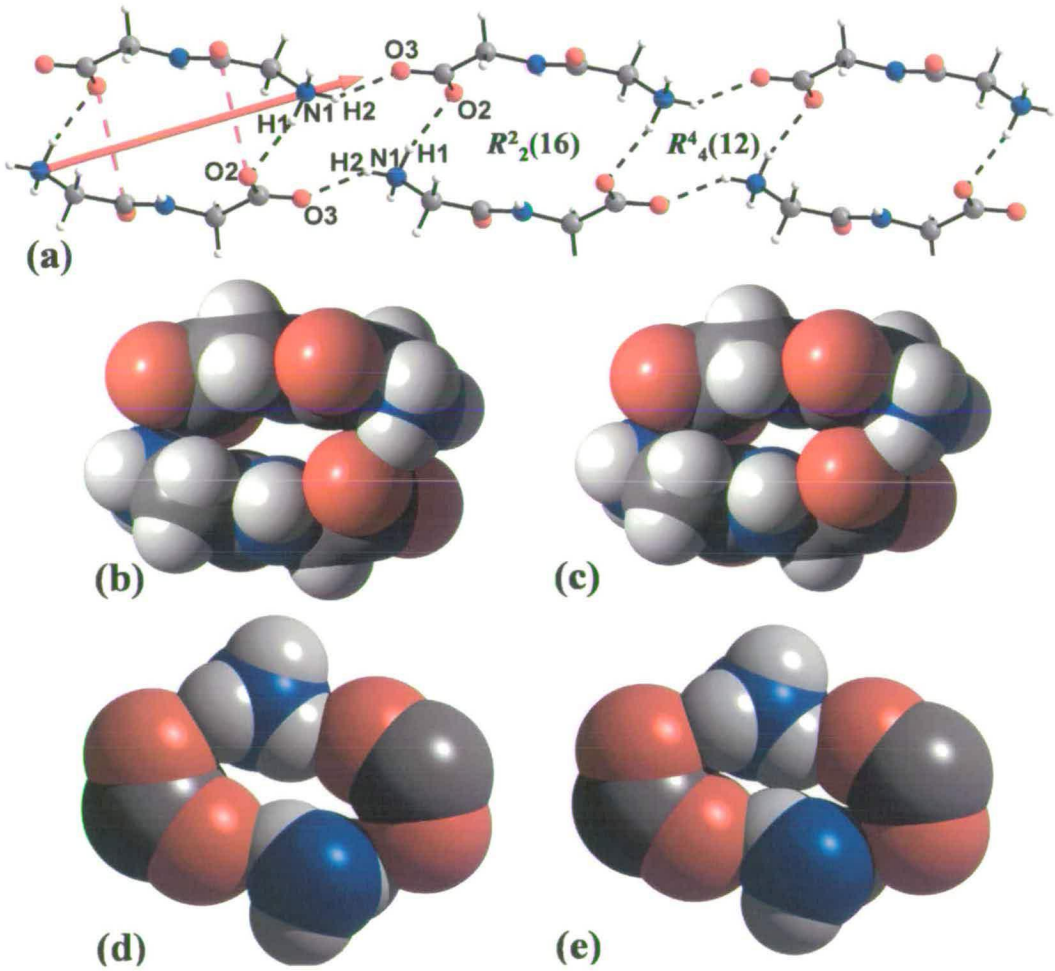

Figure 6.4: (a) Ball and stick model showing the formation $R^2_2(16)$ and $R^4_4(12)$ ring motifs under ambient pressure conditions between GLYGLY layers. Weak C=O…C=O interactions are drawn as pink dotted in the far left motif, while NH…O H-bonds are drawn as black dotted lines. The largest component of the strain tensor is drawn as a red arrow in (a). Space filling plots for $R^2_2(16)$ and $R^4_4(12)$ motifs in α-GLYGLY at ambient pressure (b & d), and 4.7 GPa (c & e) are drawn at the same scale and direction. For clarity, only the ammonium and carboxyl groups are included for comparison in d & e. Note that voids within $R^2_2(16)$ and $R^4_4(12)$ ring motifs close-up on increasing pressure. Colour scheme is the same as that in Figure 6.2.

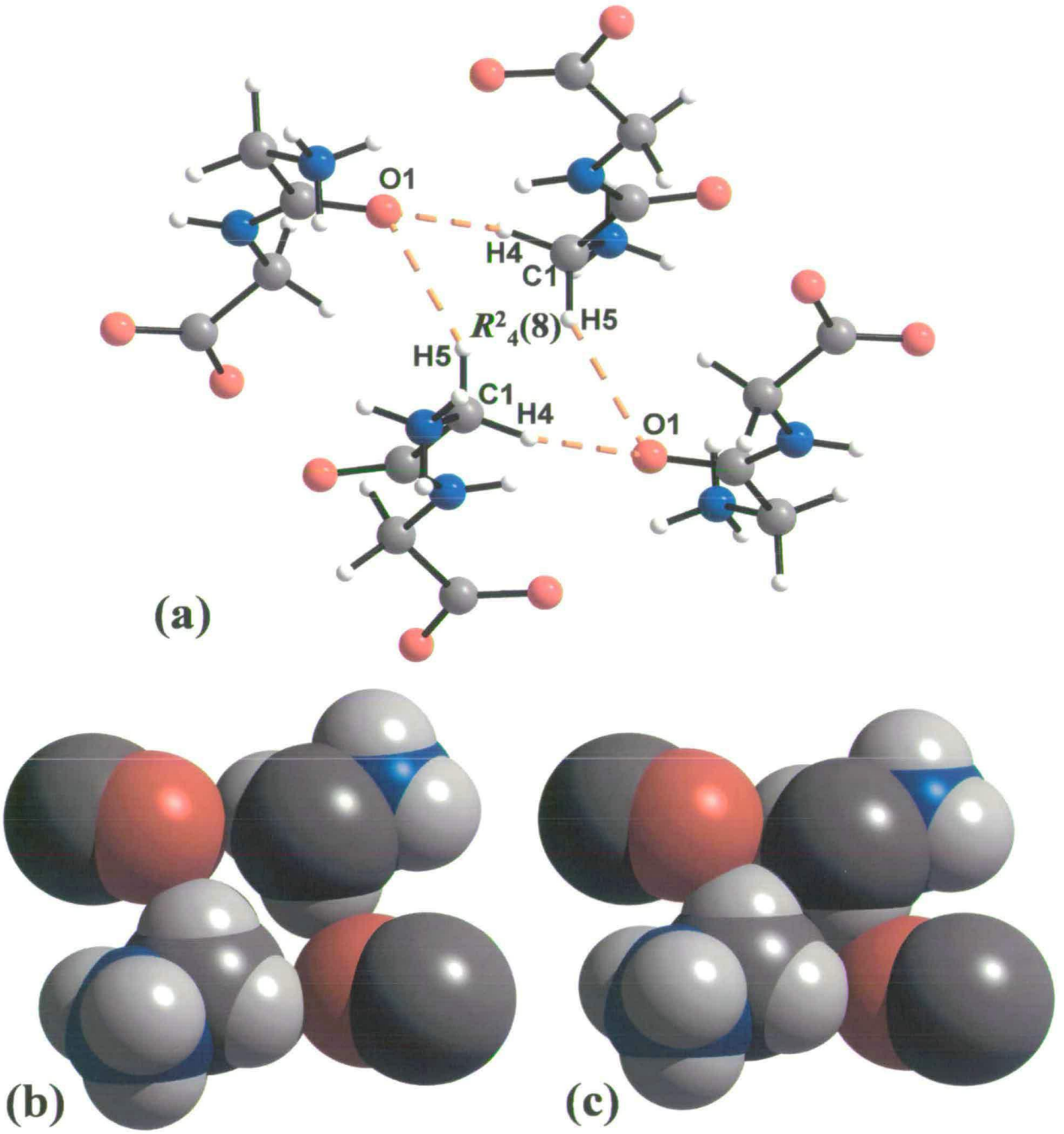

Figure 6.5: (a) Ball and stick model showing the formation of $R^2_4(8)$ ring motifs via CH...O H-bonds acting between layers of GLYGLY molecules, CH…O H-bonds are drawn as orange dotted lines. Space-filling plots of $R^2_4(8)$ ring motifs at (b) ambient pressure and (c) 4.7 GPa are shown, drawn at the same scale and direction. In both (b) and (c), only those atoms involved in the formation of the ring, carbonyl C atoms and ammonium groups are shown for clarity. Colour scheme is the same as that in Figure 6.2.

C=O...C=O interactions have been discussed in detail by Allen *et al.* (1998) and are thought to be important in the stabilisation of α-helices and β-sheets (Maccallum *et al.*, 1995). In α-GLYGLY, C=O...C=O interactions occur within the β-sheet like layers between adjacent carbonyl groups (Figure 6.2a). A typical *d*(O...C) distance of *ca* 3.6 Å is reported for the average of 12 sets of secondary structural features (Maccallum *et al.*, 1995). This value is in agreement with that measured for α-GLYGLY under ambient pressure conditions [3.573(2) Å]. Carboxyl-carboxyl and carboxyl-carbonyl interactions are formed between the GLYGLY layers. One such interaction occurs between pairs of C4=O2 bonds and is aligned in an anti-parallel fashion, another, C4=O2...C2=O1, forms a sheared parallel motif (Allen *et al.* 1998).

6.4.2 Effect of pressure on the unit cell dimensions.

α-GLYGLY was found to be stable to 5.4 GPa. However the refined parameters of data collected at 5.4 GPa were imprecise and therefore only structural data to 4.7 GPa are reported here and used for comparison with the ambient pressure structure.

The response of the lattice parameters of α-GLYGLY to pressure is anisotropic, with the largest principal component of the strain tensor formed between the β-sheet-like planes, making an angle of 69.22(6)° with the (1 0 -1) plane. The most compressible unit cell dimension (Figure 6.6) is the *a*-axis which reduces by 11.2%, with the *b* and *c*-axes reducing by 3.8% and 3.6% respectively between ambient pressure and 5.4 GPa. The β-angle also reduces by 6.61°. Between ambient pressure and 5.4 GPa the volume of α-GLYGLY reduces by 15.2%; most of the compression takes place in the first 1.4 GPa, with a reduction in volume of 8.0%. The gradient of the graph of pressure *versus* volume (Figure 6.6) reduces markedly at pressure just before the break-up of the crystal.

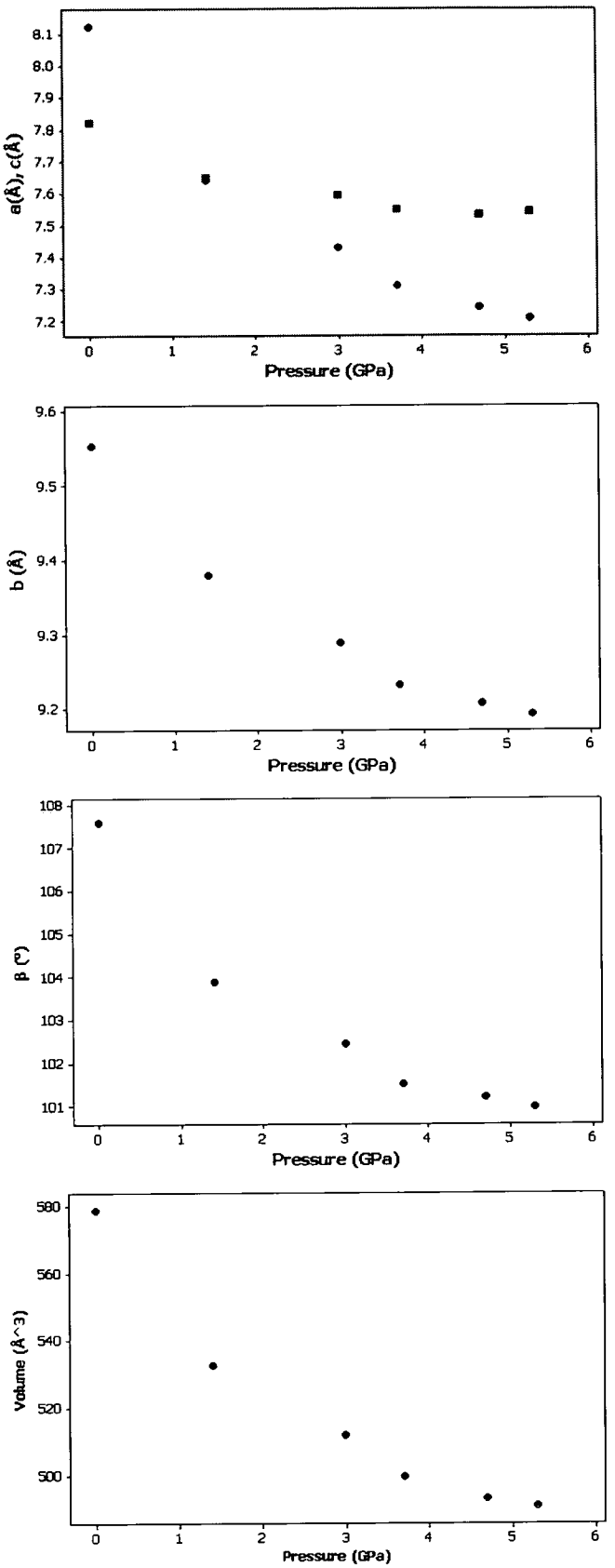

Figure 6.6: Variation of lattice parameters *a*, *b*, *c* (Å), β (°) and volume (Å^3) of α-GLYGLY as a function of pressure (GPa). Variation of *a* and *c* are shown on the same graph, with black circles and squares, respectively.

6.4.3 Conformational analysis of the β-sheet motif.

The structural analogy between the structure of the layers in α-GLYGLY and β-sheet motifs found in proteins was referred to above. Similar observations have been applied to N-formyl-L-Met-L-Val trihydrate (Chetterjee & Parthasarathy *et al.*, 1984) and L-His-Gly chloride (Steiner, 1997), which form parallel and anti-parallel β-sheet-like motifs, respectively.

In anti-parallel β-sheets, the conformational angles C(O)-N(H)-C_α-C(O) (ϕ) and N(H)-C_α-C(O)-N(H) (ψ) adopt typical values of -139° and +135° under ambient pressure conditions, although these values can vary somewhat (Voet & Voet, 1995). In α-GLYGLY, these torsion angles can be defined ϕ1, ψ1, ϕ2 and ψ2 leading from the free ammonium end, to the free carboxyl end and correspond to the torsion angles about N1-C1, C1-C2, N2-C3 and C3-C4 (Table 6.3). ϕ1 is therefore 'unconventional' in the sense that it cannot be defined within the dipeptide molecule; rather, we use the carboxyl oxygen atom O3 to which N1 is H-bonded (labelled $O3^{iii}$ in Tables 6.2 and 6.3). At ambient pressure, ϕ1 and ψ1 are -154.77(10)° and -152.38(13)° respectively, while ϕ2 and ψ2 measure -155.06(14)° and 169.70(14)° respectively.

These torsion angles, particularly for ψ are quite far from those expected for anti-parallel β-sheet structure. This is not surprising because of the flexibility of the glycine residues, in particular the ammonium end, which is primarily optimised for H-bonding within the structure. Nevertheless, on increasing pressure to 4.7 GPa the molecules remain fairly inflexible with both ϕ1 and ψ1 increasing by +3.4° and +1.1° respectively, while ϕ2 and ψ2 decrease and increase by only -3.5° and +2.2° respectively.

Pressure/GPa	0	1.4	3.0	3.7	4.7	Δ
H-bonds formed between the β-sheet-like layers						
N1H1..O2[i] N1..O2	2.7541(18)	2.737(9)	2.730(8)	2.723(8)	2.725(9)	0.029
N1H1..O3[ii] N1..O3	3.202(2)	3.042(6)	2.972(6)	2.928(6)	2.925(7)	0.277
H-bonds formed within the β-sheet-like layers						
N1H2..O3[iii] N1..O3	2.7223(19)	2.674(9)	2.657(8)	2.649(8)	2.624(9)	0.098
N1H3..O2[iv] N1..O2	2.7913(18)	2.755(6)	2.731(6)	2.708(6)	2.713(7)	0.078
N2H6..O1[v] N2..O1	2.9567(18)	2.861(6)	2.814(5)	2.783(5)	2.772(5)	0.185
C-H...O Hydrogen Bonds						
C1H4..O1[v] C1..O1	3.214(2)	3.160(7)	3.133(7)	3.119(7)	3.125(7)	0.089
C1H5..O1[vi] C1..O1	3.348(2)	3.252(9)	3.207(8)	3.180(8)	3.160(9)	0.188
C3H8..O2[vii] C3..O2	3.593(2)	3.356(7)	3.265(6)	3.221(6)	3.202(7)	0.391
C3H8..O3[vi] C3..O3	3.603(2)	3.382(8)	3.308(7)	3.282(7)	3.251(7)	0.352
C=O...C=O Interactions						
C2=O1..C2=O1[iv]	3.573(2)	3.480(6)	3.435(6)	3.404(6)	3.395(6)	0.178
C4=O2..C2=O1[i]	3.274(2)	3.105(7)	3.014(7)	2.939(7)	2.909(7)	0.365
C4=O2...C4=O2[vii]	3.405(2)	3.127(7)	3.022(7)	2.976(7)	2.952(7)	0.453

Symmetry operators:

i	1-*x*,1-*y*,-*z*	v	1-*x*,1/2+*y*,1/2-*z*
ii	1+*x*,1/2-*y*,1/2+*z*	vi	*x*,1/2-*y*,1/2+*z*
iii	1+*x*,*y*,1+*z*	vii	-*x*,1-*y*,-*z*
iv	1-*x*,-1/2+*y*,1/2-*z*		

Table 6.2: Hydrogen bonding parameters, and C=O...C=O interactions in α-GLYGLY. Donor-acceptor distances are in Å. The Δ column refers to the 4.7 GPa distance subtracted from the distance at ambient pressure.

	Pressure (GPa)	
	0	4.7
O3^{iii}-N1-C1-C2 (ϕ1)	-154.77(10)	-151.4(4)
N1-C1-C2-N2 (ψ1)	-152.38(13)	-151.3(6)
C2-N2-C3-C4 (ϕ2)	-155.06(14)	-158.6(6)
N2-C3-C4-O3 (ψ2)	169.70(14)	171.9(5)

Table 6.3: Torsion angles ϕ and ψ (°) in α-GLYGLY as a function of pressure. For numbering refer to text (iii = 1+*x*,*y*,1+*z*).

6.4.4 NH...O hydrogen bonds

Variation in hydrogen bonding parameters between ambient pressure and 4.7 GPa are given in Table 6.2. Since all H-atoms were placed geometrically, N...O distances are used to quantify the relative compressibility of the H-bonds. The most compressible of the NH...O H-bonds is the longer interaction in the bifurcated N1H1...O2/O3 H-bond, which interacts between the β-sheet-like layers. The shorter of these bonds, N1H1...O2, is the least compressible H-bond in the system. The next most compressible H-bond, N2H6...O1, is the interaction between neighbouring peptide groups which interact within the β-sheet-like layers (Figure 6.2a). In a study of the mean geometries of C-H...O and N-H...O H-bonding interactions in parallel and anti-parallel β-sheets (Fabiola *et al.*, 1997), the mean distance for this particular N-H...O H-bond is 2.89 Å, that is, slightly shorter than observed in α-GLYGLY at ambient pressure. This interaction runs in the same direction as the second largest component of the strain tensor, which is parallel **b** and is shown as a red arrow in Figure 6.2a.

N1H2...O3 shortens more than N1H3...O2, even though the latter is the longer bond at ambient pressure. N1H2...O3 decreases in length to 2.624(9) Å at 4.7 GPa. This distance is very short: a search of the Cambridge Database reveals that there are no ambient-pressure amino acid structures (out of 213 hits) with NH...O interactions shorter than N1...O3 at 4.7 GPa. The shortest interaction observed under ambient pressure conditions [2.661(2) Å] was observed in L-arganine L-glutamate trihydrate (DUSMAF; Suresh *et al.*, 1986). Even at 3.0 GPa N1H2...O3 is compressed below this value

[2.657(8) Å]. Short NH...O H-bonds have also been observed in L-cystine [2.690(18) Å; Moggach *et al.*, 2005a] at 3.7 GPa, and ε-glycine [2.59(4) Å; Dawson *et al.*, 2005].

6.4.5 CH...O hydrogen bonds

The most compressible of the CH...O H-bonding interactions is the bifurcated system, C3H8...O2/O3, formed between the β-sheet-like layers. The C...O distances in this interaction decrease in length by 0.39 and 0.35 Å between ambient pressure and 4.7 GPa, that is, substantially more than any of the NH...O bonds.

C1H4...O1 reduces by a relatively modest 0.089 Å between ambient pressure and 4.7 GPa, measuring 3.125(7) Å at 4.7 GPa. In anti-parallel β-sheets the mean C...O distance for this type of interaction is typically 3.27 Å (Fabiola *et al.*, 1997), with minimum and maximum values under ambient conditions of 2.91 Å and 3.50 Å respectively (3.50 Å being the cut-off distance used in the study).

6.4.6 C=O...C=O interactions

The least compressible of the C=O...C=O interactions, C2=O1...C2=O1, interacts within the β-sheet like layers and decreases in length by 0.178 Å between ambient and 4.7 GPa. This interaction runs in the same direction as the second largest component of the strain tensor and its compression is comparable to that of N2H6...O1, which also interacts within the layers, between adjacent peptide groups (reducing in length by 0.185 Å). The most compressible C=O...C=O interaction is formed between carboxyl groups, C4=O2...C4=O2, with d(C...O) decreasing by 0.453 Å. This interaction, which measures 2.952(7) Å at 4.7 GPa interacts between the layers and is the most compressible interaction in the structure.

The last of the C=O...C=O interactions, C4=O2...C2=O1, interacts between adjacent carboxyl and carbonyl groups and decreases by 0.365 Å between ambient pressure and 4.7 GPa. This interaction, like that of C4=O2...C4=O2, interacts between the layers and is the shortest of the three C=O...C=O interactions at 4.7 GPa, measuring 2.909(7) Å.

6.5 *Discussion*

6.5.1 Anisotropic compression of α-GLYGLY.

In previous pressure studies of L-serine-I and hexagonal L-cystine we have ascribed trends in the relative compressibility of CH...O and NH...O H-bonds to the closing up of voids within *R*-type ring motifs which exist under ambient pressure conditions. These voids are conveniently visualised in α-GLYGLY by comparing space-filling plots of ring motifs between ambient pressure and 4.8 GPa.

In α-GLYGLY there are five *R*-type ring motifs: all of these contain voids at the ring-centres, and all become smaller as pressure increases. These *R* motifs can be split into two categories, those within the GLYGLY layers [$R^2_2(10)$ and $R^4_4(18)$], and those between the layers [$R^2_3(6)$, $R^2_2(16)$ and $R^4_4(12)$]. The largest voids formed within the layers are those at the centre of $R^4_4(18)$ ring motifs (Figure 6.2), and these are very far from being completely closed at 4.7 GPa. Increasing pressure would be expected to close this void still further, but N1H2...O3 measures 2.624(9) Å at 4.7 GPa, and in other amino acids attainment of an NH...O distance as short as this has been observed to be a prelude to a phase transition. This is consistent with the break-up of the crystal which ensues above 4.7 GPa. Of the three H-bonds involved in the formation of the $R^4_4(18)$ rings, the most compressible is N2H6...O1, which is also the longest of the three at ambient pressure. Very small voids can also be observed within $R^2_2(10)$ ring motifs which also close-up on increasing pressure to 4.7 GPa.

Between the layers, the closure of voids can also be observed within $R^4_4(12)$, $R^2_3(6)$ and $R^2_2(16)$ ring motifs (Figure 6.3b/c, 6.4b/c and 6.4d/e, respectively). This is achieved by a sliding action of the layers across each other and moving closer together, rather than direct compression of N1H1...O2, which is the least compressible of the NH...O H-bonds formed. The combination of the sliding of the layers and their movement closer together accounts for the direction of the largest component of the strain tensor, which is illustrated in Figure 6.4a. As the layers are compressed together the H-bond about H1 becomes more bifurcated (Figure 6.3b/c); as in the case of N2H6...O1, described above, this occurs though compressions of a relatively long H-bond (N1H1...O3).

The compression of the layers leads to shortening of two C=O...C=O interactions. C4=O2...C4=O2 reduces by 0.453 Å, while C4=O2...C2=O1 compresses to become the shortest of its type in α-GLYGLY, although still substantially longer [2.909(7) Å] than the

shortest value observed under ambient pressure conditions [2.521(2) Å, Kapplinger *et al.*, 1999].

Our work on other amino acids has shown that compression is accompanied by an increase in the number and strength of CH...O contacts. Hence the void in the $R^2_4(8)$ ring motifs formed between C1H4...O1 and C1H5...O1, which interact between the β-sheet like layers, closes-up on increasing pressure (Figure 6.5b-c). The longest CH...O H-bond is the bifurcated interaction C3H8...O2/3, which experiences the greatest shortening (Table 6.2).

To summarise, compression of α-GLYGLY proceeds via the reduction in void sizes. Voids close in such a way as to decrease the distances of stabilising interactions like H-bonds and dipolar contacts, but once a contact has become very short (in this case N1H2...O3), the crystal begins to break-up, presumably as a result of a phase change. The largest reductions in interaction distances tend to occur for those contacts which are longest at ambient pressure. In α-GLYGLY these longer interactions are formed between the β-sheet-like layers, and it is understandable therefore that the direction of greatest compression lies in the same direction.

6.5.2 Hirshfeld surface analysis.

Hirshfeld surfaces are constructed by partitioning space within a crystal structure into regions where the electron density from a sum of spherical atoms (the promolecule) dominates over the sum of the electron density of the crystal (the procrystal) (McKinnon *et al.*,2004). In this study, Hirshfeld surfaces were constructed using the program CrystalExplorer (Wolff *et al.*, 2005). Figure 6.7 shows the distance external to the surface to the nearest nucleus in another molecule (d_e) mapped onto the surface in two different ranges 0.68-2.31 Å [labelled (i)] and 1.1-1.5 Å [labelled (ii)]. Each surface is shown in three orientations at ambient pressure (top row, a-c) and 4.7 GPa (bottom row, d-f).

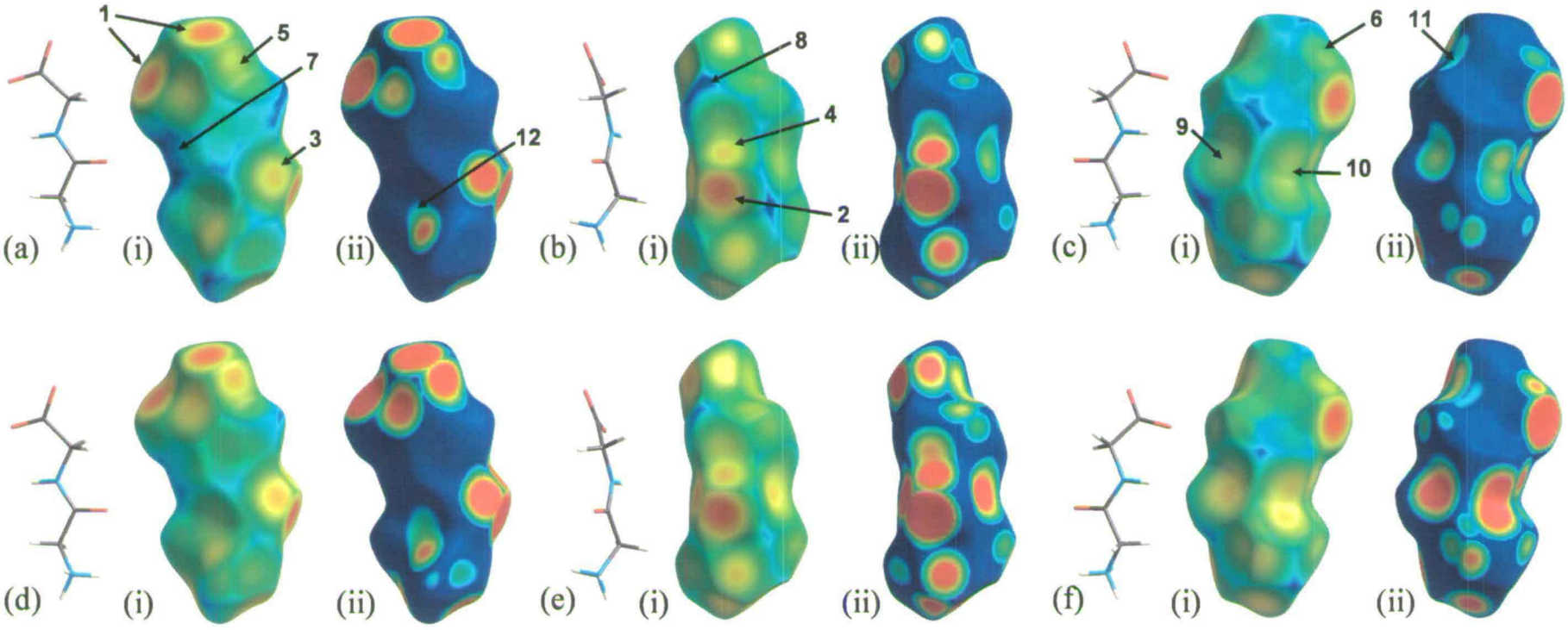

Figure 6.7: The Hirshfeld surface of GLYGLY at (a-c) ambient temperature and pressure, and (d-f) 4.7 GPa. The surface at both ambient pressure and 4.7 GPa have been separated into three orientations where (a & d) represent the GLYGLY molecule as viewed approximately perpendicular to the (1 0 -1) plane. Both (b & e) and (c & f) represent 90° increment rotations about the vertical axis from (a & d). In comparing both the ambient pressure and 4.7 GPa structures, all H-bonds have been normalised to neutron distances (C-H = 1.083 Å and N-H = 1.009 Å). Surfaces have been mapped over two ranges between [a(i)-f(i)] *d*e, 0.68 to 2.31 Å and [a(ii)-f(ii)] 1.1 to 1.5 Å. The molecules beside the surfaces have been added for clarity, for numbers refer to text. Colour scheme C grey, N blue, O red and H white.

In Figure 6.7a(i)-f(i), red regions on the surface arise from short values of d_e, (i.e. H-bond acceptors) while flat green regions around the ammonium group and peptide N2H6...O1 H-bond, correspond to H-bond donors. Blue regions correspond to long contacts. On increasing pressure to 4.7 GPa, there are fewer blue regions (longer contacts) and more red regions (short contacts), consistent with the general shortening of contacts at high-pressure [Figure 6.7a(i)-f(i)]. The decrease in lengths of NH...O H-bonds from the ammonium moiety and the peptide H-bond can be seen in Figures 6.7 a(i)/d(i) and b(i)/e(i), as an increase in the size of the red regions labelled 1 and 2. The yellow regions labelled 3 and 4 in Figure 6.7 a(i) and b(i), which are derived from C1H5...O1 and C1H4...O1, respectively, become redder in the corresponding regions of Figures 6.7 d(i) and e(i), indicating a shortening of these contacts at 4.7 GPa. The substantial shortening of the bifurcated H-bond C3H8...O2/O3 appears in regions 5 [Figure 6.7a(i)/d(i)) and 6 (Figure 6.7c(i)/f(i)].

In Figure 6.7(a(i)-c(i)), blue regions on the surfaces correspond to voids in the structure. As these voids become smaller at high-pressure the surfaces become greener. For example, the darkest blue region, labelled 7 in Figure 6.7a(i), corresponds to voids in $R^2_2(16)$ ring motifs (*cf* Figure 6.4b) between the β-sheet-like layers in the structure. Region 8 [Figure 6.7 b(i)] corresponds to voids in the middle of $R^4_4(18)$ ring motifs; the reduction in the size of this void can be seen in the corresponding region of Figure 6.7e(i). Notably, this void appears on the surface beside the C3-H7 bond, the only one of its type not involved in the formation of a CH...O H-bond, although a contact is formed between C3H7...O1, this contact is long, even at 4.7 GPa (3.311 Å). This contact, although it is long, does appear on the surface in Figure 6.7c(i) labelled 9. The region becomes markedly more yellow at 4.7 GPa [Figure 6.7f(i)] again representing clearly the compression between the layers.

The region in Figure 6.7c(i) labelled 10 is a close contact between two H-atoms attached to the CH_2 groups of adjacent ammonium moieties between layers. This region becomes markedly more yellow at 4.7 GPa showing the compression of non-polar side groups of the dipeptide toward each other on increasing pressure.

The compression of the C=O...C=O groups is not nearly as clear on the surfaces in Figure 6.7a(i)-f(i). In part this is because they are masked by much shorter contacts between NH...O and C=O. These contacts can be made clearer by mapping d_e on the surface over a shorter range (see Figure 6.7a(ii)-f(ii)). This not only enhances the

C=O...C=O interactions, but makes the increase in strength of CH...O and NH...O contacts much clearer. However, the regions in which void closure takes place becomes much more difficult to see, and therefore both sets of surfaces mapped over different ranges are included in Figure 6.7.

C4=O2...C4=O2, the most compressible interaction appears in region 11 [Figure 6.7c(ii)]. The increase in size of the blue/green region on Figure 6.7f(ii) corresponds to the shortening of this interaction on increasing pressure. The final C=O...C=O interaction, C4=O2...C2=O1 is the shortest of the three C=O...C=O interactions at 4.7 GPa, and can be seen in region 12 (Figure 6.7a(ii)). Again, the size of this region increases in Figure 6.7d(ii), and demonstrates the closing up of voids within $R^2_2(16)$ ring motifs between the layers (Figure 6.4b/c). Notably, this is the shortest of the C=O...C=O interactions at 4.7 GPa, and thus accounts for why the C4=O2...C2=O1 contact is markedly clearer in appearance on the surface than that formed by C4=O2...C4=O2.

6.5.3 Fingerprint plots

A *fingerprint plot* is a plot of d_e against d_i (the distance from the surface to the nearest atom in the molecule itself). It can be used to encode information on overall packing characteristics (Figure 6.8). The number of longer contacts decreases as the points at larger values of d_e become less frequent at 4.7 GPa: these interactions are formed across the voids within the *R*-type ring motifs. The overall shortening of these longer contacts are related to the fingerprint plots by a decrease in the maximum values of d_e between ambient pressure (2.303) and 4.7 GPa (2.196). The two long spikes in both plots represent NH...O H-bonds, specifically the shortest d_e value at 4.7 GPa is caused by N1H2...O3, the shortest of the NH...O H-bonds at this pressure. In previous studies, such as that of L-cystine, NH...O H-bonds have been found to be less compressible than 'softer' CH...O interactions. This is represented clearly in the fingerprint plot, as the NH...O spikes become less pronounced as the rest of the plot moves toward the origin.

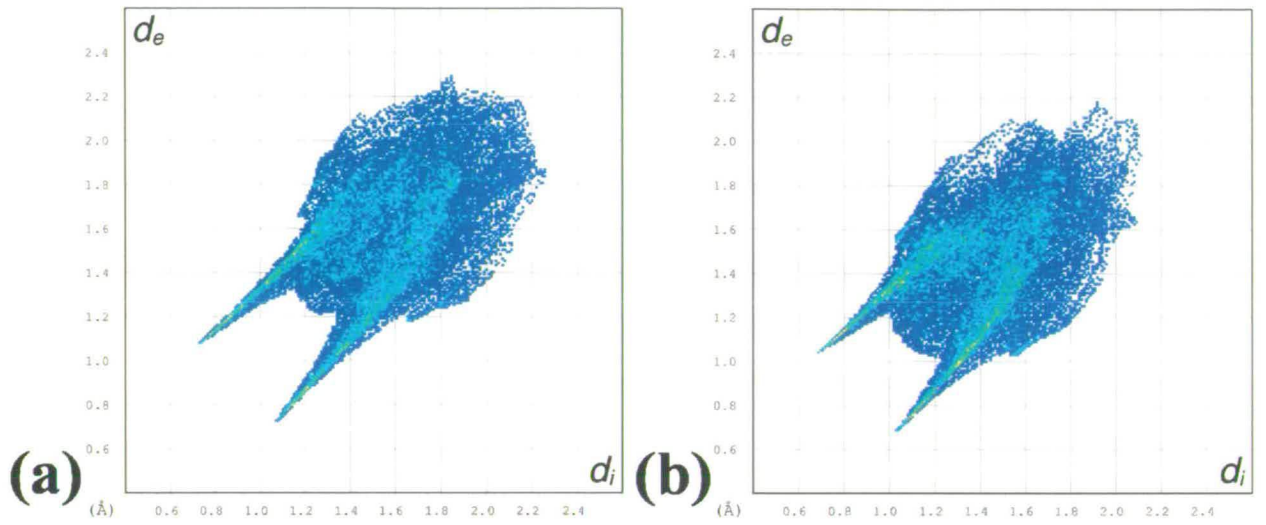

Figure 6.8: Two-dimensional fingerprint plots for α-GLYGLY at (a) ambient temperature and pressure and (b) 4.7 GPa.

6.6 Conclusions

We have described the effect of pressure on the crystal structure of α-GLYGLY. The structure can be considered to consist of layers of GLYGLY molecules which stack perpendicular to the (1 0 -1) direction, which are made up of $R^2_2(10)$ and $R^4_4(18)$ ring motifs constructed via NH...O H-bonding interactions. Ring motifs are also formed between layers, again by NH...O H-bonding interactions in $R^4_4(12)$, $R^2_2(16)$ and $R^2_3(6)$ ring motifs. The arrangement of GLYGLY molecules within each layer resembles that of an anti-parallel β-sheet motif observed in protein structures, where in α-GLYGLY, the molecules in the β-sheet motif are linked through NH...O H-bonds rather than conventional covalent amide links. The conformational changes in the pressure regime studied are quite modest, and the same might be expected of β-sheets.

The structure was found to be stable to 5.4 GPa, though structural data were only reported to 4.7 GPa. α-GLYGLY undergoes anisotropic compression in which the principal effect is to compress voids in the structure, particularly those between the layers. This compression continued until, at 5.4 GPa, the sample began to break apart and no structural data could be extracted. At 4.7 GPa the length of N1H2....O3 reduced in size to the minimum distance usually observed under ambient pressure conditions (*c.a.* 2.6 Å) for this type of interaction, and it is possible that relief of these close contacts drives the phase transition.

The compression of both NH...O and soft CH...O interactions are also described using Hirshfeld surfaces. These clearly show the reduction in the sizes of voids and a decrease in length of CH...O, NH...O and C=O...C=O interactions with increasing pressure, both between, and within the layers. Hirshfeld surfaces are an effective means to gain an overall view of the environment of molecules at increasing compress in an anisotropic fashion.

6.7 References

Allen, F. H. (2002). *Acta Cryst. B***58**, 380-388.

Allen, F. H., Baalham, C. A., Lommerse, J. P. M. & Raithby, P. R. (1998). *Acta Cryst. B***54**, 320-329.

Allen, F. H. & Motherwell, W. D. S. (2002). *Acta Cryst. B***58**, 407-422.

Bernal, J. D. (1931). *Z. Kristallogr. Kristallgeom. Kristallphys. Kristallchem.* **78**, 363-369.

Bernstein, J., Davis, R.E., Shimoni, L. & Chang, N-L. (1995). *Angew. Chem. Int. Ed. Engl.*, **34**, 1555-1573.

Boldyreva, E. V., Ivashevskaya, S. N., Sowa, H., Ahsbahs, H. & Weber, H.-P. (2004). *Doklady Physical Chemistry*, **396**, 111-114.

Boldyreva, E. V., Kolesnik, E. N., Drebushchak, T. N., Ahsbahs, H., Beukes, J. A. & Weber, H.-P. (2005) *Z. Krist.* **220**, 58-65.

Betteridge, P. W., Carruthers, J. R., Cooper, R. I., Prout, K., & Watkin, D. J. (2003). *J. Appl. Cryst.* **36**, 1487.

Bruker-Nonius (2002). SMART. Area-Detector Software Package, Madison, Wisconsin, USA.

Bruker-Nonius (2004a). SAINT, Version V7.12A. Area-Detector Integration Software, Madison, Wisconsin, USA.

Bruker-Nonius (2004b). APEX-II, Version V1. Area-Detector Integration Software, Madison, Wisconsin, USA.

Chatterjee, A. & Parthasarathy, R. (1984). *Int. J. Pept. & Prot. Res.* **24**, 447-452.

Crystal Impact (2004). *DIAMOND*. Version 3.0. Crystal Impact GbR, Postfach 1251, 53002 Bonn, Germany. http://www.crystalimpact.com/diamond.

Dawson, A., Allan, D. R., Clark, S. J., Parsons, S. & Ruf, M. (2004). *J. Appl. Cryst.* **37**, 410-416.

Dawson, A., Allan, D. R., Belmonte, S. A., Clark, S. J., David,W. I. F., McGregor, P. A., Parsons, S., Pulham, C. R. & Sawyer, L. (2005). *Cryst. Growth Des.* **5**, 1415-1427.

Derewenda, Z. S., Lee, L. & Derewenda, U. (1995). *J. Mol. Biol.* **252**, 248-262.

Desiraju, G. R. & Steiner, T. (1999). *The Weak Hydrogen Bond in Structural Chemistry and Biology. IUCr Monographs on Crystallography No. 9*. Oxford Univerity Press, Oxford.

Fabiola, G. F., Krishnaswamy, S., Nagarajan, V. & Pattabhi, V. (1997). *Acta Cryst. D***53**, 316-20.

Farrugia, L. J. (1999). *J. Appl. Cryst.* **32**, 837-838.

Girard, E., Kahn, R., Mezouar, M., Dhaussy, A-C., Lin, T., Johnson, J.E. & Fourme, R. (2005). *Biophysical Journal.*, **88**, 3562-3571.

Hughes, E. W. & Moore, W. J. (1949). *J. Am. Chem. Soc.* **71**, 2618-2623.

Kapplinger, I., Keutel, H. & Jager, E. G. (1999). *Inorg .Chim. Acta.* **291**, 190-206.

Kvick, A., Karaghouli, A. R. & Koetzle, T. F. (1979). *Acta Cryst. B***33**, 3796-3801.

Maccallum, P. H., Poet, R. & Milner-White, J. E. (1995). *J. Mol. Biol.* **248**, 361-373.

McKinnon, J. J., Spackman, M. A. & Mitchell, A. S. (2004). *Acta Cryst, B***60**, 627-668.

Moggach, S. A., Allan, D. R., Lozano-Casal, P. & Parsons, S. (2005a). *J. Synchrotron Rad.*, **12**, 590-597.

Moggach, S. A., Allan, D. R., Morrison, C. A., Parsons, S. & Sawyer, L. (2005b). *Acta Cryst. B***61**, 58–68.

Moggach, S. A., Allan, D. R., Parsons, S., Sawyer, L. & Warren, J. E. (2005c). *J. Synchrotron Rad.* **12**, 598–607.

Parsons, S. (2004). *SHADE*. The University of Edinburgh, Scotland.

Piermarini, G.J., Block, S., Barnett, , J.D., Forman, R.A. (1975). *J. Appl. Phys.*, **46**, 2774 - 2780

Sheldrick, G. M. (2004). *SADABS*. University of Göttingen, Germany.

Sheldrick, G. M. (1997). *XP*. University of Göttingen, Germany.

Spek, A. L. (2003). *J. Appl. Cryst.* **36**, 7-13.

Steiner, T. (1997) *Acta Cryst. C***53**, 730-732.

Suresh, C. G., Ramaswamy, J. & Vijayan, M. (1986). *Acta. Cryst.* (1986), *B***42**, 473-478.

Voet, D. & Voet, J. G. (1995). *Biochemistry* Second Edition. Wiley, New York, N.Y., USA.

Wolff, S. K., Grimwood, D.J., McKinnon, J.J., Jayatilaka, D. & Spackman, M.A. (2005). CrystalExplorer V1.5. University of Western Australia. http://www.theochem.uwa.edu.au/crystal_explorer/.

Chapter 7

Conclusions

7.1 Conclusions

This thesis has described the effect of high pressure on the crystal structures of a series of amino acids. Primarily this study has provided information about the pressure effects on the intermolecular interactions in these systems, in particular, the compression of hydrogen bonds has been studied in great detail. On increasing pressure, the general trend appears to be to force intermolecular contacts to their lower distance limits as observed under ambient pressure, after which the structure either changes (i.e. a phase transition), or the single-crystal breaks apart. Thus, in L-serine and L-cysteine, these systems underwent phase transitions to alleviate very close NH...O and S...S interactions. In α-glycylglycine, this was not the case, rather the single-crystal disintegrated on increasing pressure above 5.4 GPa. Nevertheless, the formation of a short NH...O interaction [*ca* 2.6 Å], which is at the lower distance limit for this type of hydrogen bond under ambient pressure conditions, was observed at 4.7 GPa. In L-cystine, compression of an already short S...S interaction took place which resulted in break-up of the single-crystal.

The formation of super-short hydrogen bonds within this pressure regime does not, therefore, appear to happen, rather the packing of the molecules changes to accommodate the increase with pressure.

Another trend which we observed within this family of compounds was the closure of voids observed within R-type H-bonded ring motifs on increasing pressure. Some compression within ring motifs was observed within all of the amino acids studied here. In particular, the compression of similar $R^4_4(16)$ motifs in α-glycine, and L-cystine were comparable. This may indicate that the compression of similar motifs within other amino acid structures may be similar.

Although admittedly, these conclusions are based on a very limited number of examples, they may provide insight into understanding the reasoning behind the behaviour of these molecular systems as a function of pressure.